Characterization and Localization of Intracellular Signals Emanating from an Oncogenic Mutant of the Cytokine Receptor Gp130

Von der Fakultät für Mathematik, Informatik und Naturwissenschaften
der RWTH Aachen University
zur Erlangung des akademischen Grades eines Doktors der Naturwissenschaften
genehmigte Dissertation

vorgelegt von

Diplom-Biologin

Natalia Rinis

aus Chalkis

Berichter: Professor Dr. Gerhard Müller-Newen

Professor Dr. Björn Usadel

Tag der mündlichen Prüfung: 24.04.2015

Γηράσκω δ’ αἰεὶ πολλὰ διδασκόμενος

Ich werde alt und lerne immer noch Vieles dazu

I always learn as I age

Solon

An essential part of this thesis was previously published in the following paper:

Rinis N, Küster A, Schmitz-Van de Leur H, Mohr A, Müller-Newen G. Intracellular signaling prevents effective blockade of oncogenic gp130 mutants by neutralizing antibodies. Cell Commun Signal. BioMed Central Ltd; 2014;12(1):14

Further publications:

Mohr A, Chatain N, Domoszlai T, Rinis N, Sommerauer M, Vogt M, et al. Dynamics and non-canonical aspects of JAK/STAT signalling. European Journal of Cell Biology. 2012 Jun;91(6-7):524–32.

Mohr A, Fahrenkamp D, Rinis N, Müller-Newen G. Dominant-negative activity of the STAT3-Y705F mutant depends on the N-terminal domain. Cell Commun Signal. BioMed Central Ltd; 2013;11(1):83.

Sebastian K, Detro-Dassen S, Rinis N, Fahrenkamp D, Müller-Newen G, Merk HF, et al. Characterization of SLCO5A1/OATP5A1, a Solute Carrier Transport Protein with Non-Classical Function. Deli MA, editor. PLoS ONE. Public Library of Science; 2013 Dec 20;8(12):e83257.

Witten KG, Ruff J, Mohr A, Görtz D, Recker T. Cellular uptake of fluorophore-labeled glyco-DNA–gold nanoparticles. J Nanopart Res. 2013.

Contents

Summary

IL-6 is a major regulator of the acute phase response (APR) and signals via a hexameric complex comprising two molecules IL-6, IL-6Rα and gp130, respectively. Upon formation of the signaling complex cytoplasmic Tyr-residues of the receptor get phosphorylated by receptor associated Jaks leading to the initiation of two major signaling pathways: the Jak/STAT and the MAPK/Erk pathway. Within the Jak/STAT pathway STAT1 and STAT3 are recruited to the four most membrane-distal pTyr-residues, homo- and/or heterodimerize and translocate into the nucleus to induce the expression of target genes. Among the most important target genes is the feedback inhibitor SOCS3 that binds to the pTyr 759 and exerts its action primarily via direct inhibition of the Jaks. Furthermore, SOCS3 recruits an E3-ubiquitin ligase complex leading to the degradation of its signaling partners. pTyr 759 also serves as a docking site for SHP2 and is therefore important for initiation of the MAPK/Erk pathway. This cascade leads to nuclear translocation of Erk and target gene induction. In 2009 small in-frame somatic deletions were identified within the gene encoding gp130 in benign liver tumors designated as IHCAs. These mutations target the interaction site of gp130 with IL-6 and confer constitutive and ligand-independent activity to the receptor by means of STAT3-phosphorylation and induction of SOCS3. This work focuses on the most potent of the detected deletion mutants of gp130 that is designated as CAgp130.

In the first part of this thesis we examined the processing-trafficking-signaling axis of CAgp130 in comparison to WTgp130. For this purpose WT and mutant receptor were tagged with fluorescent proteins and cell lines were generated that allowed expression of both receptors in a stable and inducible manner. Our results reveal that in contrast to WTgp130 that is prevalent in its high glycosylated form, CAgp130 is predominantly expressed in the lower glycosylated and therefore incompletely processed form. In line with these data CAgp130 accumulates in intracellular compartments that resemble the ER and Golgi and reaches the cell membrane to a much lower extent than WTgp130. We come to the conclusion that defects in processing and trafficking of CAgp130 cannot be attributed to constitutive receptor-phosphorylation, as described for several RTKs, as a receptor mutant where all Tyr-residues have been mutated does not differ in its intracellular distribution. Concerning the signaling properties, WTgp130 as well as CAgp130 lead to a full-fledged activation of the Jak/STAT pathway according to phosphorylation of the respective Tyr- and Ser-residues on STAT3 and STAT1. In contrast to WTgp130, that clearly activates the

MAPK/Erk pathway, CAgp130 just leads to its partial activation as it phosphorylates SHP2 but not Erk. We conclude that partial activation of the MAPK/Erk cascade by CAgp130 is due to its reduced cell surface expression as this pathway reportedly is strictly limited to the plasma membrane. By the use of so-called add-back mutants of CAgp130 were only single cytoplasmic Tyr-residues are available for signaling we confirmed a differential contribution of the Tyr-residues for activation of the Jak/STAT and MAPK/Erk pathways that, however, is identical to the WT.

In the second part of this thesis we investigated the spatial distribution of constitutive signaling. In order to analyze the signaling potential of CAgp130 on its way to the plasma membrane we initially tried to retain the receptor within the cell by the use of ER-retention sequences. As a second approach we utilized the trafficking-inhibitor brefeldin A and found that mutant receptor is able to activate STAT3 before reaching the cell membrane. Analysis of signaling emanating from CAgp130 located at the plasma membrane or upon its endocytosis was performed utilizing neutralizing gp130 Abs and dominant-negative dynamin, respectively. In both cases STAT3-activation did not show any perturbance leading us to the conclusion that neither cell surface CAgp130 nor CAgp130 at endosomal compartments significantly contributes to constitutive signaling. Downregulation of constitutive signaling was achieved by transfection of dominant-negative STAT3.

In the third part of this thesis we examined the role of SOCS3 that is induced by CAgp130 for downregulation of constitutive signaling. Our results using the Y759F mutant of gp130 reveal that signaling emanating from CAgp130 is inhibited by SOCS3 to a certain extent. Further data indicate a possible role of SOCS3 in lysosomal degradation of the receptor mutant as CAgp130 but not its Y759F mutant gets stabilized in the presence of inhibitors of lysosomal degradation.

Zusammenfassung

IL-6 spielt eine wichtige Rolle bei der Regulation der Akutphase Reaktion (APR) und vermittelt seine Signale über einen hexameren Komplex, der aus je zwei Molekülen IL-6, IL-6Rα und gp130 aufgebaut ist. Nach Ausbildung des signalisierenden Komplexes kommt es zur Phosphorylierung von Tyr-Resten auf der zytoplasmatischen Seite des Rezeptors durch assoziierte Jaks und zur nachfolgenden Aktivierung von hauptsächlich zwei Signalwegen: den Jak/STAT- und MAPK/Erk-Signalwegen. Im Rahmen des Jak/STAT-Signalweges werden STAT1 und STAT3 an die vier C-terminalen pTyr-Reste von gp130 rekrutiert, homo- und/oder heterodimerisieren und translozieren in den Zellkern um die Expression von Zielgenen zu induzieren. Zu den wichtigsten Zielgenen zählt der Inhibitor SOCS3, der an das pTyr 759 bindet und seine Wirkung primär über eine direkte Inhibierung der Jaks ausübt. Für SOCS3 wurde ein sekundärer Wirkmechanismus beschrieben, der auf die Rekrutierung eines E3-Ubiquitin-Ligase Komplexes basiert und den Abbau der Signaltransduktionspartner von SOCS3 zur Folge hat. Das pTyr 759 dient zusätzlich der Rekrutierung von SHP2 und spielt dadurch eine wichtige Rolle für die Initiierung der MAPK/Erk-Signalkaskade. Am Ende dieser Kaskade stehen die nukleäre Translokation von Erk und die Induktion der Expression von Zielgenen. Im Jahr 2009 wurden kleine somatische Deletionen im gp130-Gen von Leber-Adenomen entdeckt, die als IHCAs bezeichnet werden. Diese Mutationen sind an der Interaktionsfläche von gp130 und IL-6 lokalisiert und haben eine konstitutive und liganden-unabhängige Aktivierung des Rezeptors zur Folge, die anhand der Phosphorylierung von STAT3 und Induktion von SOCS3 festzustellen ist. Diese Arbeit fokussiert auf jene gp130-Mutante für welche die stärksten aktivierenden Effekte nachgewiesen wurden. Sie wird als CAgp130 bezeichnet.

Im ersten Abschnitt dieser Doktorarbeit wurden die Prozessierung, der Transport und die Signaltransduktion von CAgp130 verglichen zu WTgp130 untersucht. Aus diesem Grund wurden Konstrukte kloniert, die die Expression beider Rezeptoren als fluoreszierende Fusionsproteine ermöglichten. Desweiteren wurden Zelllinien für eine stabile und induzierbare Expression der fluoreszierenden Rezeptoren generiert. Unsere Ergebnisse zeigen, dass im Gegensatz zu WTgp130 das hauptsächlich in der höher glykosylierten Form vorliegt die Rezeptor-Mutante überwiegend in der niedrig glykosylierten Form vorhanden ist. In Übereinstimmung mit diesen Daten akkumuliert CAgp130 in intrazellulären Kompartimenten, die dem ER und Golgi ähneln und erreicht die Zellmembran mit einer

weitaus geringeren Effizient als WTgp130. Wir schlussfolgern, dass die Unterschiede in der Prozessierung und den Transport zur Zellmembran nicht auf die konstitutive Phosphorylierung von CAgp130 zurückgeführt werden kann, wie es für zahlreiche RTKs der Fall ist, da ein Rezeptor, der keine intrazelluläre Tyr-Reste mehr aufweist und nicht phosphoryliert werden kann, keinen Unterschied in seiner Zellmembran-Lokalisation zeigt. Bezogen auf die Signaltransduktion sind sowohl WT als auch CAgp130 in der Lage den Jak/TAT Signalweg vollständig zu aktivieren. Allerdings, sorgt CAgp130 im Gegensatz zu WTgp130 nur für eine partielle Aktivierung des MAPK/Erk-Signalweges. Die partielle Aktivierung besteht in einer Aktivierung von SHP2, der allerdings keine Erk-Aktivierung folgt. Die partielle Aktivierung ist möglicherweise auf die geringe Menge von CAgp130 an der Zellmembran zurückzuführen, zumal die MAPK/Erk-Signalkaskade als Zellmembranständiger Prozess beschrieben wird. Durch die Nutzung sogenannter add-back Mutanten in denen nur einzelne Tyr-Reste der Signaltransduktion zur Verfügung stehen wurde eine differentieller Beitrag der Tyr-Reste von CAgp130 für die Signaltransduktion nachgewiesen, die allerdings identisch zum WT ist.

Im zweiten Teil dieser Arbeit haben wir die räumliche Verteilung des konstitutiven Signals untersucht. Um das Signaltransduktionspotential von Rezeptor-Molekülen auf dem Weg zur Zellmembran zu untersuchen wurde anfangs eine Retention mittels geeigneter ER-Retentionssequenzen ausprobiert. In einem zweiten Ansatz wurde der Inhibitor Brefeldin A eingesetzt, der intrazelluläre Transportprozesse inhibiert. Anhand dieser Versuche haben wir herausgefunden, dass CAgp130 eine Aktivierung von STAT3 herbeiführen kann noch bevor es die Zellmembran erreicht. In weiteren Versuchen wurde das Signalisierungspotential von CAgp130 auf der Zellmembran und nach seiner Endozytose untersucht. Mit Hilfe antagonistisch wirkender Antikörper gegen gp130 und durch den Einsatz von dominant negativem Dynamin konnte gezeigt werden, dass weder konstitutiv aktiver Rezeptor an der Zellmembran noch endozytierte Rezeptor-Moleküle einen signifikanten Beitrag zum konstitutiven Signal beitragen. Die konstitutive Aktivität des Rezeptors konnte erst durch Transfektion von dominant negativem STAT3 runterreguliert werden.

Im dritten Abschnitt haben wir die Rolle von SOCS3, welches durch den konstitutiven Rezeptor induziert wird, in der Inhibierung des konstitutiven Signals untersucht. Durch den Einsatz der Y759F Mutante von CAgp130 konnten wir zeihen, dass die CAgp130-vermittelte Signaltransduktion durch SOCS3 runterreguliert werden kann. Weitere Daten lassen eine

Rolle von SOCS3 für den lysosomalen Abbau von CAgp130 vermuten, zumal CAgp130 allerdings nicht seine Y759F Mutante durch lysosomale Inhibitoren stabilisiert wird.

1. Introduction

Cytokines are small proteins that act as major mediators of intercellular communication in multicellular organisms. They are synthesized by various cell types like monocytes/macrophages, T- and B-lymphocytes, fibroblasts and endothelial cells mostly upon stimulation. Unlike hormones that are stored in glands as preformed molecules cytokines are secreted immediately upon synthesis [1].

Cytokines exert their function in nano- to picomolar concentrations through specific cell surface receptors. They are involved in the regulation of multiple physiological processes like survival, growth and differentiation and are key regulators of the immune response. Uncontrolled cytokine signaling is connected to several pathophysiological conditions like acute and chronic inflammatory diseases, cancer and autoimmune diseases [2].

Cytokines can act in an autocrine (when affecting the producing cell itself), paracrine (when affecting cells adjacent to the producing cell) and in rare cases endocrine manner (when acting on distant cells). Their mode of action is often described as redundant as similar biological effects can be achieved by different cytokines and pleiotropic meaning that a single cytokine can act on many different target cells [3].

The classification of the quite heterogenous group of cytokines has been performed in the past on the basis of engaged receptors and structural similarities. Of major biological and clinical importance is the ongoing classification according to the pro- and anti-inflammatory properties of cytokines [1] (Figure 1).

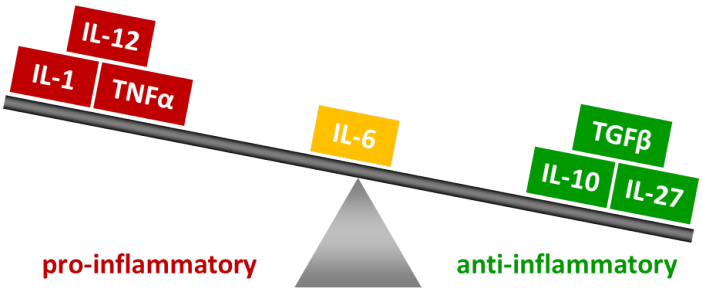

Figure 1 – Classification of prominent cytokines according to their pro- and anti-inflammatory properties [4]. A definite assignment of pro- or anti-inflammatory properties is possible for a minority of cytokines. Most cytokines e.g. IL-6 exert both [5] depending on the cellular context and environmental factors.

This kind of classification represents a serious challenge as cellular activities of cytokines depend on numerous factors like cytokine concentration, nature and activation state of the target cells and the cell microenvironment including the presence of other cytokines.

1.1. IL-6-type cytokines and their receptors

IL-6 (interleukin-6) type cytokines are characterized by a four-α-helix bundle structure [6]. Members of this family have pro- and anti-inflammatory properties and are major players in hematopoiesis, in acute phase and immune responses. The family of IL-6-type cytokines comprises IL-6 and IL-11, IL-27, IL-31, LIF (leukaemia inhibitory factor), OSM (oncostatin M), CNTF (ciliary neurotrophic factor), CT-1 (cardiotrophin-1) and CLC (cardiotrophin-like cytokine) [7]. The most prominent functions of these cytokines are summarized in Table 1.

IL-6-type cytokine	Functions
IL-6	APR [8] Further information in section 1.2.1.
IL-11	• Thrombopoiesis [9] • Inhibition of adipogenesis [10]
IL-27	• Regulation of T cell responses [4] • B cell differentiation and activation [11]
IL-31	• Promotion of skin disorders [12] • Regulation of allergic diseases [13]
LIF	• Blastocyst implantation [14] • Survival factor for neurons [15]
OSM	• Inhibition of the proliferation of cells derived from melanomas [16] • Bone formation and destruction [17]
CNTF	• Proliferation of neural stem cells in mice [18] • Nerve regeneration *in vivo* [19]
CT-1	• Induction of cardiomyocyte hypertrophy [20] • Survival of motorneurons [21]
CLC	Survival factor for motor neurons [22]

Table 1 – Major functions of IL-6-type cytokines. Abbreviations used: APR – acute phase response.

Among IL-6-type cytokines CLC and IL-27 are so-called composite cytokines and need further components in order to bind to their respective receptor. CLC forms prior to binding to its cognate receptor a heterodimeric complex with CLF-1 (cytokine-like factor-1) [23] and IL-27

is comprised out of the cytokine p28 and the soluble receptor EBi3 (Epstein-Barr virus-induced gene) [24] (Figure 2). The latest discovered IL-6-type cytokine is IL-35 and a composite cytokine as well. It is composed of p35 that is a cytokine subunit of IL-12 and EBi3 [25],[26].

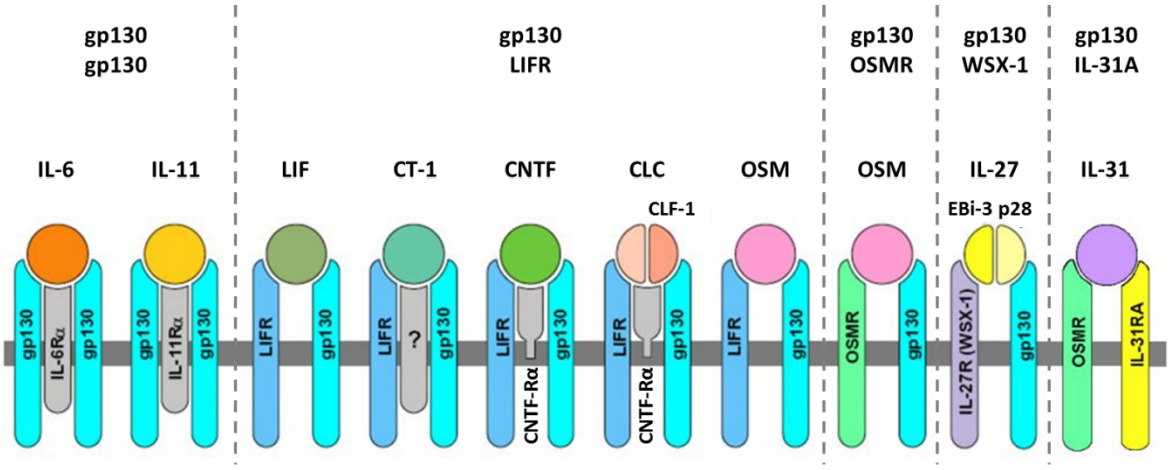

Figure 2 – IL-6-type cytokines and their receptors (modified from [7]). For details see text.

IL-6-type cytokines signal via class I cytokine receptors harboring at least one CBM (cytokine binding module) on their extracellular part. CBMs are comprised of two FNIII(fibronectin type III)-like domains with four concerved Cys-residues in the N-terminal FNIII-like domain and a WSXWS-motif (W – tryptophan, S – serine and X an arbitrary aa (amino acid)) in the C-terminal FNIII-like domain [7].

Signaling is mediated by receptor complexes that are comprised out of a non-signaling α-receptor that binds the respective cytokine and delivers it to the signaling homo- or heterodimeric β-receptor. An α-receptor is required in the case of IL-6, IL-11, CNTF and CLC (Figure 2). It is still unclear whether CT-1 needs an α-receptor [27]. Almost all IL-6-type cytokines utilize the signal transducing β-receptor gp130 with the exception of IL-31. IL-31 signals via a heterodimeric OSMR/IL-31RA receptor complex [28] with IL-31RA also known as GPL (gp130-like receptor). IL-6 and IL-11 signal via gp130 homodimers whereas LIF, CT-1, CNTF and CLC use a heterodimeric gp130/LIFR receptor complex. IL-27 signals via a heterodimeric gp130/IL-27R complex and OSM is the only IL-6-type cytokine able to signal through two different heterodimeric receptor complexes: gp130/LIFR and gp130/OSMR [7] (Figure 2).

In a simplified view every cytokine binds to its respective receptor and leads to activation of intracellular pathways. However, when combined, cytokines, hormones and other stimuli can affect each other in an additive, synergistic or antagonistic way, generating a regulatory network designated as cross-talk. Cross-talk occurs at the level of activated signaling pathways as well as at the level of cytokine-receptor interactions allowing a single cytokine to utilize different receptor combinations [2].

1.2. IL-6-mediated signal transduction

1.2.1. IL-6

IL-6 was initially described in 1983 as hepatocyte-stimulating factor because of its regulatory effect on the synthesis of APPs (acute phase proteins) in the liver [29]. The arrangement of its four helices results in an up-up-down-down topology apparent in Figure 3 [30]. IL-6 comprises three receptor binding sites: site I for the interaction with the IL-6Rα and sites II and III that mediate the interaction with gp130 [31].

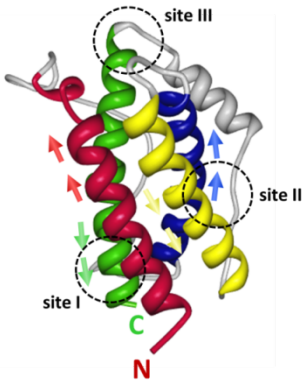

Figure 3 – Structure of IL-6 (modified from [7]). The helices of the four-α-helix bundle structure of IL-6 are highlighted in different colours as well as the interaction sites of IL-6 with the IL-6Rα and gp130. For details see text.

Today it is known that IL-6 is the major regulatory cytokine of the APR (acute phase response). It is produced upon injury, infection and because of neoplastic growth or immunological disorders by leukocytes, fibroblasts and endothelial cells. Upon its production it contributes to the systemic part of the APR and exerts a wide spectrum of pleiotropic actions [8] some of which are summarized in Figure 4.

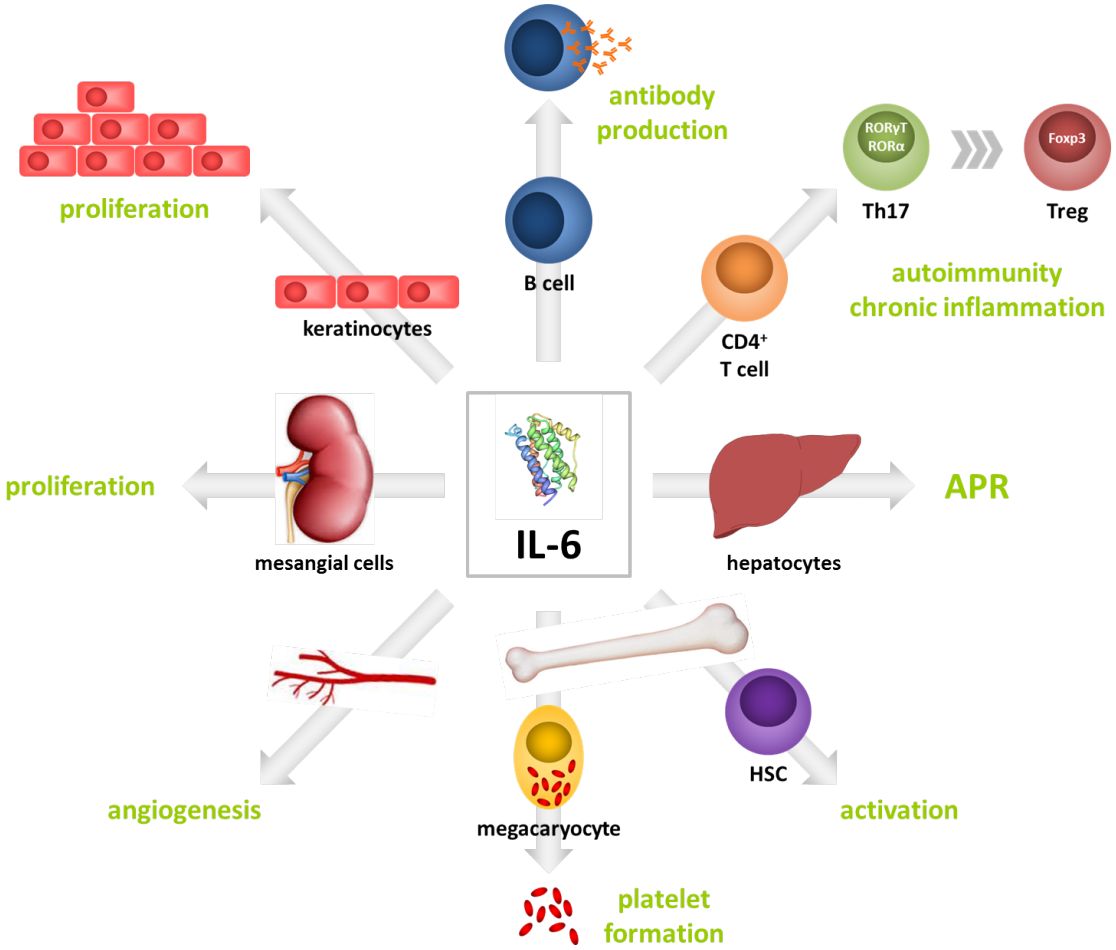

Figure 4 – Pleiotropic effects of IL-6. Abbreviations used: APR – acute phase response, HSC – hematopoietic stem cell, Th17 – IL-17 producing T cells, Treg – regulatory T cells. For details see text.

In the APR IL-6 upregulates APPs such as CRP (C-reactive protein) that is a well established biomarker for inflammation and SAA (serum amyloid A). In contrast to these positive APPs that are upregulated negative APPs like fibronectin and transferrin are downregulated [8].

In a more immunological context IL-6 together with TGFβ (transforming growth factor β) promotes the differentiation of naïve $CD4^+$ T cells into IL-17 producing Th17 cells that promote autoimmunity. At the same time IL-6 inhibits the TGFβ-induced generation of regulatory T cells designated as Treg. The resulting Th17/Treg imbalance leads to the breakage of immunological tolerance and is of pathological importance for various autoimmune and chronic inflammatory diseases [32]. IL-6, also designated as B cell stimulatory factor-2, stimulates B cells for Ab (antibody) production and induces $CD8^+$ T cells to generate cytotoxic T cells [8].

In the hematopoietic system IL-6 induces the maturation of megakaryocytes into platelets and the activation of hematopoietic stem cells [33].

IL-6 induces VEGF (vascular endothelial growth factor). Excess VEGF production leads to enhanced angiogenesis and increased vascular permeability that are inflammatory features. IL-6 further promotes the proliferation of keratinocytes and production of collagen in dermal fibroblasts thereby possibly promoting autoimmune skin diseases like systemic sklerosis and psoriasis. Furthermore, it stimulates the growth of myeloma/plasmacytoma and mesangial cells [33].

1.2.2. IL-6Rα

IL-6Rα is a type I transmembrane protein with its C-terminus localized within the cytoplasm. According to its molecular weight of 80 kDa IL-6Rα is often designated as gp80 – glycoprotein of 80 kDa. Its extracellular part consists of three domains (Figure 5). Domain 1 is an Ig(Immunoglobulin)-like domain and is dispensable for biological activity [34]. Domains 2 and 3 are FNIII-like domains and form the CBM [7].

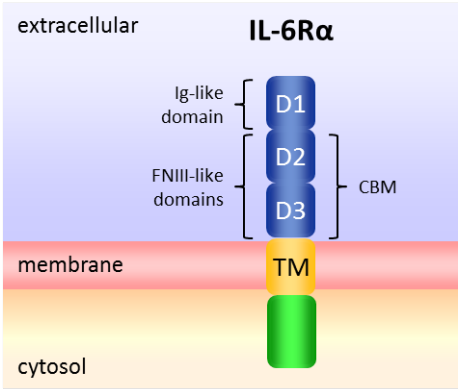

Figure 5 – Schematic representation of the membrane-bound form of IL-6Rα. Abbreviations used: CBM – cytokine binding module, FNIII – fibronectin type III, Ig – immunoglobulin. For details see text.

In contrast to gp130 that is ubiquitously expressed IL-6Rα expression is restricted to certain cell types like hepatocytes, some epithelial cells and leukocytes [5]. The IL-6Rα is not involved in the intracellular signal transduction cascade [7], however, its extracellular part is important for the formation of the signaling complex. Cells lacking IL-6Rα are completely unresponsive to IL-6 as gp130 has no measurable affinity for IL-6 [35]. In general IL-6 first binds to the IL-6Rα with low affinity before the IL-6/IL-6Rα complex can bind to gp130 with a 100fold affinity. However, even cells without membrane-bound IL-6Rα can be stimulated with the help of a soluble form of IL-6Rα abbreviated as sIL-6Rα in a process called trans-

signaling [5]. This soluble receptor can be generated by two distinct mechanisms: differential splicing or limited proteolysis by two members of the ADAM (A Disintegrin and Metalloproteinase) family, namely ADAM 10 and 17 [36]. Regulation of sIL-6Rα levels is supposed to occur via shedding of the membrane-bound receptor [37].

1.2.3. Gp130

Gp130 – glycoprotein 130 – is the common signal transducing receptor subunit for the family of IL-6-type cytokines. In contrast to IL-6Rα gp130 is ubiquitously expressed, however, in low amounts. HEK cells exhibit less than 1000 molecules/cell [38] and human HepG2 cells around 2000 molecules/cell [1]. Mice deficient for gp130 die at day 12.5 post coitum and display hematological and myocardial abnormalities [39].

Gp130 is synthesized as a precursor with an apparent molecular weight of 130 kDa and gets processed within 45-60 min to a mature form of 150 kDa [40]. Its processing comprises – similar to other transmembrane proteins – the attachment of O- and N-linked oligosaccharides in the ER and throughout the Golgi. Gp130 gets N-glycosylated at 9 out of 11 potential glycosylation sites [41]. It remains unclear whether glycosylation is a prerequisite for the localization and activation of the receptor. Yanagisawa et al. report that in neuroepithelial cells treated with the N-glycosylation-inhibitor tunicamycin gp130 reaches the cell surface, however, cannot form a heterodimer with LIFR upon stimulation [42]. In contrast to that Waetzig et al. report that a gp130 mutant where all N-glycosylation sites have been mutated is severely hampered on its way to the cell membrane and gets degraded by the proteasome. Small amounts of gp130 detectable at the cell membrane, however, are able to signal suggesting that glycosylation is important for the stability of the receptor but not for its signaling activity [43].

Gp130 is similar to the IL-6Rα a type I transmembrane protein. Its extracellular part has a modular structure and consists of six distinct domains (Figure 6). Domain 1 is an Ig-like domain and domains 2-6 are FNIII-like domains. The first three domains have been shown to be important for ligand binding [44] with domains 2 and 3 forming the CBM. The three membrane-proximal domains 4-6 transmit structural changes upon ligand binding to the transmembrane and intracellular part of the receptor enabling signal transduction to occur [45].

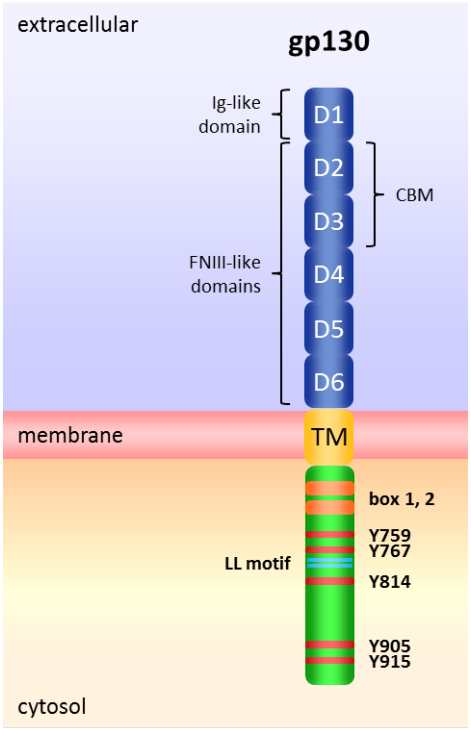

Figure 6 – Schematic representation of gp130. Abbreviations used: CBM – cytokine binding module, FNIII – fibronectin type III, Ig – immunoglobulin. For details see text.

The intracellular part of gp130 comprises two membrane-proximal conserved domains called box 1 and 2 which are connection sites for the Jaks (Janus kinases) [46]. Jaks play a pivotal role in gp130-mediated signal transduction as gp130 does not have an intrinsic tyrosine kinase activity. Gp130 has been shown to associate with Jak1, 2 and Tyk2 [7]. Among these kinases Jak1 plays a critical role as in cells without Jak1 IL-6 signal transduction is strongly impaired [47]. As shown by FRAP (fluorescence recovery after photobleaching) analysis gp130 and Jak1 stably interact and can be regarded as a RTK (receptor tyrosine kinase) [48]. Among the box regions box 1 is important for receptor binding of Jaks to gp130 as its deletion or mutation of two critical Pro-residues abrogates Jak binding [49]. Box2 is also important for Jak binding in terms of increasing the affinity of the Jaks for the receptor [50]. Besides the boxes the interbox region is also critical as the mutation of a single residue abrogates Jak binding and receptor signaling activity [51].

Upon IL-6 stimulation a rapid internalization and degradation of the receptor is observed leading to the loss of IL-6 binding sites, a mechanism important to prevent overstimulation [52],[53]. A stretch of 10 aa crucial for efficient endocytosis [54] and a dileucine-motif important for ligand-dependent internalization were identified within the cytoplasmic region of gp130 [55]. Furthermore, endocytosis of gp130 was shown to occur in a constitutive and

ligand-independent manner through constitutive association with the AP-2 (adaptor protein-2) adaptor complex [56].

Finally, in the intracellular part of gp130 five out of six Tyr-residues get phosphorylated upon stimulation and function as recruitment sites for transcription factors and further signaling components. Tyrosine at position 683 is the most membrane-proximal Tyr-residue and the only one without a recruiting function. The next Tyr-residue Y759 binds upon its phosphorylation to SHP2 (src homology domain 2 (SH2) containing protein tyrosine phosphatase 2) and further recruits the feedback inhibitor SOCS3 (suppressor of cytokine signaling) [57]. The four remaining Tyr-residues Y767, Y814, Y905 and Y915 act upon their phosphorylation as recruiting sites for STAT(signal transducer and activator of transcription)-factors [7].

1.2.4. IL-6/IL-6Rα/gp130 complex

The initial event of IL-6-induced signal transduction is the formation of a ternary hexameric IL-6/IL-6Rα/gp130 complex (Figure 7).

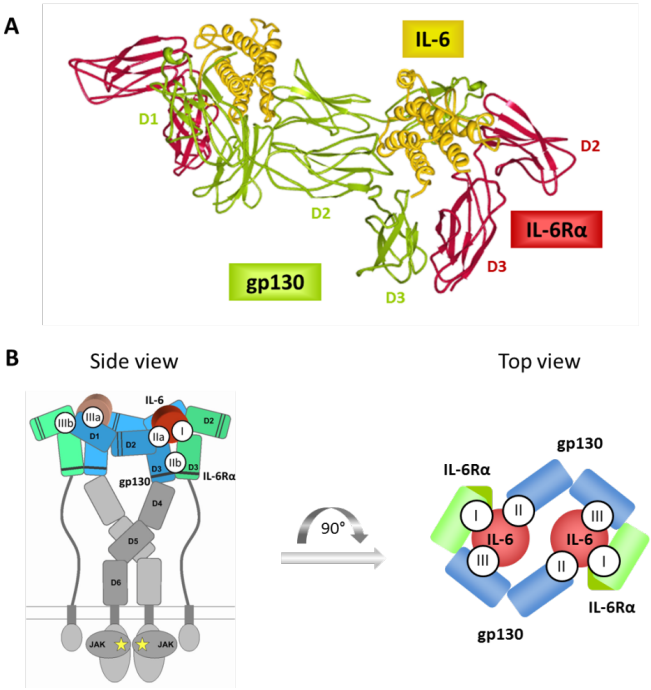

Figure 7 – Structure of the hexameric IL-6/IL-6Rα/gp130 complex. (A) Crystal structure of the IL-6/IL-6Rα/gp130 complex (modified from [58]). The components of the complex are highlighted in different colours: IL-6 in yellow, D2 and D3 of IL-6Rα in red and D1-3 of gp130 in green. **(B)** Schematic representation of the signaling complex (modified from [59]). Depicted are the side (left) and top (right) view of the signaling complex as well as decisive interaction sites. For details see text.

The structure of the hexameric signaling complex was resolved in 2003 by Boulanger et al. using the crystal structure of a soluble complex consisting of human IL-6, the two FNIII-like domains of human IL-6Rα (D2 and D3) and the three N-terminal domains of gp130 (D1-D3). This hexameric complex is built up sequentially out of two molecules IL-6, IL-6Rα and gp130 respectively. In the very first step site I within the IL-6 molecule interacts with the non-signaling α receptor and a binary IL-6/IL-6Rα complex is formed. This complex interacts via site II of IL-6 with a single gp130 molecule. The resulting trimeric complex interacts via site III of IL-6 with domain I of a gp130 molecule that is itself also captured in a trimeric IL-6/IL-6Rα/gp130 complex [58]. The resulting hexameric IL-6/IL-6Rα/gp130 complex is depicted in Figure 7.

1.2.5. Signaling pathways activated by IL-6

Upon formation of the IL-6/IL-6Rα/gp130 signaling complex Jaks that are associated with the cytoplasmic part of gp130 come in close proximity and get activated via autophosphorylation and/or transphosphorylation [60],[61]. Activated Jaks phosphorylate Tyr-residues on the cytoplasmic part of gp130. The pTyr-motifs serve as recruitment sites for transcription factors and adaptor proteins. The IL-6-induced activation of gp130 initiates two major signaling pathways: the Jak/STAT pathway and the MAPK/Erk cascade [7]. An additional signaling cascade that gets activated by IL-6 is the PI3K/Akt pathway. However, its activation has been described to be cell type specific [62].

1.2.5.1. Jak/STAT pathway

Activation of the Jak/STAT pathway involves the recruitment of STAT1 and STAT3 to phosphorylated Tyr-residues at positions 767, 814, 905 and 915 of gp130 [7]. The recruitment of STAT factors has been shown to be mediated by their SH2 domain [63]. STAT3 preferentially binds to pTyr-motifs with the consensus sequence YXXQ (Y – tyrosine, Q - glutamine and X an arbitrary aa) and therefore binds to the four membrane-distal pTyr-residues of gp130. STAT1 binds to pTyr-residues within the more restricted consensus sequence YXPQ (P – prolin) and therefore gets recruited to the most membrane-distal Y905 and Y915 [63]. Work by Schmitz et al. demonstrated differential contribution of the potential recruitment sites for the activation of STAT3 [64]. Upon recruitment STAT proteins get phosphorylated by Jaks at conserved Tyr-residues namely Y705 for STAT3 [65] and Y701 for

STAT1 [66]. They form homo- and heterodimers that translocate to the nucleus and initiate the transcription of target genes. One of the most prominent target genes of STAT3 is the feedback inhibitor SOCS3 [67] as depicted in Figure 8.

STAT1 and STAT3 are also phosphorylated at the Ser-residue 727 [68],[69]. The responsible serine kinase has not been unambiguously identified yet. Amongst several candidate kinases are the SAPKs (stress activated protein kinases), JNK (c-jun N-terminal kinase) and p38 as well as Erk (extracellular signal regulated kinase) [7]. Ser-phosphorylation of STAT1 has been shown to be important for the maximal activation of transcription [70]. In addition Ser-phosphorylation has been implicated in a non-canonical function of STAT3 within mitochondria [71],[72].

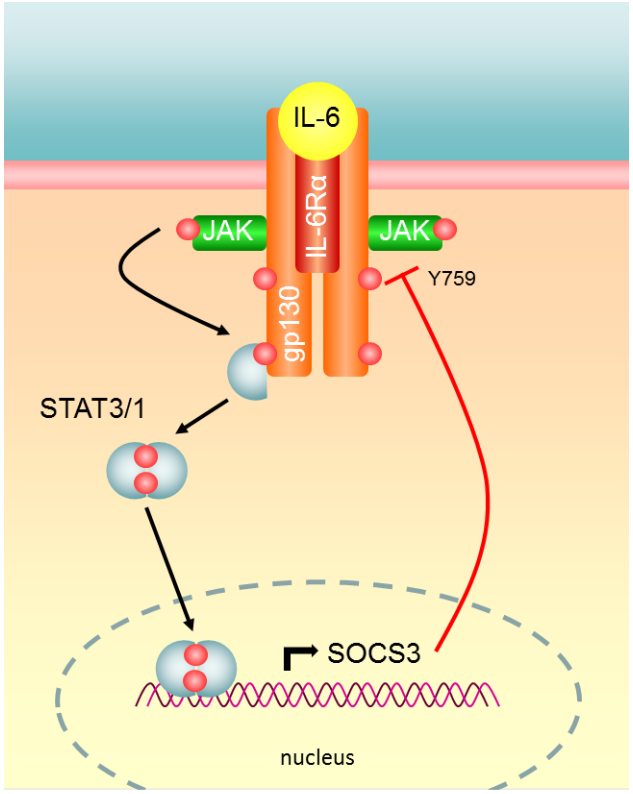

Figure 8 – Schematic representation of the Jak/STAT pathway. Upon formation of the IL-6/IL-6Rα/gp130 signaling complex Jaks associated with the cytoplasmic part of gp130 undergo autophosphorylation and/or transphosphorylate and activate each other. They phosphorylate cytoplasmic Tyr-residues of the receptor that recruit STAT1 and STAT3. Upon their phosphorylation STAT proteins form homo- and heterodimers that translocate into the nucleus and drive transcription of target genes e.g. the feedback inhibitor SOCS3. For details see text.

1.2.5.2. MAPK/Erk pathway

Activation of the MAPK/Erk cascade involves the recruitment of the tyrosine phosphatase SHP2 to Y759 within gp130 [73]. Upon recruitment SHP2 acts as an adaptor protein and

associates with Grb2 (growth factor receptor-bound protein 2). Grb2 acts as an adaptor protein itself and binds the guanine nucleotide exchange factor SOS (son of sevenless). A crucial step in the activation cascade is the recruitment of SOS to the plasma membrane where it can activate the small G protein Ras (rat sarcoma) and converts it into its GTP-bound form. The recruitment of SOS to the plasma membrane is facilitated through the constitutive interaction of Grb2 with Gab1 (Grb2 associated binding protein 1) [74],[75]. Gab1 binds via its PH(pleckstrin homology)-domain specifically to PdtIns(phosphoinositide)-(3,4,5)P_3 [76],[77] that is exclusively found in the plasma membrane [78]. Ras-GTP activates the MAPK (mitogen activated protein kinase) cascade by phosphorylating and thereby activating the serine/threonine kinase Raf1 (Ras associated factor 1). Raf1 activates MEK (MAP-Erk-kinase) that itself activates Erk [7]. Erk translocates into the nucleus and drives transcription of target genes as depicted in Figure 9.

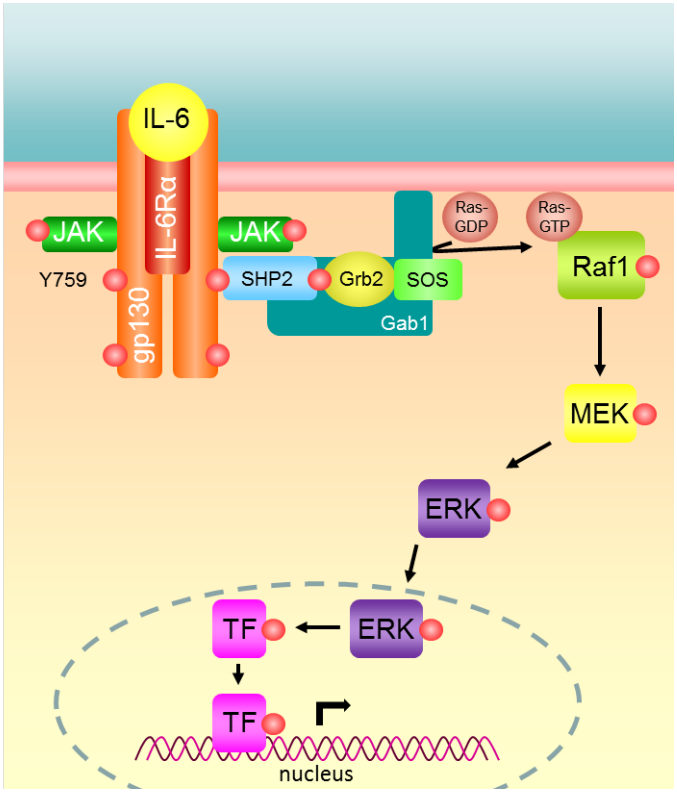

Figure 9 – Schematic representation of the MAPK/Erk pathway. The initial steps are identical to the activation of the Jak/STAT pathway. SHP2 gets recruited to Y759 of gp130 and recruits Grb2 that itself recruits SOS. SOS recruitment to the plasma membrane is important for activation of Ras and is mediated by Gab1. Upon its activation Ras initiates the MAPK cascade that ends with the activation and nuclear translocation of Erk. For details see text.

1.2.5.3. PI3K/Akt pathway

As already mentioned IL-6-mediated activation of the PI3K/Akt pathway is reported to be cell type specific [62]. PI3K (phosphatidyl inositol 3 kinase) consists out of two subunits: the regulatory subunit p85 and the catalytic subunit p110. Gp130 recruits the subunit p85 via Gab1 and thereby activates p110. Activation of PI3K leads to phosphorylation of PtdIns(4,5)P2 and production of PtdIns(3,4,5)P3 where the protein kinases PDK1 (phosphoinositide-dependent kinase-1) and Akt bind to. Upon its recruitment to the plasma membrane PDK1 activates Akt [79].

1.2.6. Downregulation of IL-6-mediated signaling

Negative regulation of signaling pathways is equally important to their activation in order to prevent prolonged signaling. Especially in the case of IL-6-induced STAT3-phosphorylation where a longer persisting or even constitutive signaling has been associated with chronic inflammatory conditions and cancer, mechanisms that downregulate signaling are indispensable.

The most important negative regulators that are being utilized within the Jak/STAT pathway are the tyrosine phosphatase SHP2, PIAS (protein inhibitors of activated STATs) proteins and the members of the SOCS family of feedback inhibitors [7]. After a short introduction of SHP2 and PIAS proteins the focus will be set on SOCS proteins.

1.2.6.1. SHP2

The protein tyrosine phosphatase SHP2 exerts its negative regulatory function on signaling by its recruitment to the phosphorylated Y759 of gp130 [73]. Upon binding to the receptor SHP2 unfolds and gets enzymatically active [80]. A potential substrate of SHP2 is gp130 as well as Jaks and STATs [81].

1.2.6.2. PIAS proteins

PIAS proteins are important transcriptional regulators of the Jak/STAT pathway as they inhibit DNA binding of activated STAT proteins and hence transcription of their target genes. Within the family of PIAS proteins that comprises five mammalian members PIAS1 inhibits DNA binding of STAT1 [82] and PIAS3 DNA binding of STAT3 [83].

1.2.6.3. SOCS proteins – Focus on SOCS3

The family of SOCS proteins comprises eight mammalian members: CIS (cytokine inducible SH2 protein) and SOCS1-7 [67],[84],[85]. Common structural features of all SOCS proteins are the central SH2 domain that mediates binding to pTyr-motifs and the C-terminal SOCS-box [86] that are depicted for SOCS3 in Figure 10. The SOCS-box is involved in the degradation of SOCS3 binding partners [87].

Stimulation with IL-6 leads to the induction of four proteins of the SOCS family: CIS and SOCS1-3 [7]. Among those SOCS1 and SOCS3 are the most potent inhibitors but it is rather SOCS3 that is responsible for inhibiting IL-6 signal transduction *in vivo* [88]. In contrast to the other SOCS proteins SOCS1 and SOCS3 contain a short sequence upstream of the SH2 domain termed KIR (kinase inhibitory region) (Figure 10).

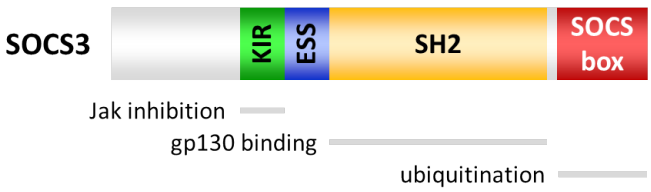

Figure 10 – Schematic representation of SOCS3. The functional roles of the individual domains are indicated. Abbreviations used: KIR – kinase inhibitory region, ESS – extended SH2 domain.

SOCS3 exerts its inhibitory activity utilizing two different modes of action. The primary mechanism of SOCS3 action is the direct inhibition of the catalytic activity of Jaks. The inhibitory effect is mediated by the KIR [89] that is partially blocking the substrate binding groove of the kinase. In contrast, ATP binding remains unperturbed [90] making SOCS3 to a non-competitive inhibitor with regards to ATP binding.

In its second mode of action SOCS3 is able to recruit an E3-ubiquitin ligase complex and induces the ubiquitination and subsequent degradation of signaling components. Of central importance in this facet of SOCS3 action is the SOCS-box that was reported to recruit elongin B and C [87] as well as Cullin5 [91]. Cullin5 is the scaffold for the CRL (Cullin-RING ligase) family of ubiquitin ligases [92]. Its C-terminal part binds to activated ubiquitin whereas the N-terminal part recruits the substrate. Recently Kershaw et al. reconstructed a SOCS3 based E3-ubiquitin ligase complex *in vitro* and reported that SOCS3 was able to catalyze ubiquitination of Jak2 and gp130 [93].

1.3. Inflammation and cancer

1.3.1. The link between inflammation and cancer

Cancer – in medical terms malignant neoplasia – is a disease characterized by unrestrained cellular division and expansion. In general carcinogenesis is thought to depend on disruption of the checkpoints that limit cell division and on activation of signals that accelerate cellular growth [94]. In addition to these mechanisms inflammation has emerged over the last ten years to play a decisive role in the development of cancer including its initiation and promotion [95].

An inflammatory response generally consists of three major steps: In the first step neutrophils are recruited to the site of injury. They release chemotactic factors and recruit monocytes that differentiate into macrophages. Macrophages affect endothelial, epithelial and mesenchymal cells of the local environment by the production of cytokines and growth factors upon their activation. The key concept of normal inflammation as it occurs upon injury is that it is self-limiting. This self-limiting property can be attributed to the consecutive production of pro- and anti-inflammatory cytokines that is overruled in chronic inflammation [96].

The link between inflammation and cancer as it has been elaborated in the past decade consists of two pathways: the extrinsic and the intrinsic pathway [97].

The extrinsic pathway refers to chronic inflammatory conditions that increase cancer risk [97]. The inflammatory response of the extrinsic pathway precedes tumor development and can be attributed to several causes including environmental exposure, microbial infection as well as immune deregulation and autoimmunity [95]. In particular material from tobacco smoke can cause COPD (chronic obstructive pulmonary disease) that is associated with higher lung cancer risk [98]. Persistent infections with Helicobacter pylori are associated with gastric cancer [99] and infections with hepatitis B or C viruses are linked to a higher incidence of HCCs (hepatocellular carcinomas) [100]. An example for a chronic inflammatory disease linked to autoimmunity is IBD (inflammatory bowel disease) that is associated with higher risk of colorectal cancer [101]. However, not all chronic inflammatory diseases increase cancer risk [102].

In contrast to the extrinsic pathway the intrinsic pathway refers to the type of inflammation that follows tumor development [95] and is driven by genetic alterations such as the ones found in oncogenes [97]. Members of the Ras and MYC family are the most frequently

mutated oncogenes in human cancers. Oncogenic components of the Ras-Raf signaling pathway induce the production of pro-inflammatory cytokines and chemokines [103],[104]. MYC promotes cell-autonomous proliferation and formation of an inflammatory microenvironment. In a mouse model of MYC-induced cancer of the β-cells MYC induces the pro-inflammatory cytokine IL-1β thereby promoting the first wave of angiogenesis [105].

The role of inflammation in tumor initiation consists of providing the mutational hits that send a normal cell on the tumorigenic track. It has been proposed that an inflammatory environment can increase mutation rates mainly by the production of ROS (reactive oxygen species) and RNI (reactive nitrogen intermediates) by activated immune or epithelial cells [106]. Inflammation-induced mutagenesis can further inactivate or repress mismatch repair response genes [107] or upregulate AID (activation-induced cytidine deaminase). AID promotes immunoglobulin gene class switching by deamination of cytosines in DNA. It has been shown to be upregulated in many types of cancer [108] and induces genomic instability [107]. A further mechanism by which inflammation may promote tumor initiation is via the production of growth factors and cytokines that confer a stem cell-like phenotype upon tumor progenitors or stimulate stem cell expansion as shown for STAT3 [109]. This leads to the enlargement of the cellular pool targeted by environmental mutagens.

In tumor promotion inflammation can contribute by increasing cell proliferation and reducing cell death. The predominant portion of inflammation-driven pro-tumorigenic effects is exerted at the level of tumor promotion and involves besides increased proliferation and enhanced survival the so-called angiogenic switch that provides small dormant tumors the blood supply necessary for growth [110]. The main transcription factors activated by tumor-promoting cytokines are NF-κB, STAT3 and AP-1 (activator protein-1) [95]. Among them NF-κB and STAT3 are activated in the majority of cancers and act as nonclassical oncogenes whose activation does not result from mutation themselves but depends on signals produced by neighboring cells or mutational activation of upstream signaling components.

Finally, even the most critical aspect of cancer namely metastasis requires close collaboration between the tumor, immune and inflammatory as well as stromal cells [95].

As a result of inflammation tumors get infiltrated by immune cells that play a pivotal role in modulation of the tumor microenvironment and thereby in tumor development. The presence of these cells and the pro- or anti-inflammatory millieu that they generate are

according to the current perception one of the most important hallmarks of cancer-related inflammation [95]. By affecting the cytokine and chemokine composition of the tumor microenvironment these cells determine whether tumor-promoting inflammation or anti-tumor immunity will prevail. Among the cells that are found within tumors and the tumor microenvironment are innate immune cells including macrophages, mast cells and dendritic cells as well as cells of the adaptive immunity such as T and B lymphocytes [111]. Among the most important players are TAMs (tumor-associated macrophages) that represent an important source of cytokines [97].

1.3.2. The IL-6-STAT3 axis at the interface of inflammation and cancer

As already mentioned in the last section the connection between inflammation and cancer can be subdivided in an extrinsic and an intrinsic pathway [97]. In the first case inflammation precedes and enhances cancer risk, in the second case cancer caused by genetic alterations is responsible for the generation and maintenance of inflammatory conditions. In both cases the stage is set by an inflammatory microenvironment that contains inflammatory cells and mediators.

The IL-6-STAT3 axis is important for both ex- and intrinsic pathways linking cancer and inflammation.

As already discussed in section 1.2.1. IL-6 is an important factor for induction of the APR. The vast majority of the IL-6-mediated effects on inflammation-induced carcinogenesis depend on its ability to activate the pseudo-oncogene STAT3. The contribution of the IL-6-STAT3 axis in the feed-forward loop of cancer and inflammation is commonly subdivided into five categories:

Effects on cell proliferation and survival

Activation of STAT3 by IL-6 promotes cell cycle progression and proliferation through upregulation of MYC, cyclin D1, cyclin B1 (late G1 to G1/S phase proteins) and cdc2 (G2/M phase protein) as well as downregulation of the Cdk (cyclin-dependent kinase) inhibitor p21 [112].

Furthermore, activated STAT3 upregulates survival genes of the intrinsic apoptosis pathway such as Bcl-X_L, Bcl-2 and Mcl-1 [113]-[115] along with the survival and proliferation marker

survivin [116]. STAT3 can also inhibit the extrinsic apoptosis pathway by transcriptionally downregulating the death receptor Fas in cooperation with c-Jun [117].

Effects on angiogenesis, invasion and metastasis

STAT3 upregulates growth and transcription factors important for angiogenesis like VEGF [118],[119] and HIF1α (hypoxia-inducible factor 1α) [120]. In this context HIF1α has been reported to bind to the VEGF gene promotor and initiate VEGF-A transcription upon recruitment of further transcription factors like phosphorylated STAT3 [121].

Excessive STAT3-activation has been shown to promote metastasis of melanoma cells to the brain, a fact that has been associated with the induction of tissue-degrading MMPs (matrix metalloproteinases) such as MMP-2 [122]. In epithelial-mesenchymal transition that is the first step of metastasis STAT3 was shown to induce the key regulators Snail and Twist [123]. Snail is a repressor for E-cadherin transcription in epithelial cells and loss of E-cadherin is thought to be a key event in the transition process [95].

Metabolism

STAT3 that is phosphorylated at Y705 promotes aerobic glycolysis and reduces oxidative phosphorylation [124]. This metabolic shift known as the Warburg effect is mediated by the STAT3 target gene HIF1α. HIF1α is known to increase the transcription of all glycolytic enzymes as well as PDK1 (pyruvat dehydrogenase kinase 1) that inhibits the entry of pyruvat into the citric acid cycle and therefore leads to the production of lactic acid [125]. The tumor is able to proliferate and gets protected from ROS that form during mitochondrial respiration at the same time [126].

Lastly the role of STAT3 in metabolism has been dominated by a non-canonical function of STAT3 within mitochondria. According to findings by Wegrzyn and Gough STAT3 phosphorylated at S727 localizes within mitochondria where it augments the electron transport chain and facilitates Ras-dependent transformation [71],[72].

Immunity

Among the most important immunological aspects of STAT3 action is the antiinflammatory response (AIR) driven by the immunosuppressive cytokine IL-10. STAT3 activated by IL-10 induces several AIR factors that subsequently repress proinflammatory genes primarily on a

transcriptional level [127]. Furthermore, STAT3 plays an important role in T cell differentiation as shortly mentioned in section 1.2.1.. Activated STAT3 is a major regulator of the balance between Th17 cells and Treg (regulatory T) cells [128]. Through its sustained activation the balance is tipped in favour of Th17 cells that play a crucial role in several autoimmune diseases [129]. Th17 cells are further crucial for defence against extracellular bacteria and fungi [32].

1.3.3. IHCAs – A model for inflammation-induced carcinogenesis

Hepatocellular adenomas (HCAs) are rare benign liver tumors predominantly found in women and associated with obesity, alcohol abuse [130] and intake of oral contraceptives [131]. Bleeding and malignant transformation of these adenomas to HCCs occur in 30-50% and 5% of the cases, respectively. In the last ten years HCAs were molecularly classified in four subgroups depending on whether the occuring mutations are inactivating HNF1α (hepatocyte nuclear factor 1α), activating β-catenin or activating STAT3. Remaining unclassified adenomas were summarized in a fourth group [132].

HCAs with mutations leading to STAT3-activation are designated as inflammatory HCAs (IHCAs) and represent 50% of HCAs. As the name already suggests IHCAs have an inflammatory phenotype characterized by inflammatory infiltrates largely localized to arterial vessels.

The first mutations that were found to confer constitutive activation of STAT3 were identified in a genome-wide transcriptome analysis of four IHCAs in 2009 [133]. Rebouissou et al. reported on somatic gain-of-function mutations within the *IL6ST* gene that encodes the signaling receptor subunit gp130. Mutations of gp130 were found in about 60% of IHCAs and included primarily small in-frame deletions and one in-frame duplication within exon 6 of the *IL-6ST* gene. The functional consequences of these mutations were besides a constitutive and ligand-independent activation of STAT3, the induction of the major feedback inhibitor SOCS3 and further downstream target genes like *STAT3* itself and the acute phase genes *CRP* and *SAA*. Constitutive activation can be explained when taking into account the structural consequences of gp130 mutations for its interaction with IL-6. All mutations are localized within domain 2 of the CBM of gp130 and are predicted to disrupt key residues in the gp130/IL-6 interface. By targeting the binding site of gp130 for IL-6 gp130 mutations might resemble IL-6 binding and initiate the sequence of structural rearrangements along the

receptor that finaly end in signal transduction. In later studies constitutive activation of STAT3 by gp130 was shown to be dependent on Jak1 but not Jak2 or Tyk2 [134].

A second source of STAT3 activating mutations within the Jak/STAT pathway was found to be STAT3 itself. In 2011 Pilati et al. reported that a subset of IHCAs lacking mutations within gp130 harbored somatic mutations within the STAT3 gene [135]. Most of the identified mutations were aa substitutions within the SH2 domain that drives homodimerization of STAT3.

In a large approach initiated this year by a strong French consortium the focus was placed on the improvement of molecular classification of HCAs to provide a more personalized care for patients in the future. Beyond the mutations in gp130 and STAT3 further somatic mutations confering to constitutive STAT3-activation were identified [132]. Most importantly activating mutations were found in the gene encoding Jak1.

These findings provide a so far unique example for the addiction of benign tumorigenesis to mutational alterations of a single signaling pathway namely the Jak1/STAT3 pathway.

1.3.4. Constitutively active receptors

Constitutively active gp130 as it was detected within IHCAs [133] is far from being the only receptor whose ligand-independent activity shows disease-related consequences. In nearly each of the four major classes of cell surface receptors alone members that exhibit constitutive activity can be found.

Within the family of GPCRs (G protein-coupled receptors) constitutive activity is specified as the ability of a receptor to adopt an active conformation in the absence of an agonist [136]. Agonists play a major role in stabilizing the active state within the two-state model of GPCR-activation [137]. Constitutive activity has been observed for 60 WT GPCRs as well as for disease-related mutants [136]. Prominent GPCRs that exhibit an agonist-independent activity are amongst others the receptors for the thyroid-stimulating hormone (TSH) – TSHR – and cholecystokinin B [CCK_2) – CCK_2R. Within TSHR single point mutations in several transmembrane domains or the N-terminus lead to adenoma or hyperplasia associated with hyperthyroidism [138]-[140]. In the case of CCK_2R coincidence of several single point mutations leads to gastric tumors in mice [141]. Furthermore, mutations conferring constitutive activity to the luteinizing hormone LHR cause male precocious puberty [142].

Besides gp130, constitutive activity has been reported for several other cytokine receptors such as the erythropoietin receptor EPOR and the leptin receptor LepR. In the case of EPOR a single aa change in the extracellular part of the receptor confers constitutive activity and has been reported to be tumorigenic [143],[144]. Within LepR an aa substitution at position 269 renders the receptor persistently active and results in the obese phenotype of the fatty rat [145]. The most recent report on a constitutive cytokine receptor is the thrombopoietin receptor MPL that is found in patients with primitive myelofibrosis and essential thrombocythemia [146].

The most prominent cell surface receptors concerning constitutive activity and its disease-related effects are RTKs, which in contrast to cytokine receptors harbor an intrinsic kinase activity. Particularly class III RTKs, which are characterized by five extracellular Ig-like domains and two intracellular kinase domains are frequently mutated leading to hematopoietic malignancies [147]. Among those the platelet derived growth factor receptors PDGFRα and β get persistently activated due to chromosomal translocations that lead to the generation of fusion genes. These rearrangements are frequently seen in patients with myeloid malignancies. A further mechanism of RTK-activation consists of mutations of the juxtamembrane domain. The juxtamembrane domain prevents formation of the active conformation by interacting with N- and C-terminal kinase lobes and serves as a negative regulatory element. For c-Kit activating mutations of the juxtamembrane domain were first identified in mast cell lines [148],[149]. Mutations within this domain are found in mastocytosis [150] and GISTS (gastrointestinal stromal tumors) [151]. In the case of the RTK FLT3R (Fms-like tyrosine kinase 3) mutations of the juxtamembrane domain are in-frame tandem duplications (ITDs) [152]. FLT3-ITD is found in 20% of AML cases.

1.4. Aim of the study

The initial goal of this work was to investigate the signaling properties of constitutively active gp130. Among the numerous somatic mutations conferring constitutive activity to the receptor the most potent one – a deletion of residues 186 to 190 – was chosen. The receptor mutant is designated as CAgp130 (Constitutively Active gp130) throughout this work. Besides activation of the Jak/STAT pathway the focus was set on activation of the MAPK/Erk and PI3K/Akt cascades.

A further important issue was a possible spatial regulation of the constitutive activity of CAgp130. As the constitutive activity of the mutant receptor occurs in a ligand-independent manner the question came up whether localization of the receptor at the plasma membrane was of any importance for the quality and/or quantity of its signaling outcome. In this context the signaling potential of the receptor on its biosynthetic route to the plasma membrane as well as its signaling potential upon its endocytosis were set in the focus.

Among the important issues that arise in the context of spatial regulation of constitutive signaling are its consequences for the design of therapeutic approaches. The localization of signaling receptors within the cell dictates whether constitutive activity will be abrogated by agents applied on the cell surface or requires agents that act within the cell.

A further point of debate focused on the feedback inhibitor SOCS3 and its ability to downregulate signaling emanating from CAgp130. In this context the question came up whether SOCS3 could also exert its secondary mode of action by recruiting an E3-ubiquitin ligase. SOCS3 could thereby possibly downregulate its signaling partners especially the mutant receptor.

2. Materials & Methods

Materials and methods are described according to standard protocols used in the Institute of Biochemistry and Molecular Biology, RWTH Aachen University, and modified regarding individual differences in experimental procedures.

2.1. Materials

2.1.1. Chemicals

Applied chemicals were of pro-analysis grade. Aqueous solutions were prepared with ddH_2O.

2.1.2. Cytokines and soluble receptors

IL-6	Recombinant human IL-6 was expressed in *E. coli* using the method of Arcone et al. [153]
sIL-6R	Recombinant human sIL-6R was expressed with a baculovirus system using the method of Weiergräber et al. [154]
OSM	Human OSM was purchased from Peprotech

Table 1 – Cytokines and soluble receptors

2.1.3. Antibodies

Antibody	Directed against	Property	Host	Purchased from	Application
actin (I-19)	C-terminus of actin	polyclonal	goat	Santa Cruz Biotechnology sc-1616	WB
Alexa405-conjugated anti-mouse	mouse IgG	polyclonal	goat	Life Technologies A31553	FACS
Alexa633-conjugated anti-mouse	mouse IgG	polyclonal	goat	Life Technologies A-21052	FACS

APC-conjugated anti-mouse	mouse IgG	polyclonal	goat	Dianova 115-136-146	FACS
B-P4	gp130 domain 4-6	monoclonal	mouse	Kindly provided by Dr. J. Wijdenes	FACS
B-P8	gp130 domain 3	monoclonal	mouse		FACS
B-R3	gp130 domain 2	monoclonal	mouse		FACS
B-T2	gp130 domain 1	monoclonal	mouse		FACS
Erk1/2	C-terminus of Erk1	polyclonal	rabbit	Cell Signaling #9102	WB
GAPDH (6C5)	GAPDH	monoclonal	mouse	Santa Cruz Biotechnology sc-32233	WB
GFP	full length GFP	polyclonal	goat	Rockland 600-103-215	WB
gp130 (M20)	C-terminus of gp130	polyclonal	rabbit	Santa Cruz Biotechnology sc-656	WB, IP
HRP-conjugated anti-goat	goat IgG	polyclonal	rabbit	DAKO 00045307	WB
HRP-conjugated anti-mouse	mouse IgG	polyclonal	goat	DAKO 00058737	WB
HRP-conjugated anti-rabbit	rabbit IgG	polyclonal	goat	DAKO 00052233	WB

lamin A/C (636)	lamin preparation	monoclonal	mouse	Santa Cruz Biotechnology sc-7292	WB
pAkt(S473)	phosphorylated S473 of Akt	polyclonal	rabbit	Cell Signaling #9271	WB
pErk1/2 (T202/Y204)	phosphorylated T202 and Y204 of Erk1	monoclonal	rabbit	Cell Signaling #4370	WB
pp38 (T180/Y182)	phosphorylated T180 and Y182 of p38	polyclonal	rabbit	Cell Signaling #9211	WB
p38	full length p38	polyclonal	rabbit	Cell Signaling #9212	WB
pSAPK/JNK (T183/Y185)	phosphorylated T183 and Y185 of SAPK/JNK	polyclonal	rabbit	Cell Signaling #9251	WB
pSHP2(Y542)	phosphorylated Y542 of SHP2	polyclonal	rabbit	Cell Signaling #3751	WB
pSTAT1(Y701)	phosphorylated Y701 of STAT1	polyclonal	rabbit	Cell Signaling #9177	WB
pSTAT3(Y705)	phosphorylated Y705 of STAT3	polyclonal	rabbit	Cell Signaling #9131	WB
pSTAT3(S727)	phosphorylated S727 of STAT3	polyclonal	rabbit	Cell Signaling #9134	WB
pY (4G10)	pTyr residues	monoclonal	mouse	Upstate 05-321	WB
pY99	pTyr residues	monoclonal	mouse	Santa Cruz Biotechnology sc-7020	WB
SAPK/JNK	full length JNK2	polyclonal	rabbit	Cell Signaling #9252	WB

SHP2	N-terminus of SHP2	polyclonal	rabbit	Cell Signaling #3752	WB
SOCS3 (M20)	C-terminus of SOCS3	polyclonal	goat	Santa Cruz Biotechnology sc-7009	WB
STAT3	N-terminus of STAT3	monoclonal	mouse	BD Transduction Laboratories 610189	WB
STAT1	full length STAT1	polyclonal	rabbit	Cell Signaling #9172	WB

Table 2 – Applied antibodies

2.1.4. Plasmids

Plasmids that were previously constructed in our lab are summarized in Table 3. Depicted plasmids were used to generate further plasmids listed in Table 4 or were directly transfected into cells.

pSVL-WTgp130-CFP/-YFP and pSVL-WTgp130	eukaryotic expression vector, AmpR • contains the cDNA of human gp130 that is fused at its C-terminus with CFP, YFP or is not fluorescently labeled
pSVL-EG(FFFFFF)	contains the cDNA of a chimeric receptor comprised of the extracellular part of the EPOR (E) and the intracellular part of gp130 (G) all six cytoplasmic Tyr-residues of gp130 have been mutated to Phe-residues [64]
pSVL-EG(YFFFFF) pSVL-EG(FYFFFF) pSVL-EG(FFYFFF) pSVL-EG(FFFYFF) pSVL-EG(FFFFYF) pSVL-EG(FFFFFY)	contain the cDNA of chimeric EPOR/gp130 receptors in which all except for one cytoplasmic Tyr-residue at a time have been mutated to Phe-residues

pSVL-gp130-YFYYYY-myc	contains the cDNA of human gp130 with the second most membrane-proximal Tyr-residue (position 759) mutated to a Phe-residue and with a myc-tag at its C-terminus
pcDNA5/FRT/TOspecial	eukaryotic expression vector that originates from pcDNA5/FRT/TO (Life Technologies) and harbors a modified MCS, AmpR • contains a tetracycline-inducible expression cassette and a FRT site • HygR – located downstream of the FRT site and lacking a promotor and the ATG start codon
pcDNA5/FRT/TOspecial-STAT3-mCherry	contains the cDNA of human STAT3 that is fused at its C-terminus with mCherry
pOG44	eukaryotic expression vector, AmpR • contains the cDNA of the Flp recombinase
pCR2.1-TOPO	cloning vector, AmpR, KanR
pMSCV-IRES-GFP	contains an IRES that is followed by a cDNA encoding GFP • AmpR
pcDNA3.1(−)-HA-hu-dynamin-K44A	contains the cDNA of human dynamin that is fused at its N-terminus with an HA-tag and harbors an aa substitution at position 44 rendering dynamin dominant-negative • AmpR
pcDNA3-SOCS3	contains the cDNA of human SOCS3

Table 3 – Available plasmids

Plasmid	Insert
pcDNA5/FRT/TOspecial-WTgp130-CFP/-YFP/-mCherry and pcDNA5/FRT/TOspecial-WTgp130	WTgp130-CFP/-YFP/-mCherry and WTgp130
pcDNA5/FRT/TOspecial-CAgp130-CFP/-YFP/-mCherry and pcDNA5/FRT/TOspecial-CAgp130	CAgp130-CFP/-YFP/-mCherry and CAgp130 CAgp130 ≡ gp130del(Y186-Y190)

pcDNA5/FRT/TOspecial-CAgp130-6F-YFP	CAgp130-6F-YFP all six cytoplasmic Tyr-residues of CAgp130 have been mutated to Phe-residues
pcDNA5/FRT/TOspecial-CAgp130-Y915-YFP pcDNA5/FRT/TOspecial-CAgp130-Y905-YFP pcDNA5/FRT/TOspecial-CAgp130-Y814-YFP pcDNA5/FRT/TOspecial-CAgp130-Y767-YFP pcDNA5/FRT/TOspecial-CAgp130-Y759-YFP pcDNA5/FRT/TOspecial-CAgp130-Y683-YFP	CAgp130-Y915-YFP CAgp130-Y905-YFP CAgp130-Y814-YFP CAgp130-Y767-YFP CAgp130-Y759-YFP CAgp130-Y683-YFP all cytoplasmic Tyr-residues of CAgp130 except for the depicted one have been mutated to Phe-residues
pcDNA5/FRT/TOspecial-WTgp130-mCherry-V5-KKYN/-FLKKTN/-TLRKRIR/-HRRRSRSCREDQKPV	WTgp130-mCherry-V5-KKYN/-FLKKTN/-TLRKRIR/-CD74 WTgp130-mCherry is C-terminally tagged with the V5-tag and different ER-retention sequences: KKYN and FLKKTN are Lys-based ER-retention sequences, TLRKRIR and the ER-retention sequence HRRRSRSCREDQ KPV found in CD74 are Arg-based sequences
pcDNA5/FRT/TOspecial-CAgp130-mCherry-V5-KKYN/-CD74	CAgp130-mCherry-V5-KKYN/-CD74
pcDNA3.1(+)-IRES-GFP	IRES-GFP
pcDNA3.1(+)-HA-hu-dynamin-K44A-IRES-GFP	HA-hu-dynamin-K44A-IRES-GFP
pcDNA5/FRT/TOspecial-CAgp130-Y759F-YFP/-mCherry	CAgp130-Y759F-YFP/-mCherry CAgp130-YFP/-mCherry with an aa substitution at position 759 from a Tyr-residue to a Phe-residue

pcDNA5/FRT/TOspecial-CAgp130-K648R-mCherry	CAgp130-K648R-mCherry CAgp130-mCherry with an aa substitution at position 648 from a Lys-residue to an Arg-residue
pcDNA5/FRT/TOspecial-CAgp130-K648R-mCherry	CAgp130-K648R-mCherry CAgp130-mCherry with an aa substitution at position 648 from a Lys-residue to an Arg-residue

Table 4 – Generated plasmids

2.1.5. Primers and oligonucleotides

Primers and oligonucleotides were purchased from MWG-Biotech and are listed and grouped in Table 5 according to their application.

Mutant/Fusion protein	Forward 5´→3´	Reverse 5´→3´
CAgp130 (section 2.2.10.1.)	AGC CTC CGG ACT CTA GCG ACT GTT GAT TTT GTT AAC ATT GAA GTC TGG G	TTC AAT GTT AAC AAA ATC AAC AGT GCA TGA GGT GGG CCC TCT TAA ATA GGT GCG
WTgp130-mCherry (section 2.2.10.2.)	CCG GTC GCG ATA TCG GTG AGC AAG GGC GAG GAG	AGA GTC GCG GAT CCT TTA CTT GTA CAG CTC GTC C
WTgp130-mCherry-V5-KKYN (section 2.2.10.6.)	GTA CTG AGG GAC AAG TAG CCG GTC GGT AAG CCT ATC CCT AAC CCT CTC CTC GGT CTC GAT TCT ACG GC	GCA TGG ATC CTT AAT TGT ACT TCT TAG CGG CCG CCT CGA GGA CCG GTG GCT TGT ACA GCT CGT CC GGC CGC CGT AGA ATC GAG ACC GAG GAG AGG GTT AGG GAT AGG CTT ACC GA
WTgp130-mCherry-V5-FLKKTN (section 2.2.10.6.)	GGC CGC TTT CCT GAA GAA GAC CAA CTA AG	GAT CCT TAG TTG GTC TTC TTC AGG AAA GC
WTgp130-mCherry-V5-TLRKRIR (section 2.2.10.6.)	GGC CGC TAC CCT GCG GAA GCG AAT CCG GTA AG	GAT CCT TAC CGG ATT CGC TTC CGC AGG GTA GC

WTgp130-mCherry-V5-CD74 (section 2.2.10.6.)	GGC CGC TCA CCG GCG GCG GAG CCG GAG CTG CCG GGA GGA CCA GAA GCC CGT GTA AG	GAT CCT TAC ACG GGC TTC TGG TCC TCC CGG CAG CTC CGG CTC CGC CGC CGG TGA GC
HA-hu-dynamin-K44A-IRES-GFP (section 2.2.10.7.)	CGA GCA AGC ATA TCT TTG CC	GCA TCG AAT TCT TAG AGG TCG AAG GGG GGC
CAgp130-K648R-mCherry (section 2.2.10.9.)	GCG AGA CCT AAT TAG AAA ACA CAT CTG GCC	GGC CAG ATG TGT TTT CTA ATT AGG TCT CGC

Table 5 – Applied primers and oligonucleotides

2.1.6. Bacterial strains

The bacterial strain *E. coli* JM83 was used for conventional cloning and plasmid preparation. Site-directed mutagenesis was performed with the bacterial strain DH5α.

2.1.7. Eukaryotic cells

Cell line	Properties
HEK293	Adherent growing cell line derived from human embryonic kidney cells
HEK293 stably transfected with IL-6Rα	Kindly provided by Dr. Anna Dittrich
HepG2	Adherent growing cell line derived from a HCC
Flp-In T-REx 293	HEK293 cells with a single integrated FRT site at an active genomic locus allowing stable integration and expression of a transgene Stable expression of the Tet-repressor

Table 6 – Cell lines

Flp-In T-REx 293 cells were stably transfected with the non-tagged, YFP- and mCherry-tagged variant of WTgp130 and CAgp130. Furthermore, cell lines were generated for stable expression of CAgp130-mCherry-V5-CD74 and CAgp130-mCherry-V5-KKYN as well as CAgp130-Y759F-mCherry. Cells stably expressing STAT3-Y705F-YFP were kindly provided by Dr. Anne Mohr.

2.2. Molecular biology methods

2.2.1. Culturing and storage of prokaryotic cells

Prokaryotic cells were cultured in LB medium in a shaking incubator at 180 rpm or on LB agar at 37°C. Both – LB medium and LB agar – were supplemented with 100 µg/ml Amp (ampicillin) to exclusively allow the growth of transformed bacteria. Long-term storage of bacteria was performed in LB medium with 20% glycerol at -80°C.

LB medium

25 g LB medium powder (Roth)

ad 1 l H_2O

LB agar

LB medium with 2% agar (bacteriological grade) (MP Biomedicals)

2.2.2. Isolation of plasmid-DNA

Small amounts of plasmid-DNA were isolated from 3 ml bacterial cultures using the QIAprep Spin Miniprep Kit (Qiagen). DNA isolation was performed according to the manufacturer´s instructions and DNA was eluted in 30 µl H_2O suitable for chromatography (Merck).

Plasmid-DNA on preparative scale was isolated from 250 ml bacterial cultures using the HiSpeed Plasmid Maxi Kit (Qiagen) according to the manufacturer´s instructions. In the final step DNA was eluted with 1 ml chromatography H_2O.

Isolated plasmid-DNA was stored at -20°C.

2.2.3. Restriction of plasmid-DNA

Restriction enzymes were purchased from NEB (New England Biolabs) and Roche.

Restriction of plasmid-DNA was performed under the conditions specified by the manufacturer for the respective restriction enzyme. For simultaneous restriction with two different restriction enzymes the required reaction conditions had to be identical. Otherwise restrictions were performed sequentially with an intermediate DNA precipitation using LiCl (section 2.2.4.).

Restriction of plasmid-DNA for analytical purposes was performed with 0.1-0.5 µg DNA in a reaction volume of 10-20 µl. Preparative restrictions were performed with 1 µg plasmid-DNA in order to isolate the vector and 2 µg plasmid-DNA to isolate the insert. The reaction volume varied from 50-100 µl depending on the concentration of the required DNA solutions. The volume of applied restriction enzymes never exceeded 10% of the total reaction volume.

The volume of restriction enzymes required for each reaction was calculated using the following formula:

$$\text{restriction enzyme [µl]} = \frac{\text{lambda phage genome [bp]} * \text{restriction sites within the plasmid} * \text{amount of plasmid DNA to be restricted [µg]}}{\text{plasmid DNA to be restricted [bp]} * \text{restriction sites within the lambda phage genome} * \text{activity of the restriction enzyme [U/µl]}}$$

2.2.4. LiCl precipitation of plasmid-DNA

Precipitation of plasmid-DNA with LiCl was performed as an intermediate step between treatment with restriction enzymes that required deviating reaction conditions. Upon completion of the first restriction the reaction mixture was incubated for 90 min with 150 µl H_2O, 1 µl glycogen, 5 µl 8 M LiCl solution and 200 µl isopropanol at -20°C. Precipitated plasmid-DNA was pelleted by centrifugation at 13200 rpm for 30 min at 4°C. Upon removal of the supernatant the pellet was washed with 300 µl 70% ethanol and was centrifugated once more at 13200 rpm for 5 min at 4°C. The pellet was allowed to dry at rt before starting the next restriction.

2.2.5. Agarose gel elektrophoresis

Upon restriction plasmid-DNA was mixed with 10fold DNA loading buffer. Samples were loaded on a 1% agarose gel that was prepared with TAE buffer supplemented with 0.1 µg/ml EtBr (ethidium bromide). Gel electrophoretic separation of DNA fragments was performed in TAE buffer with 0.1 µg/ml EtBr for about 40 min at 100 V. The molecular weight of resulting DNA fragments was estimated using the 1 kb DNA Ladder (Life Technologies).

10fold DNA loading buffer

25% Ficoll 400.000

0.4% xylene cyanol blue

0.4% bromophenol blue

TAE buffer

40 mM tris

20 mM acetic acid

1 mM EDTA pH 8.0

2.2.6. Extraction of DNA fragments from agarose gel

Extraction of DNA fragments from agarose gels was performed using the QIAquick Gel Extraction Kit (Qiagen). In the final step DNA was eluted with 30 µl chromatography H_2O.

2.2.7. Measurement of DNA concentration

Concentration and purity of DNA samples were measured using the NanoDrop ND-1000 Spectrophotometer (ThermoScientific). DNA concentration was assessed using the absorbance at 260 nm. The ratio of sample absorbance at 260 and 280 nm was used to assess DNA purity with a ratio of 1.8 indicating a pure DNA preparation.

2.2.8. Ligation

Ligation of isolated DNA fragments was performed using the enzyme T4 DNA Ligase (NEB). In general 35 ng isolated plasmid-DNA were ligated with a certain amount of insert DNA that was calculated according to the following formula:

$$\text{amount of insert [ng]} = \frac{5 * \text{amount of plasmid [ng]} * \text{insert [bp]}}{\text{plasmid [bp]}}$$

Ligations were performed for 60 min at rt in a reaction volume of 20 µl.

2.2.9. Transformation of bacteria with plasmid-DNA

For transformation 10 µl of the ligation sample were mixed with 50 µl competent bacteria. The mixture was incubated for 20 min on ice and for further 90 s at 42°C. Transformed bacteria were plated on Amp containing LB agar and plates were incubated o/n at 37°C.

2.2.10. Cloning procedures

2.2.10.1. CAgp130-YFP

Plasmid pSVL-WTgp130-YFP (previously generated in our lab) was digested with XhoI and BamHI and the obtained fragment was cloned into pcDNA5/FRT/TOspecial resulting in the plasmid pcDNA5/FRT/TOspecial-WTgp130-YFP.

For generation of CAgp130 harboring the deletion Y186-Y190 within domain D2 of gp130 fusion PCR was performed using pcDNA5/FRT/TOspecial-WTgp130-YFP as a template. In the first step two independent PCRs were performed on the sequences flanking the sequence to be deleted. Two primer-pairs were designed – one for the left and one for the right side of the deletion with complementary overhangs at the fusion site (in bold): senseP1 – 5´-AGC CTC CGG ACT CTA GCG-3´, antisenseP1 – 5´-**TTC AAT GTT AAC AAA** ATC AAC AGT GCA TGA GGT GGG-3´, senseP2 – 5´-**ACT GTT GAT** TTT GTT AAC ATT GAA GTC TGG G-3´, antisenseP2 – 5´-CCC TCT TAA ATA GGT GCG-3´. Through substitution of a single base (underlined) resulting in a silent mutation a HpaI restriction site was generated to easily distinguish CAgp130 from WTgp130 constructs. Next, the fusion PCR was performed using primers senseP1 and antisenseP2. The PCR product was first subcloned into pCR2.1-TOPO. The resulting plasmid pCR2.1-TOPO-CAgp130 was digested with XhoI and Asp718 and cloned into pcDNA5/FRT/TOspecial-WTgp130-YFP generating the plasmid pcDNA5/FRT/TOspecial-CAgp130-YFP.

A generalized PCR scheme and the applied PCR programs are summarized in the following scheme:

Generalized PCR scheme
100 ng template
50 pmol sense and antisense primer
25 nmol dNTPs
5 µl 10fold Taq DNA polymerase buffer
0.5 µl Taq DNA polymerase
ad 50 µl H_2O

PCR1	PCR2	Fusion PCR
94°C 120 s	94°C 120 s	94°C 120 s
55°C 90 s ←	50°C 90 s ←	50°C 90 s ←
72°C 90 s (30x)	72°C 90 s (30x)	72°C 120 s (30x)
94°C 60 s →	94°C 60 s →	94°C 60 s →
72°C 240 s	72°C 240 s	72°C 240 s

2.2.10.2. mCherry-tagged variants of WTgp130 and CAgp130

For generation of mCherry-tagged receptor constructs mCherry-cDNA was amplified by PCR using the plasmid pcDNA5/FRT/TOspecial-STAT3-mCherry (previously constructed in our lab) as a template: senseP – 5´-CCG GTC GCG ATA TCG GTG AGC AAG GGC GAG GAG-3´, antisenseP – 5´-AGA GTC GCG GAT CCT TTA CTT GTA CAG CTC GTC C-3´. The PCR product was subcloned into pCR2.1-TOPO and the resulting plasmid was digested with EcoRV and

BamHI. The generated fragment was cloned into pcDNA5/FRT/TOspecial-WTgp130-YFP resulting in the plasmid pcDNA5/FRT/TOspecial-WTgp130-mCherry. For generation of mCherry-tagged CAgp130 the fragment that resulted from XhoI and Asp718 digestion of pCR2.1-TOPO-CAgp130 (section 2.2.10.1.) was cloned into pcDNA5/FRT/TOspecial-WTgp130-mCherry generating the plasmid pcDNA5/FRT/TOspecial-CAgp130-mCherry.

2.2.10.3. CFP-tagged variants of WTgp130 and CAgp130

Plasmid pSVL-WTgp130-CFP (previously constructed in our lab) was digested with XhoI and BamHI. The generated fragment was cloned into pcDNA5/FRT/TOspecial resulting in the plasmid pcDNA5/FRT/TOspecial-WTgp130-CFP. For generation of CFP-tagged CAgp130 the previously constructed pCR2.1-TOPO-CAgp130 vector (section 2.2.10.1.) was digested with XhoI and Asp718. The resulting fragment was cloned into pcDNA5/FRT/TOspecial-WTgp130-CFP generating the plasmid pcDNA5/FRT/TOspecial-CAgp130-CFP.

2.2.10.4. Non-tagged variants of WTgp130 and CAgp130

Plasmid pSVL-WTgp130 (previously generated in our lab) was digested with BstEII and BamHI and the resulting fragment was cloned into pcDNA5/FRT/TOspecial-WTgp130-YFP and pcDNA5/FRT/TOspecial-CAgp130-YFP generating plasmids pcDNA5/FRT/TOspecial-WTgp130 and pcDNA5/FRT/TOspecial-CAgp130.

2.2.10.5. Add-back mutants

For generation of add-back mutants of CAgp130 previously constructed plasmids were used [64]. New constructs were generated by three-fragment-ligation. The backbone was generated by XhoI and EcoRV digestion of pcDNA5/FRT/TOspecial-WTgp130-YFP. The extracellular part of CAgp130 was isolated upon XhoI and EcoRI digestion of pcDNA5/FRT/TOspecial-CAgp130-YFP. The intracellular part of gp130 harboring mutated Tyr-residues was generated by EcoRI and EcoRV digestion of the preexisting constructs. Following constructs were generated: pcDNA5/FRT/TOspecial-CAgp130-6F-YFP, -CAgp130-Y915-YFP, -CAgp130-Y905-YFP, -CAgp130-Y814-YFP, -CAgp130-Y767-YFP, -CAgp130-Y759-YFP and -CAgp130-Y683-YFP.

2.2.10.6. ER-retention mutants

Cloning of the ER-retention mutants was performed by generation of an intermediate construct. In a first step an oligonucleotide was synthesized that encoded the Lys-based retention-signal KKYN (underlined) and which was able to anneal to the sequence of mCherry within pcDNA5/FRT/TOspecial-WTgp130-mCherry (in bold): 5´-GCA TGG ATC CTT AAT TGT ACT TCT TAG CGG CCG CCT CGA **GGA CCG GTG GCT TGT ACA GCT CGT CC**-3´. This oligonucleotide together with a sense primer annealing downstream of WTgp130-mCherry within the vector was used in a PCR reaction to modify the C-terminus of gp130. The amplified fragment was digested with EcoRV and BamHI. The intermediate constructs (in the context of WTgp130 and CAgp130) were generated by three-fragment-ligation of the digested PCR product and the fragments resulting from digestion of pcDNA5/FRT/TOspecial-WTgp130 and pcDNA5/FRT/TOspecial-CAgp130 with BamHI and KpnI and digestion of pcDNA5/FRT/TOspecial-WTgp130-YFP and pcDNA5/FRT/TOspecial-CAgp130-YFP with KpnI and EcoRV. The resulting intermediate plasmids were digested with AgeI and NotI and the vectors were ligated with a ds oligonucleotide coding for the V5 tag: senseV5oligo – 5´-CCG GTC GGT AAG CCT ATC CCT AAC CCT CTC CTC GGT CTC GAT TCT ACG GC-3´, antisenseV5oligo – 5´-GGC CGC CGT AGA ATC GAG ACC GAG GAG AGG GTT AGG GAT AGG CTT ACC GA-3´. Ligation resulted in generation of pcDNA5/FRT/TOspecial-WTgp130-mCherry-V5-KKYN and pcDNA5/FRT/TOspecial-CAgp130-mCherry-V5-KKYN. These plasmids were digested with BamHI and NotI and the resulting vectors were ligated with ds oligonucleotides encoding further retention sequences: senseFLKKTNoligo – 5´-GGC CGC TTT CCT GAA GAA GAC CAA CTA AG-3´, antisenseFLKKTNoligo – 5´-GAT CCT TAG TTG GTC TTC TTC AGG AAA GC-3´, senseTLRKRIRoligo – 5´-GGC CGC TAC CCT GCG GAA GCG AAT CCG GTA AG-3´, antisenseTLRKRIRoligo – 5´-GAT CCT TAC CGG ATT CGC TTC CGC AGG GTA GC-3´, senseCD74oligo – 5´-GGC CGC TCA CCG GCG GCG GAG CCG GAG CTG CCG GGA GGA CCA GAA GCC CGT GTA AG-3´, antisenseCD74oligo – 5´-GAT CCT TAC ACG GGC TTC TGG TCC TCC CGG CAG CTC CGG CTC CGC CGC CGG TGA GC-3´.

2.2.10.7. K44A dynamin

For generation of the K44A dynamin construct the plasmid pMSCV-IRES-GFP (kindly provided by Dr. N. Chatain) was digested with EcoRI and SalI and the generated fragment was cloned into EcoRI and XhoI digested pcDNA3.1(+). SalI and XhoI generate complementary overhangs

and upon ligation both restriction sites are destroyed resulting in the plasmid pcDNA3.1(+)-IRES-GFP. Plasmid pcDNA3.1(+)-IRES-GFP was digested with BamHI and EcoRI providing the backbone for the next cloning step. The construct pcDNA3.1(−)-HA-hu-dynamin-K44A (kindly provided by Dr. S. Wüller) was digested with BamHI and NheI to isolate the N-terminal part of HA-hu-dynamin-K44A. To generate an EcoRI site and amplify the C-terminal part of HA-hu-dynamin-K44A PCR was performed on pcDNA3.1(−)-HA-hu-dynamin-K44A: senseP – 5´-CGA GCA AGC ATA TCT TTG CC-3´, antisenseP – 5´-GCA TCG AAT TCT TAG AGG TCG AAG GGG GGC-3´. The plasmid pcDNA3.1(+)-HA-hu-dynamin-K44A-IRES-GFP was generated by three-fragment-ligation.

2.2.10.8. CAgp130-Y759F

Plasmid pSVL-gp130-YFYYYY-myc (previously constructed in our lab) encoding gp130 with the Tyr-residue at position 759 mutated to a Phe-residue was digested with KpnI and EcoRV. The resulting fragment was ligated with the vector backbone resulting from digestion of pcDNA5/FRT/TOspecial-CAgp130 with KpnI and BamHI and the fragment generated by restriction of pcDNA5/FRT/TOspecial-WTgp130-YFP with EcoRV and BamHI. This three-fragment-ligation resulted in generation of the plasmid pcDNA5/FRT/TOspecial-CAgp130-Y759F-YFP.

For construction of the mCherry-tagged variant of CAgp130-Y759F-mCherry the approach was identical with the exception of the fragment encoding the fluorescent tag that was generated by digestion of pcDNA5/FRT/TOspecial-WTgp130-mCherry with EcoRV and BamHI.

2.2.10.9. CAgp130-K648R

In order to mutate the Lys-residue at position 648 to an Arg-residue within CAgp130 a PCR was performed using the PfuUltra DNA polymerase (Stratagene) and the following primers: senseP – 5´-GCG AGA CCT AAT TAG AAA ACA CAT CTG GCC-3´, antisenseP – 5´-GGC CAG ATG TGT TTT CTA ATT AGG TCT CGC-3´. Primers and the DNA template used, namely pcDNA5/FRT/TOspecial-WTgp130, differ in the underlined codon and this deviation finally leads to the requested mutation. The PCR product was digested with KpnI and NsiI and ligated into pcDNA5/FRT/TOspecial-WTgp130 resulting in the plasmid pcDNA5/FRT/TOspecial-WTgp130-K648R. To generate the mCherry-tagged version of

CAgp130-K648 a three-fragment-ligation was performed. The vector backbone was generated by digestion of pcDNA5/FRT/TOspecial-CAgp130 with KpnI and BamHI. The fragments resulted upon restriction of pcDNA5/FRT/TOspecial-WTgp130-K648R with KpnI and NsiI and digestion of pcDNA5/FRT/TOspecial-CAgp130-mCherry with NsiI and BamHI.

All constructs were verified by sequencing.

2.3. Cellular biology methods

2.3.1. Culturing and storage of eukaryotic cells

Eukaryotic cells were cultured in a humidified atmosphere with 5% CO_2 at 37°C. Culture media used were supplemented with 10% heat inactivated FCS (fetal calf serum) (Lonza), 60 mg/l penicillin and 100 mg/l streptomycin (Sigma) and are listed in Table 7.

Cell line	Culture media	Antibiotics
HEK293	DMEM with Glutamax	No antibiotics added
HEK293 stably transfected with IL-6Rα	DMEM with Glutamax	2 µg/ml puromycin
HepG2	DMEM/F12 with Glutamax	No antibiotics added
Flp-In T-REx 293	DMEM with Glutamax	10 µg/ml blasticidin 200 µg/ml zeocin
Flp-In T-REx 293 upon stable transfection	DMEM with Glutamax	10 µg/ml blasticidin 100 µg/ml hygromycin B

Table 7 – Cell lines, required culture media and antibiotics (additional to penicillin and streptomycin). Culture media were purchased from Life Technologies and antibiotics from Invivogen.

In general cells were cultured in 10 cm dishes. Depending on the experimental procedure cells that were 90-100% confluent were passaged with a dilution of 1:10 to further keep them in culture or seeded at a specific density to perform transfection or induce protein expression. To this end, cells were first washed with PBS (5 ml on a 10 cm dish) and detached from the dish by incubation with 1 ml trypsin(0.05%)/EDTA(0.02%) solution (Life Technologies) at 37°C for 1-5 min depending on the respective cell line. Detached cells were

resuspended in fresh medium, counted using a CasyCounter (Innovatis) when necessary and distributed on further plates.

For long-term storage 90-100% confluent cells were washed and detached from the plate as previously described. Upon resuspension in medium, cells were centrifugated at 1200 rpm for 5 min at 4°C. The cell pellet was resuspended in 1 ml ice-cold medium supplemented with 20% FCS and 10% DMSO. The cell suspension was transferred into cryotubes and the cryotubes were placed in an insulated box containing isopropanol and allowing a stepwise temperature reduction. Long-term storage of eukaryotic cells was performed at -150°C.

To thaw cells, frozen cells were warmed in a water bath at 37°C and transferred in a tube containing 9 ml medium. Upon centrifugation at 1200 rpm for 5 min at 4°C cells were resuspended in 10 ml medium and transferred on a 10 cm dish.

PBS

150 mM NaCl

2.5 mM KCl

8 mM Na_2HPO_4

1.5 mM KH_2PO_4

adjusted to pH 7.4

Inhibitors used in cell culture are summarized below:

Inhibitor	Inhibition of	Purchased from	Applied concentration
Brefeldin A	Trafficking: Inhibition of the retrograde transport from the Golgi to the ER	Sigma	100 ng/ml
Dynasore	Dynamin-dependent endocytosis	Merck	25-75 µM
Cycloheximide	Protein biosynthesis in eukaryotes	Sigma	10 µg/ml
MG132	Proteasomal degradation	Enzo	10 µM
Lactacystin		Enzo	5 µM
Chloroquine	Lysosomal degradation	Sigma	25 µM

NH_4Cl	Merck	10 mM

Table 8 – Applied inhibitors

2.3.2. Transient transfection

For transient transfection HEK293 stably transfected with IL-6Rα or not were seeded at a density of $0.4*10^6$ cells/ml 12 and 24 h prior to transfection respectively. Transfection was performed using the TransIT-LT1 transfection reagent (Mirus). In the first step the transfection reagent (applied in a ratio of 1:3 to the transfected DNA) was added dropwise to 1.4 ml of prewarmed and serum-free transfection medium Opti-MEM (Life Technologies) and the mixture was incubated for 15 min at rt. Next the DNA was added dropwise to the mixture and mixed gently with the pipette tip. Upon further 10 min of incubation at rt the transfection mixture was added dropwise to the cells to be transfected. Cells were harvested 48 h upon transfection.

2.3.3. Stable transfection of Flp-In T-REx 293 cells

The Flp-In T-REx system (Life Technologies) has been designed for generation of mammalian cells that express a GOI (gene of interest) in a stable and inducible manner.

Among the key components of the Flp-In T-REx system is the Flp-In T-REx 293 host cell line that contains two stably, independently integrated plasmids: the plasmid pFRT/lacZeo stably expresses the lacZ-Zeocin fusion gene and further introduces a single FRT site into the genome, the pcDNA6/TR plasmid harbors a blasticidin resistance and stably expresses the *tet* repressor gene. Further key components of the Flp-In T-REx system are two plasmids: plasmid pOG44 expresses the Flp recombinase and plasmid pcDNA5/FRT/TO (in this work designated as special because of alterations in the MCS (multiple cloning site)) encodes the GOI that needs to be stably expressed as well as a single FRT (Flp recombinase target) site for genomic integration.

Upon cotransfection of both plasmids – pOG44 and pcDNA5/FRT/TO-GOI – in the Flp-In T-REx 293 host cell line the Flp recombinase is transiently expressed and catalyzes a homologous recombination event between the FRT sites of pcDNA5/FRT/TO and the Flp-In T-REx 293 host cell line. Upon recombination the non-functional HygR (hygromycin B resistance) gene originally located on pcDNA5/FRT/TO aquires the SV40 promotor and ATG start codon from the lacZ-Zeocin fusion gene and becomes functional. As a result stable

transfectants remain sensitive to blasticidin and the resistance to zeocin is replaced by a hygromycin resistance.

Resistance to blasticidin is crucial as it ensures expression of the tet repressor. The tet repressor itself is required to block expression of the GOI by its binding to the operator sequences within the tet promotor. In the absence of tetracycline tet repressor molecules form homodimers that bind with high affinity to the tet operator sequences repressing expression of the GOI. Binding of tetracycline to the tet repressor homodimers causes conformational changes and the release of repressor homodimers from the operator sequences. As a result transcription of the GOI is induced.

For stable transfection Flp-In T-REx 293 cells were seeded in medium without blasticidin and zeocin at a density of $0.4*10^6$ cells/ml 24 h before transfection. Cells were cotransfected with the vectors pOG44 and pcDNA5/FRT/TOspecial harboring the GOI in a ratio of 9:1. The transfection procedure was identical to the transient transfection previously described (section 2.3.2.) and stable cells were generated according to the manufacturer´s instructions as documented in the Flp-In T-REx Core Kit manual. Single clone selection was performed with 10 µg/ml blasticidin and 300 µg/ml hygromycin B. Protein expression was induced with dox (doxycycline hyclate) instead of tetracycline as it has a longer half-life. Dox was purchased from Sigma.

2.4. Protein-chemical and immunological methods

2.4.1. Preparation of cell lysates

Upon transfection or induction and stimulation (when necessary) cells were placed on ice and washed with ice-cold PBS. Cells were scrapped off the dish in 500 µl ice-cold PBS and were transferred in Eppendorf tubes. Upon centrifugation for 5 min at 4000 rpm and 4°C the cell pellet was resuspended in RIPA lysis buffer and incubated for 30 min on ice. The lysis buffer was supplemented shortly before the lysis procedure with a series of phosphatase- and protease-inhibitors listed further below. Cellular debris was removed by centrifugation for 10 min at 13200 rpm and 4°C. The lysates were transferred in Eppendorf tubes and stored at -20°C.

RIPA lysis buffer

50 mM	tris/HCl pH 7.4
150 mM	NaCl
1 mM	EDTA
0.5%	nonidet P40
1 mM	NaF
15%	glycerol

Phosphatase- and protease-inhibitors

1 mM	Na_3VO_4
0.25 mM	PMSF
0.5 mM	EDTA
5 µg/ml	aprotinin
1 µg/ml	leupeptin

2.4.2. Determination of protein concentration

Protein concentration of lysates was measured using the Bio-Rad protein assay (Bio-Rad). The dye Coomassie blue within this assay binds to primarily basic and aromatic aa residues, especially arginine. Upon binding absorbance maximum of the dye is shifted from 465 nm to 595 nm.

In order to determine the protein concentration dye reagent was diluted in a ratio of 1:5 with H_2O and 1 ml of the diluted reagent was mixed with 3 µl of the lysate in an Eppendorf tube. The mixture was incubated for at least 5 min at rt and the absorbance was measured at 595 nm. In order to convert absorbance to protein concentration a standard curve was prepared with BSA (bovine serum albumin) to determine the required factor.

2.4.3. SDS PAA gel electrophoresis

The electrophoretic separation of proteins was performed using the method of discontinuous SDS polyacrylamide gel electrophoresis (SDS PAA gel electrophoresis or SDS PAGE). This type of electrophoresis is designated as discontinuous because of an ion step gradient that is formed and causes all proteins to focus on a single sharp band. Fractionation of denatured proteins is performed according to their approximate molecular size.

Protein samples to be analyzed were supplemented with 4fold Laemmli buffer and boiled for 5 min at 95°C. Endo H (endoglycosidase H) digestion (NEB) was performed on denatured protein samples for 1 h at 37°C according to the manufacturer´s instructions. Proteins were separated in gels composed of a 3% stacking gel and a 7.5% or 10% resolving gel. Gel electrophoresis was performed at rt with an applied current of 35 mA. To estimate the molecular weight of separated proteins the PageRuler Prestained Protein Ladder (ThermoScientific) was loaded on every gel.

4fold Laemmli buffer

40%	glycerol
20%	β-mercaptoethanol
8%	SDS
250 mM	tris/HCl pH 6.8
0.02%	bromophenol blue

Acrylamide solution (30/0.8) (AppliChem)

30%	acrylamide
0.8%	bisacrylamide

Stacking gel (3%)

4 ml	H_2O
635 µl	acrylamide solution (30/0.8)
313 µl	2 M tris/HCl pH 6.8
25 µl	20% SDS
5 µl	TEMED
40 µl	20% APS

Resolving gel (7.5%/10%)

7.1/5.9 ml	H_2O
3.6/4.8 ml	acrylamide solution (30/0.8)
3.8 ml	2 M tris/HCl pH 6.8
75 µl	20% SDS

15 µl	TEMED
75 µl	20% APS

SDS running buffer

25 mM	tris
192 mM	glycine
0.1%	SDS

2.4.4. Western blot-analysis and immunodetection

Upon electrophoretic separation proteins were transferred on a PVDF membrane (PALL) using the semidry method for western blot. At the beginning three filter papers (Whatman) were cut in the size of the gel. One filter paper was drenched in anode buffer I, the second in anode buffer II and the third in cathode buffer. The PVDF membrane that was also cut in the size of the gel was first activated for 15 s in MeOH and subsequently drenched in anode buffer II. The gel itself was equilibrated in cathode buffer. These components were stacked in the following order – from bottom to top: filter paper in anode buffer I, filter paper in anode buffer II, PVDF membrane, gel and filter paper in cathode buffer – and the transfer of proteins was performed at rt with a current of 0.8 mA/cm^2 for 60 min.

Upon transfer the PVDF membrane was incubated for 30 min in a 10% BSA solution in TBS-N buffer to block unoccupied sites of the membrane. Immunodetection was performed using a 1:1000 dilution of the primary Ab and a 1:2000 dilution of a HRP(horseradish peroxidase)-conjugated secondary Ab. Both antibodies were diluted in TBS-N buffer. Incubation with the primary Ab solution was performed o/n at 4°C and incubation with the secondary Ab solution was performed for at least 1 h at rt. In the final step of immunodetection the membrane was incubated for 1 min in ECL (enhanced chemiluminescence) solution and signals were detected with a LAS Mini 4000 (Fujifilm).

Detection of phosphorylated proteins was performed first. In order to detect further proteins on a single membrane the membrane was incubated for 25 min in stripping buffer at 70°C. In the next step the membrane was blocked and incubated with the respective Ab solutions.

Anode buffer I

0.3 M tris

20% MeOH

adjusted to pH 10.4

Anode buffer II

0.025 M tris

20% MeOH

adjusted to pH 10.4

Cathode buffer

0.04 M ε-aminohexanoic acid

20% MeOH

adjusted to pH 9.4

TBS-N buffer

20 M tris/HCl pH 7.6

140 mM NaCl

0.1% nonidet P40

Stripping buffer

62.5 mM tris/HCl pH 7.6

2% SDS

100 mM β-mercaptoethanol

2.4.5. Immunoprecipitation

Cell lysates were incubated o/n with 1 µg M20 gp130 Ab (Santa Cruz Biotechnology). Subsequently the lysate-Ab-mixture was incubated o/n with 10 µl Dynabeads Protein G (Life Technologies). Immobilized immune complexes were washed three times with RIPA lysis buffer, boiled for 5 min in 10 µl 4fold Laemmli buffer and subjected to SDS PAGE and immunoblotting.

2.4.6. Flow cytometry

Cells were washed with PBS, detached from the plate for 10 min with PBS/EDTA (10 mM), collected and washed with FACS buffer (PBS containing 5% FCS and 0.1% NaN_3). Detection of surface receptor was performed with monoclonal mouse gp130 antibodies – B-P8, B-P4, B-T2 and B-R3 – and followed by goat-anti-mouse APC(allophycocyanin)-(Dianova)/Alexa633-/Alexa405-(Life Technologies) conjugated secondary antibodies as stated in each case. Antibodies were applied in a 1:100 dilution in FACS buffer. Cells were analyzed with a FACSCanto II or a LSR Fortessa (BD Biosciences). All steps were performed on ice and with ice-cold solutions.

2.5. Confocal microscopy

For confocal microscopy 10^5 cells were seeded on 12 mm cover slips in a 12 well plate. Before seeding cover slips were coated for 30 min at rt with poly-L-lysine to improve cell adherence. Induction of protein expression (if needed) was performed 24 h upon seeding. Induced cells were washed twice with PBS and fixed with 3.7% PFA for 20 min. Fixed cells were washed twice with PBS^{++} (PBS with 0.1 mM $CaCl_2$ and 1 mM $MgCl_2$) and were incubated for 5 min with PBS^{++} containing 50 mM NH_4Cl to reduce background fluorescence. Cover slips were dipped in water and cells were mounted with Immu-mount (ThermoScientific).

Settings used for confocal images in Figure 1 and Figure 31 are summarized within the following table:

	Figure 1	**Figure 31**	
Fluorescent tag	**mCherry**	**GFP**	**mCherry**
Laser	561 nm	488 nm	561 nm
Laser intensity	1.0%	0.2%	0.4%
Detection filter	578-696	493-578	578-696
MBS	458/561	488/561/633	458/561
Resolution	1024*1024	3072*3072 (1188*1188)	
Depth	12-bit	8-bit	
Zoom	0.6	2.2	
Acquisition speed	Line 2	Line 2 (Line 4)	

Master gain	800	624	717
Digital gain	3.00	7.80	9.16
Objective	LD C-Apochromat	Plan-Apochromat	
	40x/1.1 W Korr M27	20x/0.8 M27	

Table 9 – Technical data to confocal images shown in Figure 1 (section 3.1.1.) and Figure 31 (section 3.5.). Data in brackets refer to the more detailed images in the lower half of Figure 31 and deviate from the overview images in the upper half.

3. Results

3.1. Deviations between WTgp130 and CAgp130 along the processing-trafficking-signaling axis

The initial goal of this work was to elucidate the signaling properties of the constitutively active gp130 mutant CAgp130. Upon construction of the receptor mutant, WTgp130 as well as CAgp130 were fused at their C-termini to the fluorescent proteins YFP, CFP or mCherry to facilitate application of confocal microscopy and flow cytometry. To analyze expression and signaling HEK293 cells were generated that allowed stable and inducible expression of the differentially tagged constructs. Utilizing the Flp-In T-Rex system and selecting single clones, cell lines were generated for expression of YFP-tagged WTgp130 and CAgp130 – T-REx-293-WTgp130-YFP and T-REx-293-CAgp130-YFP respectively – as well as expression of mCherry-tagged WTgp130 and CAgp130 – T-REx-293-WTgp130-mCherry and T-REx-293-CAgp130-mCherry. T-REx-293 cells belong to the few cell lines of human origin that have been engineered to allow defined chromosomal integration and inducible expression of the transgene.

3.1.1. CAgp130 demonstrates differential intracellular distribution compared to WTgp130

In initial experiments expression and intracellular distribution of WTgp130 and CAgp130 were analyzed by confocal microscopy. Induction of receptor expression was performed in T-REx-293-WTgp130-mCherry and T-REx-293-CAgp130-mCherry and fixed cells were subjected to microscopic analysis (Figure 1). Signal detected in non-treated cells is caused mainly by cellular autofluorescence and to some extent by the leakiness of the inducible cell system. Induction of receptor expression is detectable according to the emerging mCherry-signal that is clearly beyond the background level of non-induced cells. However, neither WTgp130 nore CAgp130 show the predominant cell surface localization that is expected from a cell membrane receptor. Nevertheless, there is a noticeable difference in receptor distribution between cells expressing WTgp130 and CAgp130. As it becomes clear from the confocal images and respective intensity profiles shown in Figure 1 WTgp130 is distributed throughout the cellular membrane systems whereas CAgp130 is stronger restricted in its

spatial distribution and concentrated within the cell in membrane structures that resemble the ER-Golgi compartment.

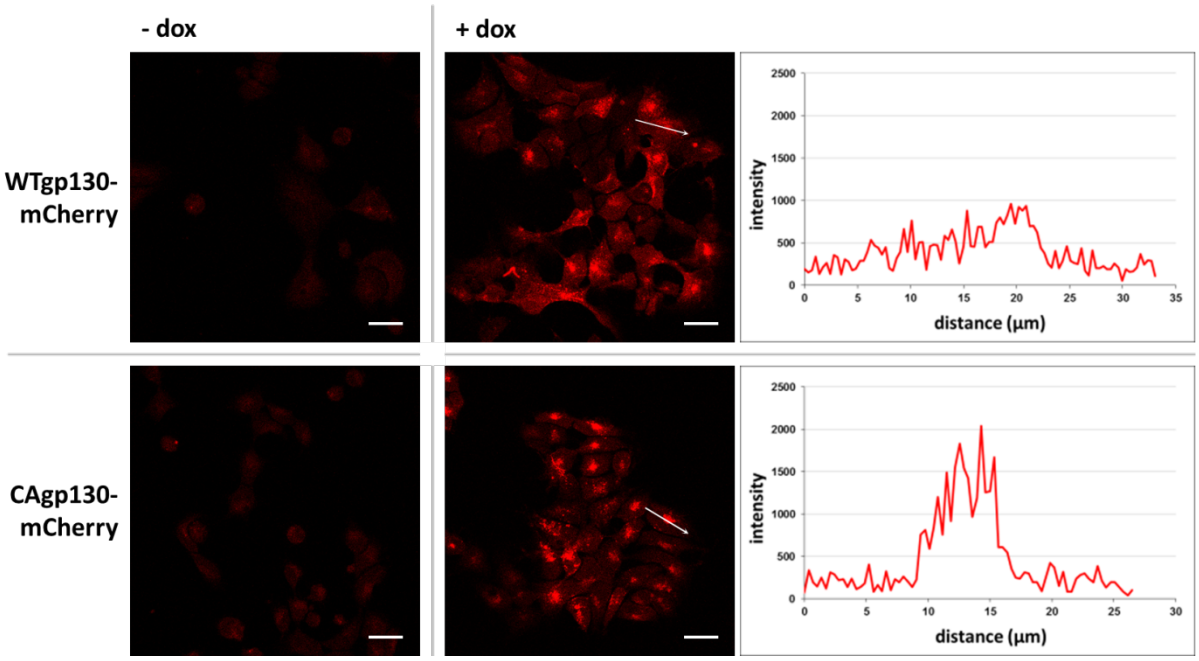

Figure 1 – WTgp130 and CAgp130 show differences in intracellular distribution. T-REx-293-WTgp130-mCherry and T-REx-293-CAgp130-mCherry were left untreated or expression was induced with 20 ng/ml dox for 48 h. Cells were fixed and receptor expression was analyzed by confocal microscopy. The diagrams represent mCherry-fluorescence intensities along the length of the white arrows. Scale bars: 20 µm.

To verify total and surface receptor expression in a quantitative manner cells stably transfected with mCherry-tagged variants of both receptors were analyzed by flow cytometry (Figure 2A). After induction of receptor expression cells were subjected to FACS-analysis. Overall receptor expression was assessed by the fluorescent tag. For verification of surface receptor expression non-permeabilized cells were immunostained with the gp130 Ab B-P8 that binds to the WT and mutant receptor with comparable efficiency (data not shown). Histograms in Figure 2A already point to differences between WTgp130 and CAgp130 concerning cell surface expression. Both receptors are expressed at comparable levels (upper panel). However, more WTgp130 seems to reach the cell surface (lower panel). Data from FACS-analysis were quantified and depicted in a diagram representing the induction of overall and surface receptor expression. The respective table documents the reduced cell surface expression of CAgp130 that is evident from the decreased ratio of surface to overall receptor expression.

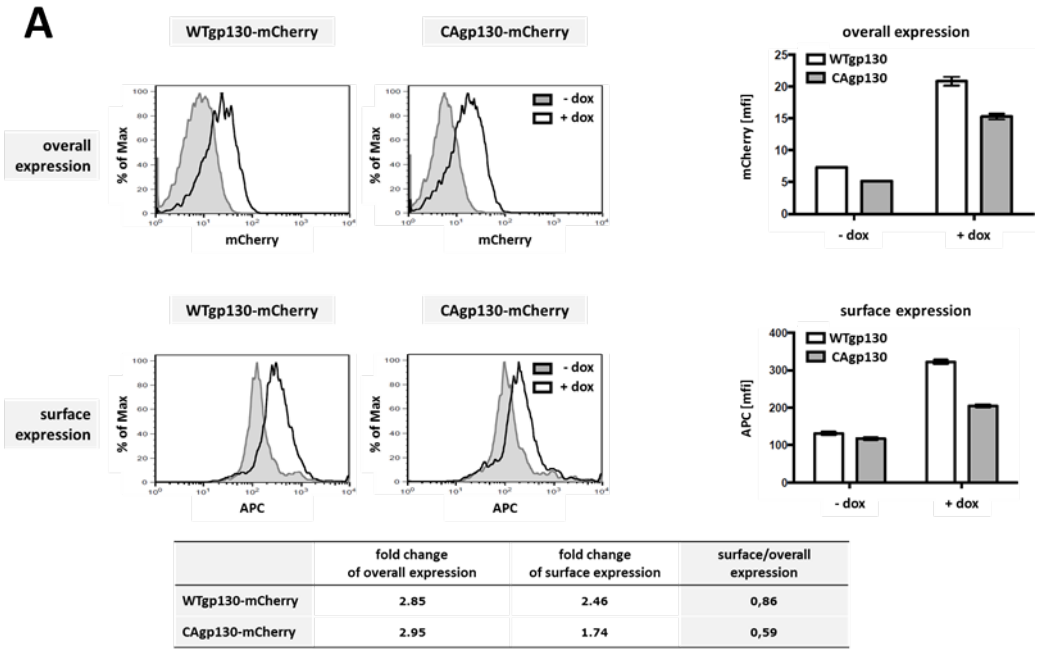

	fold change of overall expression	fold change of surface expression	surface/overall expression
WTgp130-mCherry	2.85	2.46	0,86
CAgp130-mCherry	2.95	1.74	0,59

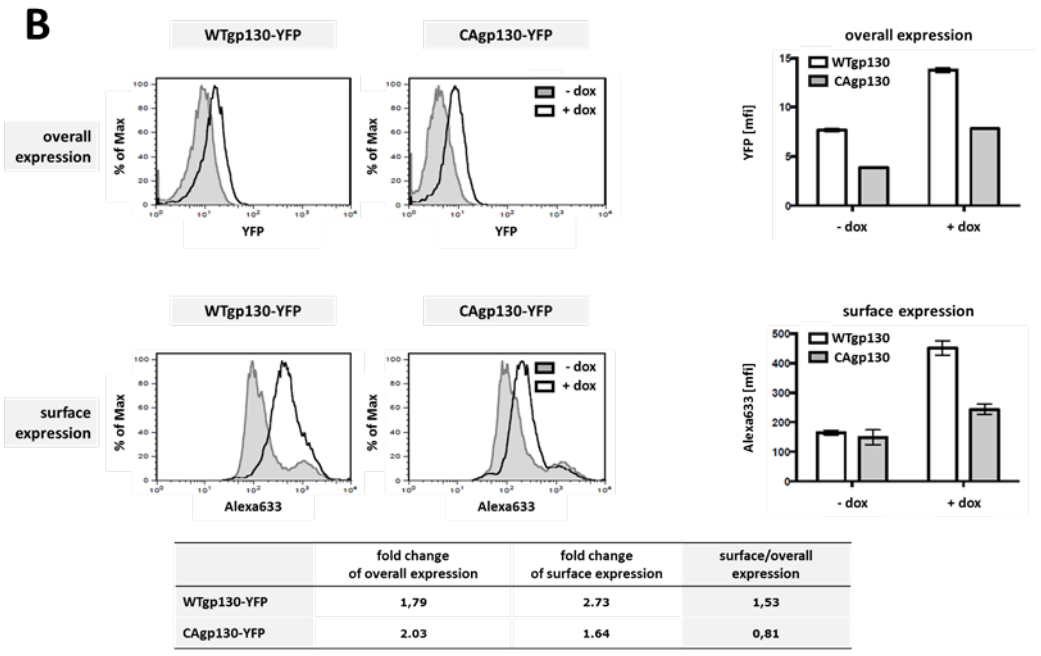

	fold change of overall expression	fold change of surface expression	surface/overall expression
WTgp130-YFP	1,79	2.73	1,53
CAgp130-YFP	2.03	1.64	0,81

Figure 2 – CAgp130 shows reduced cell surface expression compared to WTgp130. T-REx-293-WTgp130-mCherry and T-REx-293-CAgp130-mCherry **(A)** or T-REx-293-WTgp130-YFP and T-REx-293-CAgp130-YFP **(B)** were left untreated or expression was induced with 20 ng/ml dox for 24 h. Overall receptor expression was assessed by FACS-analysis of the fluorescent tag (upper panels) and surface receptor expression was determined through staining with the gp130 Ab B-P8 and an APC- **(A)** or Alexa633- **(B)** labeled secondary Ab (lower panels). Non-induced cells (filled histograms) were used as negative controls. Bar charts represent means and standard deviations from three independent experiments. Fold changes in overall and surface receptor expression as well as the ratios of surface to overall receptor expression were calculated.

In order to exclude that the reduced cell surface expression of CAgp130 is an artefact generated by the fluorescent tag of the receptor the same experiment was performed with cells stably transfected with the YFP-tagged variants of WTgp130 and CAgp130 (Figure 2B). The fluorescent tag is mandatory to still be able to monitor overall and surface receptor expression at the same time and with comparable sensitivity. However, YFP that is a GFP variant and mCherry can be considered as completely different tags. For the YFP-tagged receptor variants differences in the ratio of surface to overall receptor expression are even more pronounced than for the mCherry-tagged receptors providing evidence that mutant receptor reaches the cell surface to a lesser extent than WTgp130 independent of the tag.

3.1.2. WTgp130 and CAgp130 exhibit deviating glycosylation patterns

To verify induction of receptor expression by WB(Western blot)-analysis a time series experiment was performed. Receptor expression was induced in T-REx-293-WTgp130-YFP and T-REx-293-CAgp130-YFP for the given periods of time and receptor levels were assessed by immunoblotting (Figure 3A). Both receptors – WTgp130 and CAgp130 – can be readily detected after 4 h of induction. WTgp130 is detectable as a double band that represents the low and high glycosylated form of the receptor and appears predominantly in the high glycosylated and fully processed form as reported previously [40]. CAgp130, however, is mainly detected in the lower glycosylated and therefore immature form.

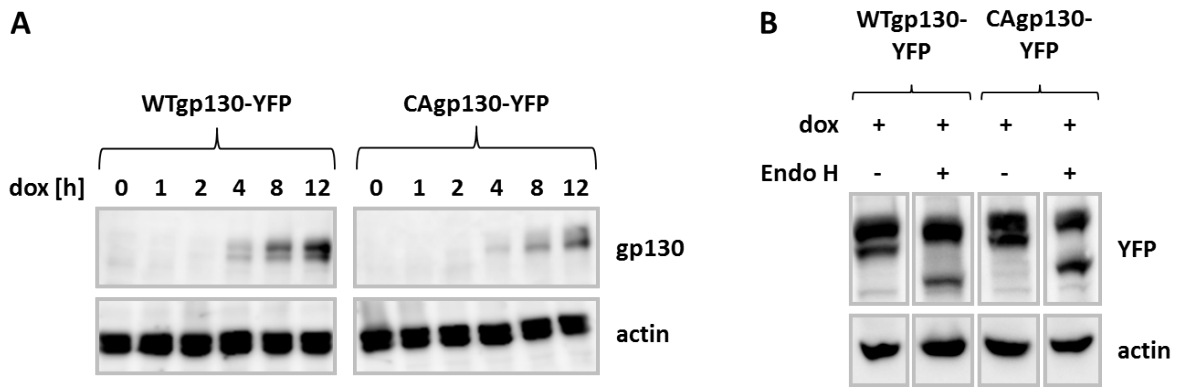

Figure 3 – WTgp130 and CAgp130 show different glycosylation patterns. (A) T-REx-293-WTgp130-YFP and T-REx-293-CAgp130-YFP were left untreated or expression was induced with 20 ng/ml dox for the indicated periods of time. TCLs were analyzed by immunoblotting using an Ab raised against a C-terminal peptide of gp130 and actin as loading control. **(B)** T-REx-293-WTgp130-YFP and T-REx-293-CAgp130-YFP were incubated with 20 ng/ml dox for 24 h. TCLs were left untreated or were subjected to Endo H digestion. Subsequently lysates were analyzed by immunoblotting using Abs against GFP/YFP and actin as loading control.

To roughly determine the glycosylation state of the two detected receptor bands TCLs (total cell lysates) of T-REx-293-WTgp130-YFP and T-REx-293-CAgp130-YFP upon induction of receptor expression were subjected to Endo H digestion (Figure 3B). Endo H removes high-mannose N-linked oligosaccharides from mainly ER-resident glycoproteins. For WTgp130 and mutant receptor the lower glycosylated form shifted upon Endo H treatment and therefore represents the high-mannose form that has not yet completely been processed in the Golgi compartment.

3.1.3. CAgp130 features aberrant signaling properties in comparison to WTgp130

3.1.3.1. CAgp130 is constitutively phosphorylated

In order to investigate signaling properties of CAgp130 and reveal possible deviations in comparison to signaling emanating from WTgp130 we first verified the phosphorylation state of the mutant receptor.

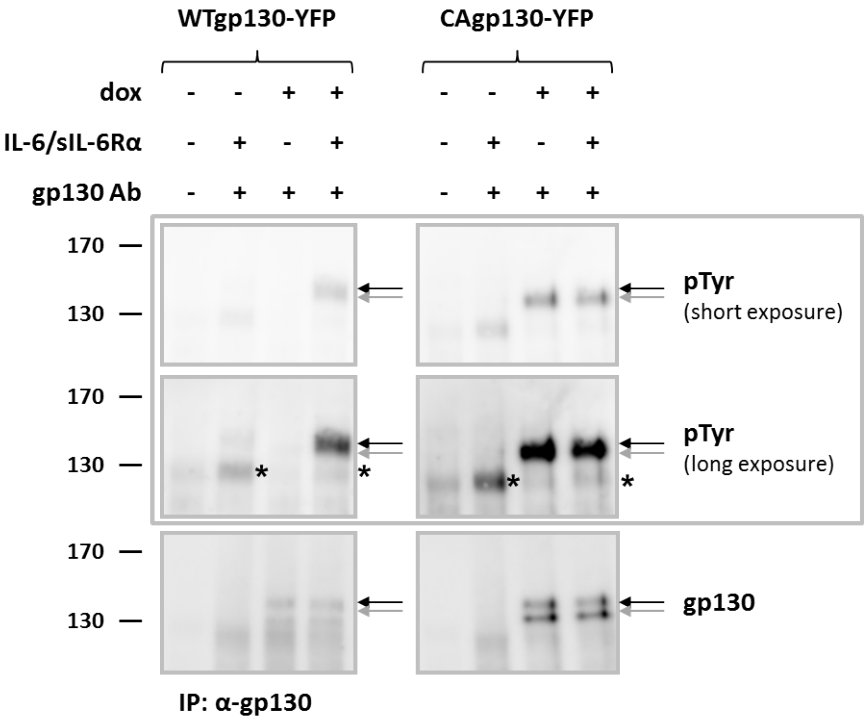

Figure 4 – CAgp130 is phosphorylated in a ligand-independent manner. T-REx-293-WTgp130-YFP and T-REx-293-CAgp130-YFP were left untreated or expression was induced with 0.5 µg/ml dox for 24 h. Cells were stimulated with 200 U/ml IL-6 and 0.5 µg/ml sIL-6Rα for 15 min or left unstimulated. Gp130 was immunoprecipitated from TCLs using an Ab against the C-terminus of gp130. Precipitates were analyzed by immunoblotting using Abs against pTyr and gp130. Asterisks mark phosphorylation-signals of endogenous gp130. Black and grey arrows mark the high and low glycosylated form of WTgp130-YFP and CAgp130-YFP respectively. Abbreviations used: IP – immunoprecipitation.

Induction of receptor expression was performed in T-REx-293-WTgp130-YFP and T-REx-293-CAgp130-YFP (Figure 4). Phosphorylation of endogenous and induced WTgp130 was induced with IL-6 and sIL-6Rα. Immunoprecipitation was performed with an Ab raised against a C-terminal peptide of gp130 that binds to both WTgp130 and CAgp130. As can be seen in the pTyr-detection of Figure 4, induced WTgp130 gets phosphorylated upon stimulation, whereas CAgp130 is phosphorylated in a ligand-independent manner. Phosphorylation of endogenous gp130 can be detected further below (marked by asterisks). For WTgp130 only the upper, fully processed form (black arrows) gets phosphorylated as it has reached the cell surface and responds to the stimulus. In the case of CAgp130, however, phosphorylation can be detected just for the lower, immature form (grey arrows). Interestingly, phosphorylation of endogenous receptor is barely detectable upon induction of WTgp130 and CAgp130.

3.1.3.2. CAgp130 activates the JAK/STAT pathway in a constitutive and ligand-independent manner

CAgp130 was initially described as a potent STAT3 activator and inducer of the feedback inhibitor SOCS3 [133].

In order to confirm the activating STAT3-phosphorylation at Y705 in our cell system and further verify phosphorylation of STAT3 at S727 and activation of STAT1 via its phosphorylation at Y701 receptor expression was induced in T-REx-293-WTgp130-YFP and T-REx-293-CAgp130-YFP. Upon stimulation cells were subjected to WB-analysis (Figure 5A). WTgp130 activates STAT3 and STAT1 only upon stimulation – in the case of endogenous gp130 – or induction and stimulation – in the case of stably transfected WTgp130-YFP. Activation of STAT3 and STAT1 gets stronger upon induction of additional gp130 – WTgp130-YFP – as far more receptor molecules are available where the transcriprion factors can bind to. CAgp130, however, activates both transcription factors without stimulation. Constitutive STAT3- and STAT1-activation also adds up to the activation caused by endogenous gp130 upon stimulation.

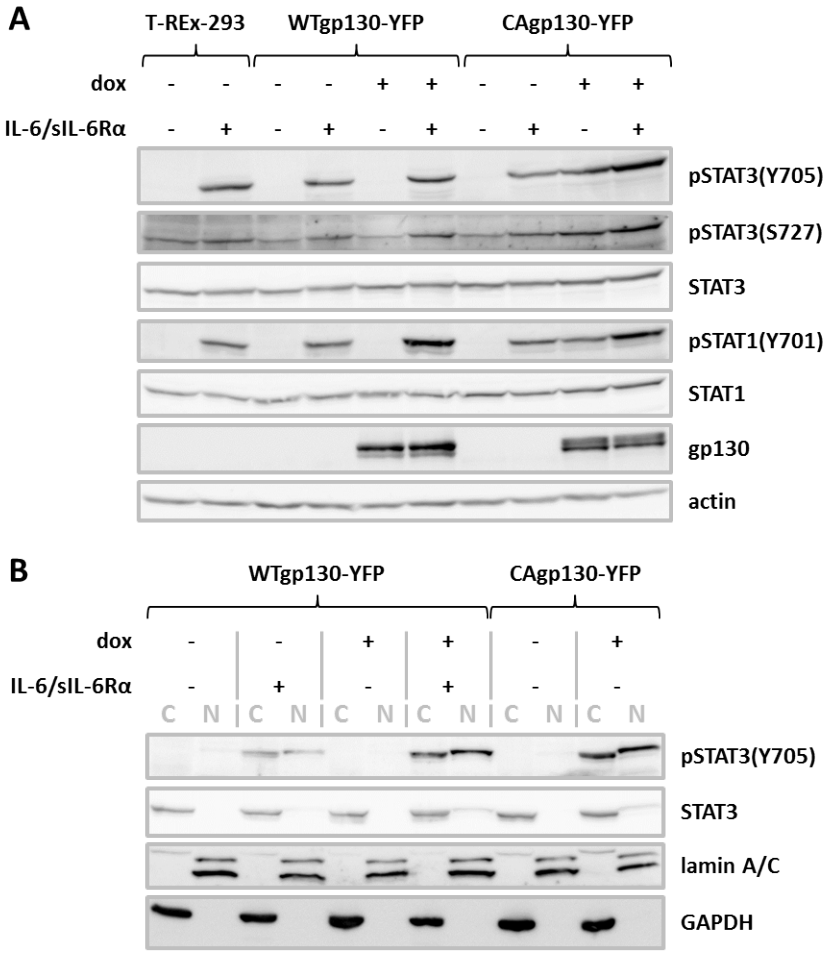

Figure 5 – CAgp130 constitutively activates the JAK/STAT pathway. T-REx-293-WTgp130-YFP and T-REx-293-CAgp130-YFP were left untreated or expression was induced with 20 ng/ml dox for 24 h. Cells were stimulated with 200 U/ml IL-6 and 0.5 µg/ml sIL-6Rα for 30 min or left unstimulated. **(A)** Activation of the JAK/Stat pathway was analyzed by immunoblotting of TCLs with Abs against pSTAT3(Y705), pSTAT3(S727), pSTAT1(Y701), STAT3, STAT1, gp130 and actin as loading control. **(B)** To verify nuclear translocation of activated STAT3 cells were subjected to a nucleus/cytosol fractionation and single fractions were analyzed by immunoblotting using Abs against pSTAT3(Y705) and STAT3. Lamin A/C and GAPDH were used as loading controls for the nuclear and cytosolic fraction respectively.

To verify whether STAT3 activated by CAgp130 translocates into the nucleus as efficiently as STAT3 activated at the stimulated endogenous gp130 or the induced and stimulated WTgp130, receptor expression was induced in T-REx-293-WTgp130-YFP and T-REx-293-CAgp130-YFP (Figure 5B). Upon stimulation cells were subjected to a nucleus/cytosol fractionation and single fractions were analyzed by immunoblotting. As can be seen in Figure 5B STAT3 activated by CAgp130 undergoes nuclear translocation as efficiently as STAT3 upon its phosphorylation at activated endogenous or induced gp130.

Further experiments were performed to determine to what extent CAgp130 is able to induce the feedback inhibitor SOCS3 compared to WTgp130 upon stimulation. Receptor expression

was induced in T-REx-293-WTgp130-YFP as well as T-REx-293-CAgp130-YFP. Subsequently parental T-REx-293 cells and T-REx-293-WTgp130-YFP were pulse-stimulated for the indicated periods of time (Figure 6). As can be seen in Figure 6 in cells expressing CAgp130, STAT3 is constitutively phosphorylated, whereas in the parental T-REx-293 cells or cells expressing WTgp130, STAT3 gets phosphorylated only upon stimulation. STAT3-activation peaks about 30 to 45 min after stimulation before declining again. SOCS3 induced in the case of T-REx-293 cells is barely detectable. However, SOCS3 induced by CAgp130 is detected at much higher levels that are comparable to SOCS3 levels triggered in cells expressing induced WTgp130 120 min after stimulation.

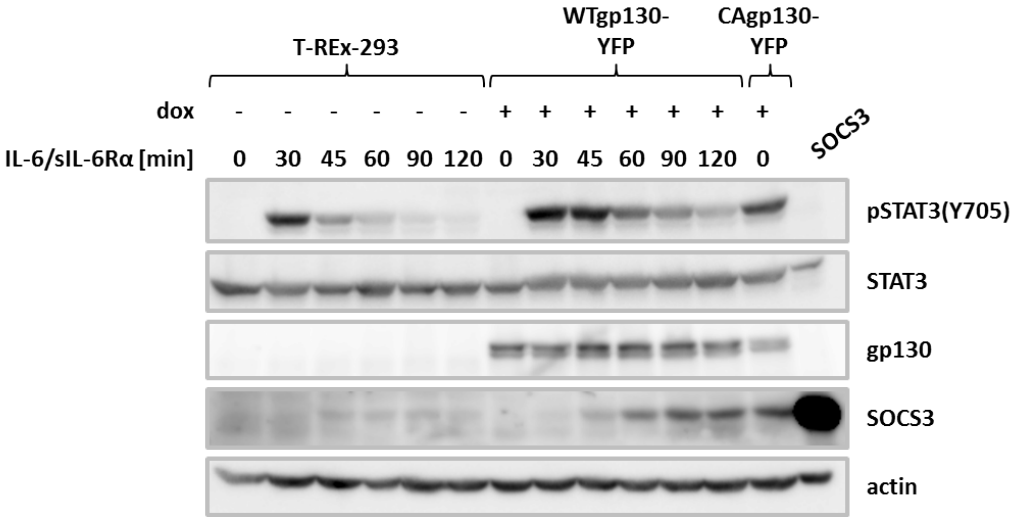

Figure 6 – CAgp130 induces the feedback inhibitor SOCS3 in a ligand-independent manner. T-REx-293-WTgp130-YFP and T-REx-293-CAgp130-YFP were left untreated or expression was induced with 20 ng/ml dox for 24 h. Cells were pulse-stimulated with 200 U/ml IL-6 and 0.5 µg/ml sIL-6Rα and the stimulus was removed after 15 min of incubation or were left unstimulated. After the indicated periods of time TCLs were analyzed by immunoblotting using Abs against pSTAT3(Y705), STAT3, gp130, SOCS3 and actin as loading control. For the SOCS3 positive control HEK293 cells were transiently transfected with a SOCS3 encoding plasmid.

3.1.3.3. Activation of the JAK/Erk pathway through CAgp130 is severely impaired

To verify activation of Erk downstream of JAK by CAgp130 we assessed phosphorylation of the major players SHP2 and Erk1/2. As for the analysis of the JAK/STAT pathway the YFP-tagged variants of WTgp130 and CAgp130 were utilized. Induction of receptor expression was performed in the respective cells and upon stimulation TCLs were used for WB-analysis (Figure 7). As expected, endogenous gp130 can activate SHP2 and Erk only upon stimulation. In cells additionally expressing WTgp130-YFP activation is stronger upon induction as far more receptor molecules are available. Surprisingly, there is just a partial activation of the

JAK/Erk axis by CAgp130. Upon induction of mutant receptor SHP2 gets heavily phosphorylated. However, there is hardly any activation of Erk1/2 detectable. Activation of the JAK/Erk cascade by CAgp130 seems to be strictly limited.

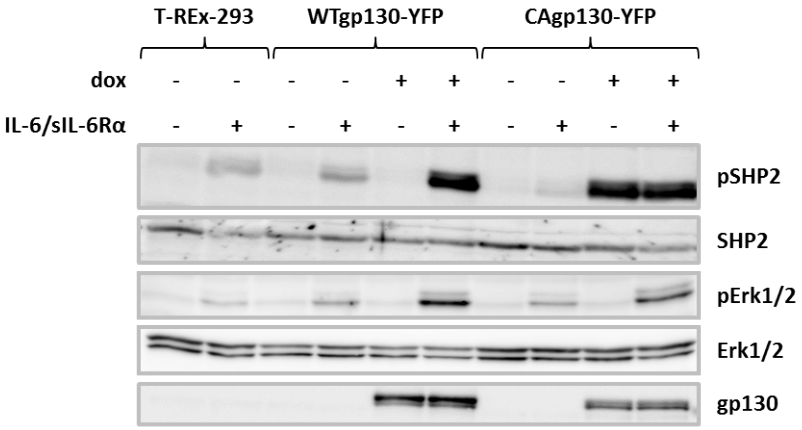

Figure 7 – CAgp130 fails to activate the JAK/Erk pathway. T-REx-293-WTgp130-YFP and T-REx-293-CAgp130-YFP were left untreated or expression was induced with 20 ng/ml dox for 24 h. Cells were stimulated with 200 U/ml IL-6 and 0.5 µg/ml sIL-6Rα for 30 min or left unstimulated. Activation of the JAK/Erk pathway was analyzed by immunoblotting of TCLs with Abs against pSHP2, pErk1/2, SHP2, Erk1/2 and gp130.

To make sure that fluorescent tags do not influence the signaling properties of CAgp130 receptor variants lacking a fluorescent tag were constructed and cell lines were generated that allowed their stable and inducible expression. As shown in Figure 8 WTgp130 activates STAT3 and Erk upon stimulation, whereas CAgp130 strongly activates STAT3 but is unable to cause Erk-activation. Therefore, Figure 8 confirms that the major signaling properties are identical between tagged and non-tagged receptors.

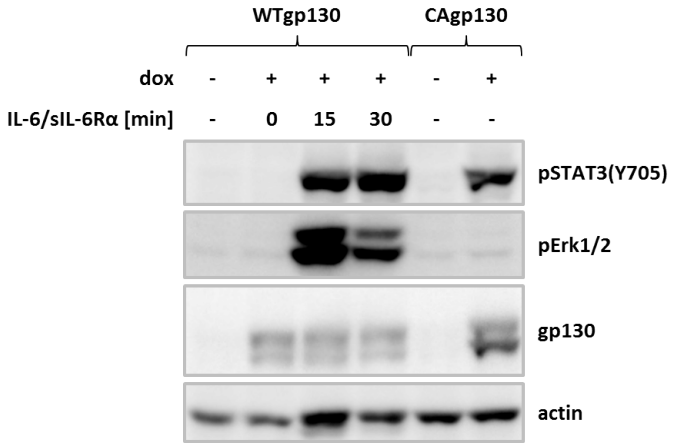

Figure 8 – Signaling properties of CAgp130 are independent of the fluorescent tag. T-REx-293-WTgp130 and T-REx-293-CAgp130 were left untreated or expression was induced with 20

ng/ml dox for 24 h. Cells were stimulated with 200 U/ml IL-6 and 0.5 µg/ml sIL-6Rα for the indicated periods of time or left unstimulated. TCLs were analyzed by immunoblotting using Abs against pSTAT3(Y705) and pErk1/2, gp130 and actin.

The group of MAPKs comprises besides Erk two SAPKs, JNK and p38 [155]. The only IL-6-type cytokine that can mediate activation of all three MAPKs is OSM through the type II OSM receptor complex [156] whereas IL-6 is only able to activate Erk. In order to make sure that CAgp130 is not able to activate any of the SAPKs receptor expression was induced in T-REx-293-WTgp130-YFP and T-REx-293-CAgp130-YFP and TCLs where probed for the activated forms of JNK and p38. HepG2 cells, which were stimulated with OSM were used to provide a positive control. As shown in Figure 9 CAgp130 activates neither JNK nor p38.

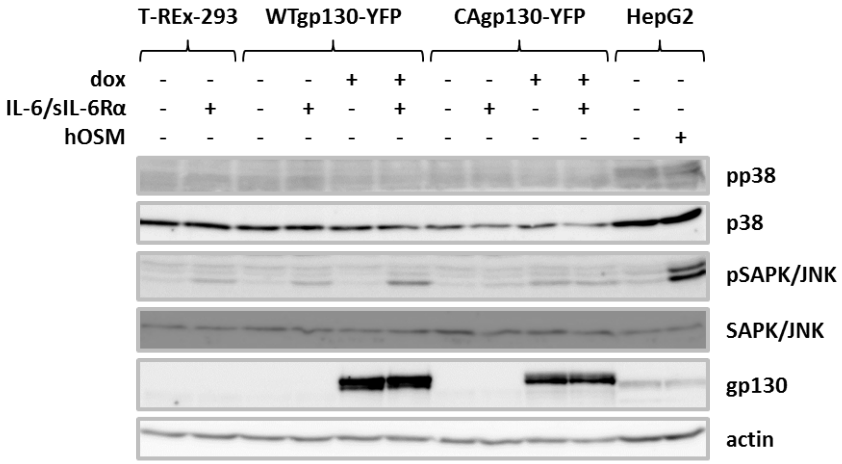

Figure 9 – CAgp130 fails to activate p38 and SAPK/JNK. T-REx-293-WTgp130-YFP and T-REx-293-CAgp130-YFP were left untreated or expression was induced with 20 ng/ml dox for 24 h. Cells were stimulated with 200 U/ml IL-6 and 0.5 µg/ml sIL-6Rα for 30 min or left unstimulated. TCLs were analyzed using Abs against pp38, pSAPK/JNK, p38, SAPK/JNK, gp130 and actin as loading control. As a positive control for the activation of p38 and SAPK/JNK HepG2 cells were stimulated with 100 ng/ml hOSM for 30 min.

A further pathway that has been reported to get activated upon IL-6 stimulation is the PI3K/Akt pathway [62]. To clarify whether CAgp130 is able to activate Akt, HEK293 cells were transiently transfected with WTgp130-CFP and CAgp130-CFP (Figure 10). With cells transfected with WTgp130-CFP a time series experiment of Akt-activation was performed. As detected in Figure 10 IL-6 does not activate the PI3K/Akt pathway in the utilized cell system as assessed by Akt-phosphorylation at S473. Whereas STAT3-phosphorylation at Y705 increases over time Akt-phosphorylation does not significantly change. Even more important CAgp130 is not able to activate Akt.

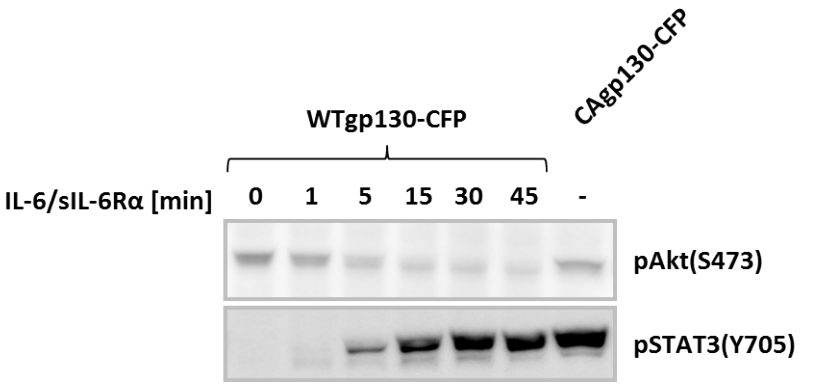

Figure 10 – CAgp130 fails to activate Akt. HEK293 cells were transiently transfected with the indicated DNA und subsequently left untreated or stimulated with 200 U/ml IL-6 and 0.5 µg/ml sIL-6Rα for the given periods of time. TCLs were analyzed by immunoblotting using Abs against pAkt(Ser473) and pSTAT3(Y705).

3.1.4. Cytoplasmic Tyr-residues of CAgp130 differentially contribute to constitutive signaling

Previous work has pointed out the importance of individual pTyr-motifs for activation of specific STAT proteins and the differential contribution of potential recruitment sites for STAT3-activation [64].

In order to define the contribution of cytoplasmic Tyr-residues of CAgp130 for activation of STAT proteins and SHP2 we generated a series of so-called add-back mutants of CAgp130, where just single cytoplasmic Tyr-residues are available for signaling (Figure 11). Furthermore, a mutant of CAgp130 without any cytoplasmic Tyr-residue was generated – CAgp130-6F-YFP – to serve as a negative control.

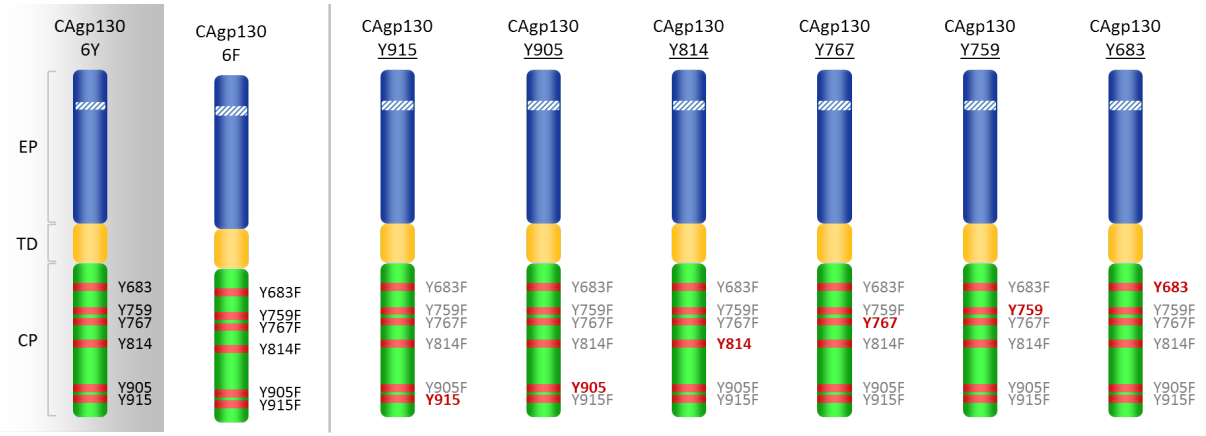

Figure 11 – Schematic overview of add-back mutants of CAgp130. Abbreviations used: EP – extracellular part with depicted del(Y186-Y190), TD – transmembrane domain, CP – cytoplasmic part.

Constructs encoding WTgp130-YFP, CAgp130-YFP, CAgp130-6F-YFP and add-back constructs were transiently transfected in HEK293 cells stably expressing IL-6Rα. Transfected cells were subjected to FACS-analysis to verify overall and surface expression of the mutants (Figure 12A). Overall receptor expression was assessed using the YFP-tag and surface receptor was stained by two different monoclonal Abs targeting distinct sites on the extracellular part of gp130. Ab B-P8 targets domain 3 (D3) of the extracellular part of gp130 and detects both WTgp130 and CAgp130. Ab B-R3 targets D2 of gp130 and does not detect CAgp130 probably because of the activating deletion located within this domain. FACS-analysis using Ab B-P8 reveals a considerably increased amount of surface WTgp130 compared to CAgp130 in agreement with the FACS data shown in Figure 2. CAgp130-6F-YFP without any cytoplasmic Tyr-residue and the series of add-back mutants do not show any difference in surface expression compared to CAgp130 indicating that single Tyr-residues do not have any impact on cell surface expression of the receptor.

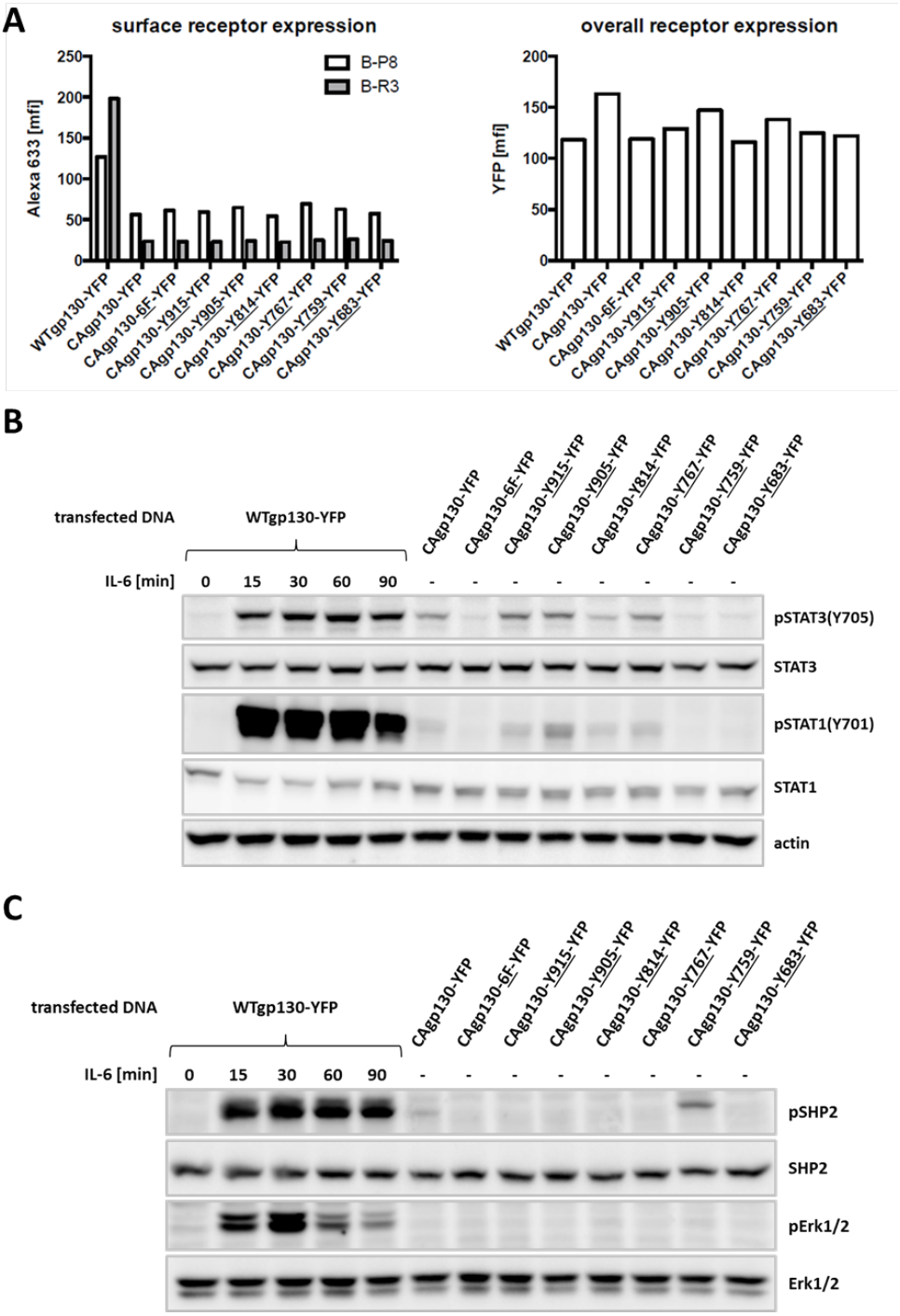

Figure 12 - Cytoplasmic Tyr-residues of CAgp130 differentially contribute to constitutive signaling. HEK293 cells stably expressing IL-6Rα were transiently transfected with WTgp130-YFP, CAgp130-YFP, CAgp130-6F-YFP or YFP-tagged add-back mutants of CAgp130. **(A)** Overall receptor expression was assessed by FACS-analysis of the fluorescent tag (right panel). Surface receptor expression was verified using the gp130 Abs B-P8 and B-R3 and an Alexa633-labeled secondary Ab (left panel). **(B)** and **(C)** Cells were stimulated with 200 U/ml IL-6 for the indicated periods of time or left untreated. TCLs were analyzed by immunoblotting. **(B)** Activation of the JAK/STAT pathway was verified by Abs against pSTAT3(Y705), pSTAT1(Y701), STAT3, STAT1 and actin as loading control. **(C)** Activation of the JAK/Erk pathway was assessed using Abs against pSHP2, pErk1/2, SHP2 and Erk1/2.

To study effector functions of single pTyr-residues of CAgp130 on the JAK/Stat axis TCLs were probed for pSTAT3(Y705) and pSTAT1(Y701). As shown in Figure 12B there are four cytoplasmic Tyr-residues that are able to bind STAT3 and STAT1 upon phosphorylation. Activation of STAT3 by CAgp130 exclusively occurs through the four distal Tyr-residues in line with findings for WTgp130 [63]. The two distal Tyr-residues seem to be favored as they lead to stronger STAT3-activation than the two membrane-proximal ones. STAT1 gets also activated through binding to the four distal Tyr-residues with the second to last pTyr being the most preferred activation site. STAT-activation through the add-back mutants is stronger than through CAgp130-YFP harboring all Tyr-residues. This might be a consequence of the fact that the STAT-activating add-back mutants lack Y759 required for feedback inhibition through SOCS3. Thus, CAgp130-YFP is to a certain extent sensitive to feedback inhibition.

With respect to activation of the JAK/Erk cascade TCLs of cells transfected with add-back mutants were probed for SHP2- and Erk-phosphorylation (Figure 12C). In line with results shown in Figure 7 phosphorylation of SHP2 but not Erk can be detected in cells transfected with CAgp130. Activation of SHP2 caused by CAgp130 can be definitely assigned to the second Tyr-residue proximal to the membrane – Y759 – in line with published data [Stahl 1995]. In cells transfected with the CAgp130 that only harbors the SHP2 recruitment site SHP2-activation is even stronger than in cells expressing CAgp130, still there is no Erk-phosphorylation detectable.

3.2. Compartimentalization of intracellular signaling emanating from CAgp130

After having thoroughly analyzed the signaling properties of CAgp130, the focus was set on spatial regulation of constitutive signaling emanating from mutant receptor.

3.2.1. Signaling potential of *de novo* synthesized CAgp130 on its way to the cell membrane

3.2.1.1. ER-retention sequences fail to cause intracellular retention of WTgp130 and CAgp130 in a cell system that allows stable expression

Initial experiments to investigate the signaling-trafficking axis of CAgp130 focused on the possibility to cause intracellular retention of the mutant receptor by the use of ER-retention signals. In this context, two Arg- and two Lys-based ER-retention sequences were taken into consideration [157]. Among the Arg-based signals was the recently described ER-retention sequence within CD74 [158].

ER-retention constructs were generated for WTgp130 and CAgp130. ER-retention sequences were fused to the C-termini of mCherry-tagged variants of both receptors. Between the fluorescent tag and the respective ER-retention sequence a V5-tag was positioned. A schematic overview of the generated constructs in the context of WTgp130 is shown in Figure 13.

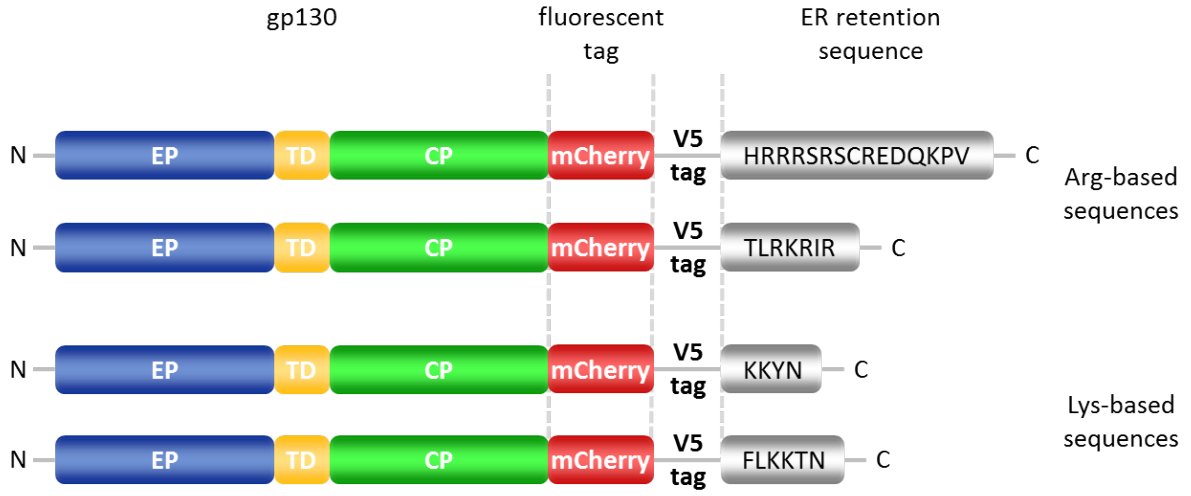

Figure 13 – Schematic overview of ER-retention mutants of gp130. ER-retention constructs consist out of the mCherry-tagged WTgp130 or CAgp130 that is fused at its C-terminus to the depicted retention sequences via a V5 tag. Abbreviations used: EP – extracellular part, TD – transmembrane domain, CP – cytoplasmic part.

Initial experiments were performed with the ER-retention constructs of WTgp130 as it was clear that it would be more difficult to demonstrate retention for CAgp130 that already shows a reduced cell surface expression compared to WTgp130. This consideration was furthermore important as first transfections were performed in a transient mode where just a fraction of treated cells harbors and expresses the transgene. In order to carry out a first verification of the chosen ER-retention sequences, ER-retention constructs of WTgp130 were transiently transfected in HEK293 cells and surface expression of transfected receptors was analyzed by FACS (Figure 14).

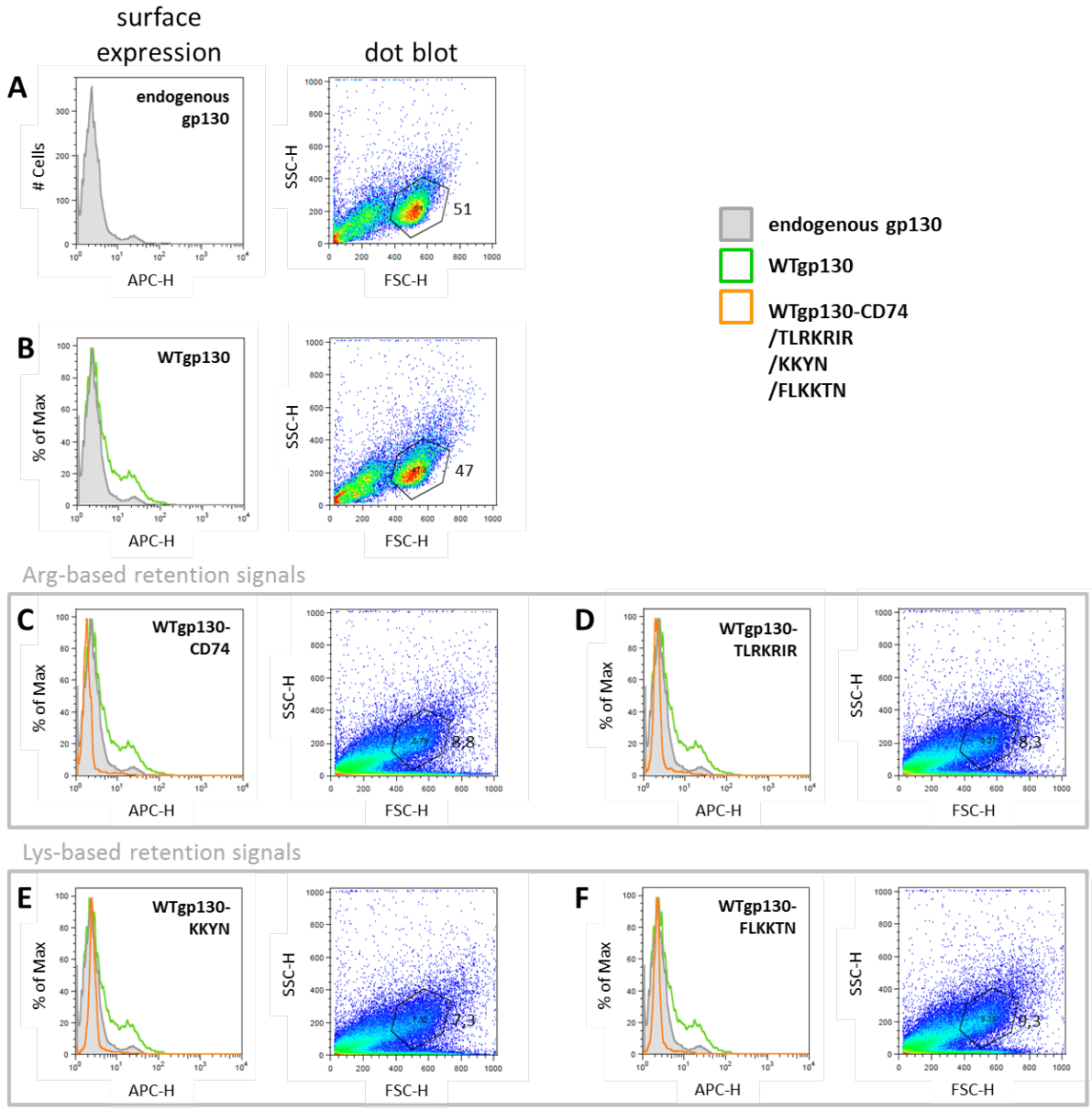

Figure 14 – Verification of retention efficiency of WTgp130 ER-retention constructs. HEK293 cells were left untransfected (grey histogram) **(A)** or were transiently transfected with equal amounts of WTgp130-mCherry (green histogram) **(B)** or ER-retention mutants of WTgp130-mCherry (orange histograms) **(C-F)** and were analyzed by FACS. Upon gating of the healthy cell population (right panels) surface receptor expression of gated cells was measured

(left panels). Surface receptor expression was verified using the gp130 Ab B-P8 and an APC-labeled secondary Ab.

Figure 14 summarizes the data on retention efficiency of the four chosen ER-retention sequences in the context of WTgp130. For every receptor construct the respective histogram (left side) and dot blot for FSC(forward scatter)/SSC(side scatter) (right side) are given. In Figure 14A non-transfected cells were analyzed and the histogram represents the signal caused by endogenous gp130. Within the dot blot the population of healthy cells was gated as evaluated by their position on the FSC and SSC axis. Figure 14B shows data from cells that were transfected with WTgp130-mCherry. As expected in the case of a transient transfection the increase of the detected signal is evident by the peak that rises on the right side of the histogram compared to untransfected cells. The respective dot blot does not show any significant changes of the main cell population on the FSC and SSC axis meaning that there are no changes in the size and granularity of the cells respectively. Figures 14C-14F show data from cells transfected with the specified ER-retention constructs of WTgp130-mCherry. Histograms of all four transfections are similar with the surface receptor expression upon transfection being even lower than the amount of endogenous gp130 measured in Figure 14A. A possible explanation for this observation is based on the existence of preformed dimers that have been described in the past [159]. According to this explanation there is a possible formation of heterodimers between endogenous gp130 and transfected ER-retention constructs of WTgp130. The retention mutant within these heterodimers could be able to capture endogenous gp130 within the cell. Also interesting are the morphological changes of transfected cells evident from the shift on the FSC/SSC. Upon transfection of ER-retention constructs cells show a dramatic shift to the lower left corner of the dot blot indicating loss of their cellular integrity. This effect obviously does not correlate with the transfection procedure itself as cells transfected with WTgp130 remain within the same gate as untransfected cells.

In a further attempt to verify whether retention sequences could be a helpful tool to investigate spatial regulation of CAgp130 WTgp130-mCherry-CD74 and CAgp130-mCherry-CD74 were stably transfected in T-REx-293 cells. As shown in Figure 15A single cell clones were obtained and tested for the expression of the transgene upon induction. Clones with the highest receptor expression levels – in the case of CAgp130-mCherry-CD74 clones 1C, 3B and 6E – were chosen for further FACS-analysis (Figure 15B). Overall receptor expression was

assessed by the fluorescent tag and surface expression was measured by the use of the gp130 Ab B-P8 and an APC-labeled secondary Ab.

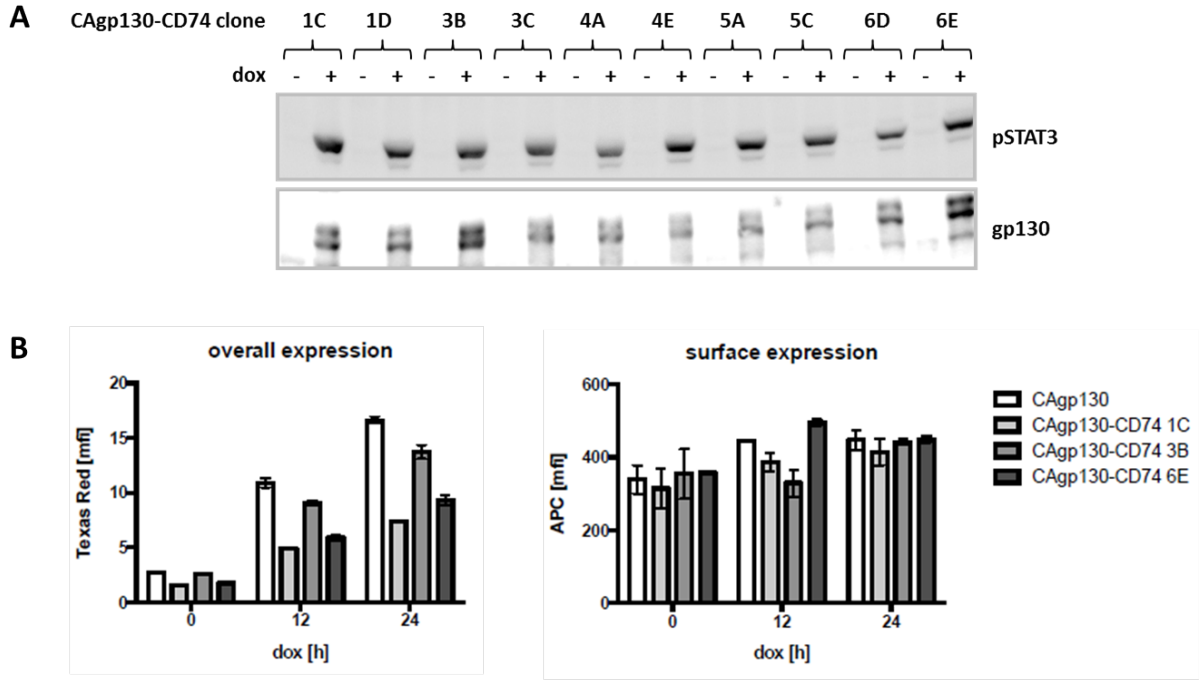

12 h dox

	fold change of overall expression	fold change of surface expression	surface/overall expression
CAgp130	4,08	1,30	**0,32**
Cagp130-CD74			
1C	3,13	1,07	**0,34**
3B	3,44	1,03	**0,30**
6E	3,47	1,40	**0,40**

24 h dox

	fold change of overall expression	fold change of surface expression	surface/overall expression
CAgp130	6,14	1,37	**0,22**
Cagp130-CD74			
1C	4,70	1,18	**0,25**
3B	5,38	1,27	**0,24**
6E	5,33	1,27	**0,24**

Figure 15 – The CD74 retention sequence fails to arrest CAgp130 within stably transfected cells. (A) Generation of T-REx-293 cells that express CAgp130-CD74 in a stable and inducible manner. Depicted clones were treated with 20 ng/ml dox for 24 h and TCLs were analyzed by immunoblotting using Abs against pSTAT3(Y705) and gp130. **(B)** Selected clones were subjected to FACS-analysis. Overall receptor expression was verified using the fluorescent tag (left diagram) and surface receptor expression was assessed using the gp130 Ab B-P8 and an APC-labeled secondary Ab (right diagram). Bar charts represent means and standard deviations from three independent experiments. Fold changes in overall and surface receptor expression as well as the ratios of surface to overall receptor expression were calculated.

Figure 15B shows changes in overall and surface receptor expression upon 12 and 24 h of induction (upper panel). In the lower panel of Figure 15B fold changes for the measured overall and surface receptor amount as well as the ratio of fold changes for both receptor populations were calculated. As evident from the calculated numbers the overall receptor amount in cells transfected with CAgp130 increases by the factor 4 upon 12 h of induction and the by factor 6 upon 24 h of induction. Surface receptor increases by factor 1 within 12 h but shows no significant increase within the next 12 h. Similar values were measured for the CAgp130-mCherry-CD74 clones. Unfortunately, clones expressing the ER-retention construct of CAgp130 do not show a markedly reduced ratio of surface to overall receptor expression neither 12 h nore 24 h upon induction, indicating that there is no retention effect. Similar results were obtained in cells stably transfected with CAgp130-mCherry-KKYN harboring the Lys-based retention signal.

3.2.1.2. The trafficking-inhibitor brefeldin A mediates intracellular retention of *de novo* synthesized WTgp130 and CAgp130

Still being interested whether signaling of CAgp130 is dependent on its presence at the cell membrane an inhibitor-based approach using the trafficking-inhibitor brefeldin A was performed. Therefore, receptor expression was induced in T-REx-293-WTgp130-YFP and T-REx-293-CAgp130-YFP. Cells were simultaneously treated with 100 ng/ml brefeldin A to prevent newly synthesized receptor from reaching the cell surface and analyzed by flow cytometry. Overall receptor expression was assessed by the YFP-tag (Figure 16B) and cell surface receptor was detected by the gp130 Ab B-P8 and an APC-labeled secondary Ab (Figure 16A). As shown in Figure 16A induction leads to the increase of receptor surface expression for both WTgp130 and CAgp130 with less CAgp130 reaching the plasma membrane. This increase is already detectable upon 4 h of induction. The combination of induction and treatment with brefeldin A causes complete retention of WTgp130 for the first 4 h. According to the FACS-analysis at the 8 h time point a small amount of WTgp130 escapes retention and appears on the cell surface. In the case of CAgp130 retention seems to be more efficient probably due to the smaller amounts of receptor that reach the plasma membrane at all. Brefeldin A in the applied concentration is able to completely retain CAgp130 within the cell even 8 h after induction. A considerable amount of surface receptor is detectable upon 8 h of induction in the vehicle control for CAgp130.

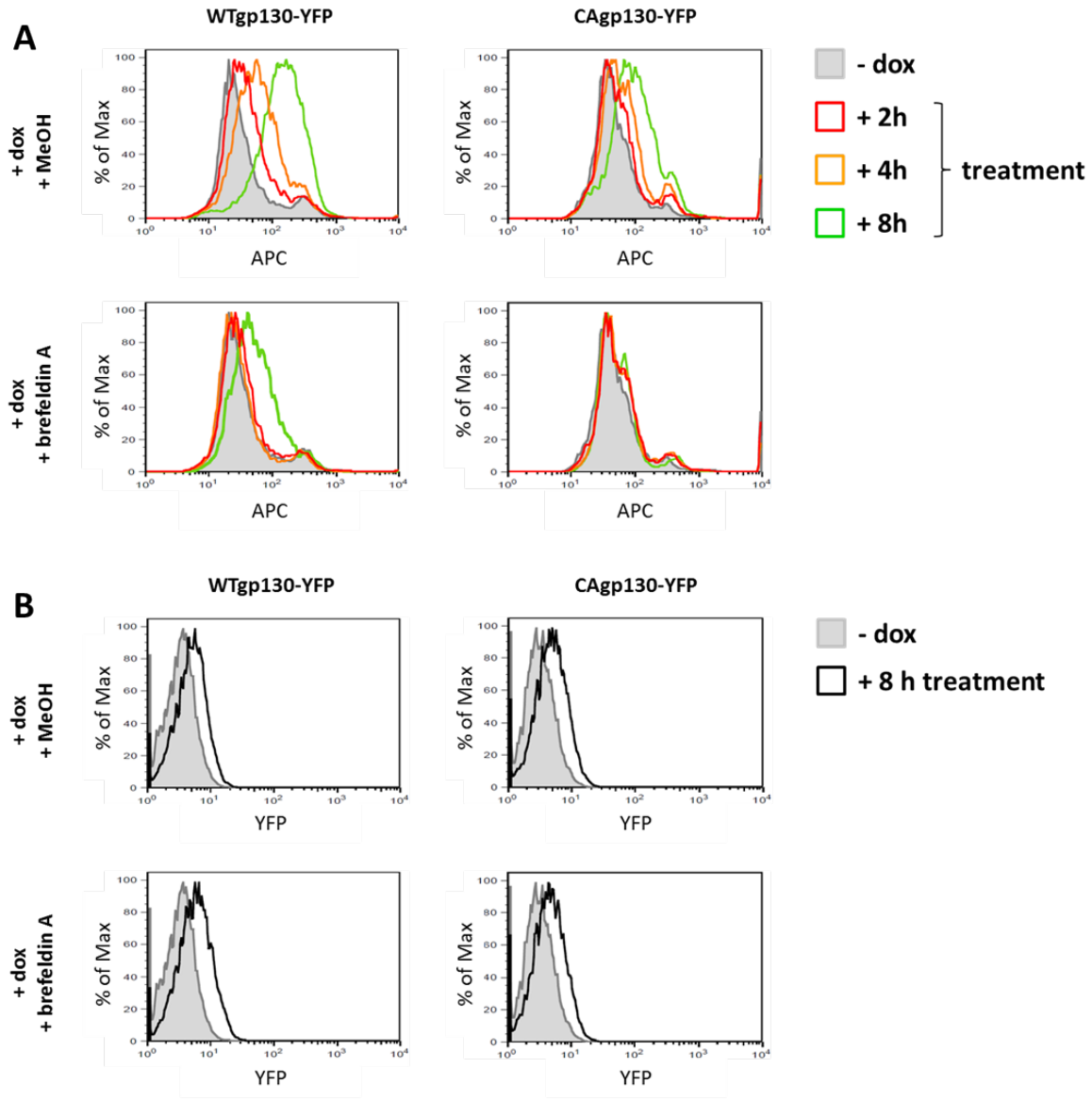

Figure 16 – Brefeldin A causes intracellular retention of *de novo* synthesized CAgp130. T-REx-293-WTgp130-YFP and T-REx-293-CAgp130-YFP were left untreated or expression was induced with 20 ng/ml dox for the indicated periods of time. Cells were simultaneously treated with 100 ng/ml brefeldin A or MeOH (vehicle). Surface receptor expression was determined by FACS-analysis using the gp130 Ab B-P8 and an APC-labeled secondary Ab **(A)** and overall receptor expression was assessed by the fluorescent tag **(B)** . Non-induced cells (filled histograms) were used as negative controls.

3.2.1.3. Intracellularly retained CAgp130 signals from the ER-Golgi compartment

In order to find out whether intracellularly retained CAgp130 is able to mediate constitutive signals from within the cell TCLs of T-REx-293-CAgp130-YFP treated with dox or a combination of dox and brefeldin A were subjected to WB-analysis and probed for CAgp130 expression and STAT3-phosphorylation (Figure 17). Upon induction increasing amounts of CAgp130 and stimulus-independent STAT3-phosphorylation can be detected. Upon treatment with brefeldin A the upper, higher glycosylated receptor band disappears. Thus,

retention of CAgp130 and generation of an ER-Golgi hybrid compartment prevent complete glycosylation of the receptor. Nonetheless, the retained receptor is still able to phosphorylate STAT3 from within the cell.

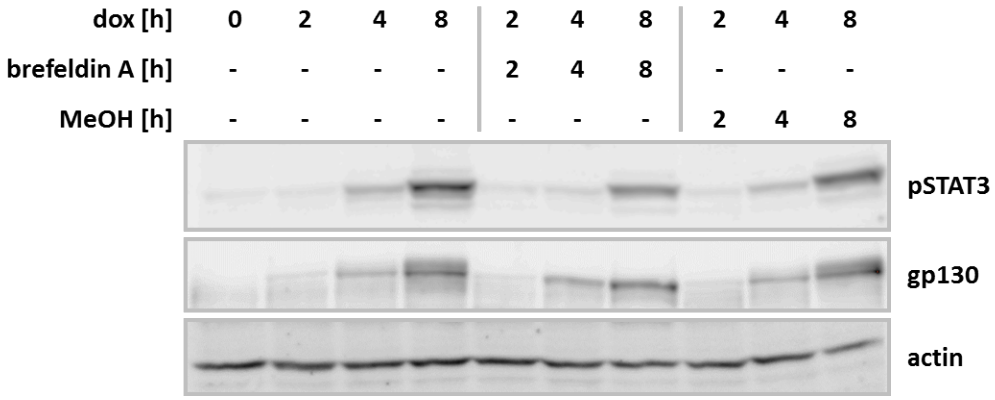

Figure 17 – *De novo* synthesized CAgp130 signals from intracellular compartments. T-REx-293-WTgp130-YFP and T-REx-293-CAgp130-YFP were left untreated or expression was induced with 20 ng/ml dox for the indicated periods of time. Cells were simultaneously treated with 100 ng/ml brefeldin A or MeOH (vehicle). TCLs were analyzed by immunoblotting using Abs against pSTAT3(Y705), gp130 and actin as loading control.

3.2.2. Signaling potential of CAgp130 upon endocytosis

After having assessed activity of *de novo* synthesized, intracellularly retained CAgp130 we further tried to elucidate whether mutant receptor is able to signal from the plasma membrane or intracellular compartments upon endocytosis.

In previous work it was reported that gp130 undergoes stimulus-independent internalization and that it is constitutively associated with the AP-2 adaptor complex [56]. These findings suggest that gp130 is constitutively endocytosed in a clathrin- and therefore dynamin-dependent way.

In two independent approaches we tried to interfere with the endocytic process of CAgp130 and analyze the consequences on its signaling activity. First experiments were performed with the dynamin-inhibitor dynasore, the second approach utilized dominant-negative dynamin.

3.2.2.1. Endocytosis-inhibitor dynasore causes cell death of T-REx-293 cells rather than inhibition of endocytosis

Initial experiments to elucidate the signaling potential of CAgp130 at the plasma membrane and upon endocytosis utilized the dynamin-inhibitor dynasore. For this purpose parental T-REx-293 cells were incubated for 30 min with increasing concentrations of dynasore starting

with low concentrations of 25 µM and reaching common applied concentrations of 100 µM. As shown in Figure 18 treated cells shift upon dynasore treatment from the gated population to the lower left corner of the dot blot. This effect is dependent on concentration and indicates detrimental effects of the inhibitor on cell morphology.

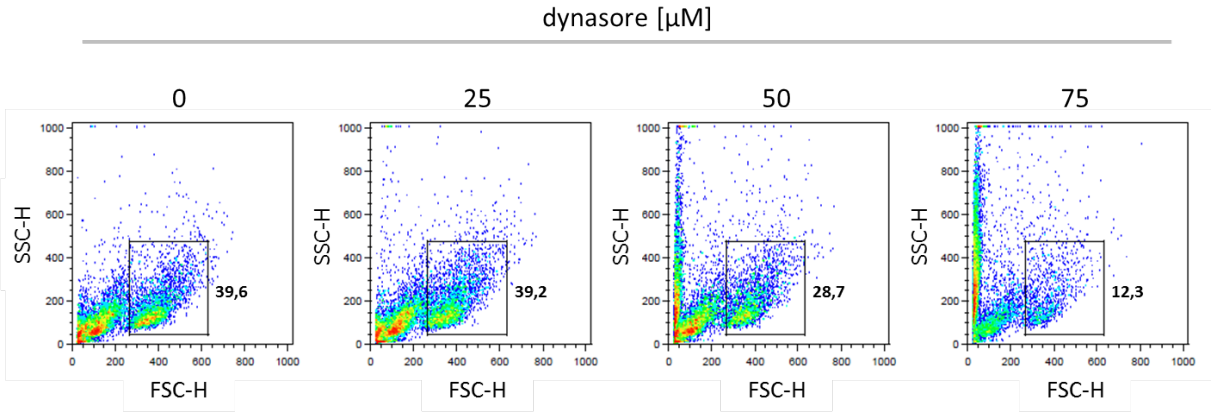

Figure 18 – Dynasore has detrimental effects on morphology of T-REx-293 cells. T-REx-293 cells were incubated for 30 min with increasing amounts of dynasore and analyzed by FACS.

3.2.2.2. Dominant-negative dynamin attenuates transferrin-uptake in T-REx-293 cells

After having observed the desintegrating effect of dynamin-inhibitor dynasore on cellular integrity of T-REx-293 cells a more elaborate approach based on dominant-negative dynamin was performed. Therefore, we utilized the dominant-negative K44A dynamin mutant. To be able to distinguish non-transfected cells from cells transfected with dynamin, a construct was generated that allows simultaneous expression of K44A dynamin and GFP separated by an IRES (internal ribosomal entry site) – K44A dynamin/GFP.

Initially, we tested functionality of dominant-negative dynamin by verification of its inhibitory effect on the dynamin-dependent transferrin-uptake in T-REx-293 cells. First experiments were performed to establish a protocol for the uptake and measurement of endocytosed transferrin in T-REx-293 cells. To determine the time frame in which transferrin-uptake occurs in these cells a time series experiment was performed with an Alexa647-conjugate of transferrin – Alexa647-transferrin (Figure 19A). As evident from the depicted histograms the strongest signal can be detected upon five min of transferrin incubation at 37°C. After 15 min of incubation the signal gets a bit weaker but stays stable till the next measurement 15 min later.

To determine the effect of temperature on transferrin-uptake and preclude false positive signals generated by unspecific binding of transferrin to the cell surface we performed experiments depicted in Figure 19B. T-REx-293 cells were incubated for 10 min on ice before being incubated with Alexa647-transferrin for 30 min on ice. A part of these cells was incubated for further 15 min on ice and washed with PBS or subjected to acid wash to remove unspecifically bound transferrin. Another set of cells was incubated for 15 min at 37°C to allow endocytosis of bound transferrin and was further washed with PBS or acidic glycin buffer to avoid again false positive signals. The left histogram in Figure 19B shows that cells incubated with transferrin at 4°C and washed with PBS generate a strong unspecific signal that can be eliminated to a great extent upon acid wash. Signal that can be detected upon acid wash indicates that endocytosis is not completely abrogated at 4°C or that some residual unspecific binding occurs. The right histogram shows that cells incubated with transferrin at 37°C commit efficient endocytosis with the generated signal being stronger than the residual signal upon incubation at 4°C and acid wash. Whether cells are washed with PBS or are subjected to acid wash does not change signal intensity that obviously completely emanates from endocytosed transferrin.

Finally, we performed transferrin competition experiments on T-REx-293 cells using two fluorescent variants of transferrin – Alexa647- and Cy3-transferrin (Figure 19C). As shown in Figure 19C incubation of cells with Alexa647-transferrin and increasing amounts of Cy3-transferrin leads to a reduction in Alexa647-transferrin-uptake and an increase in Cy3-transferrin-uptake.

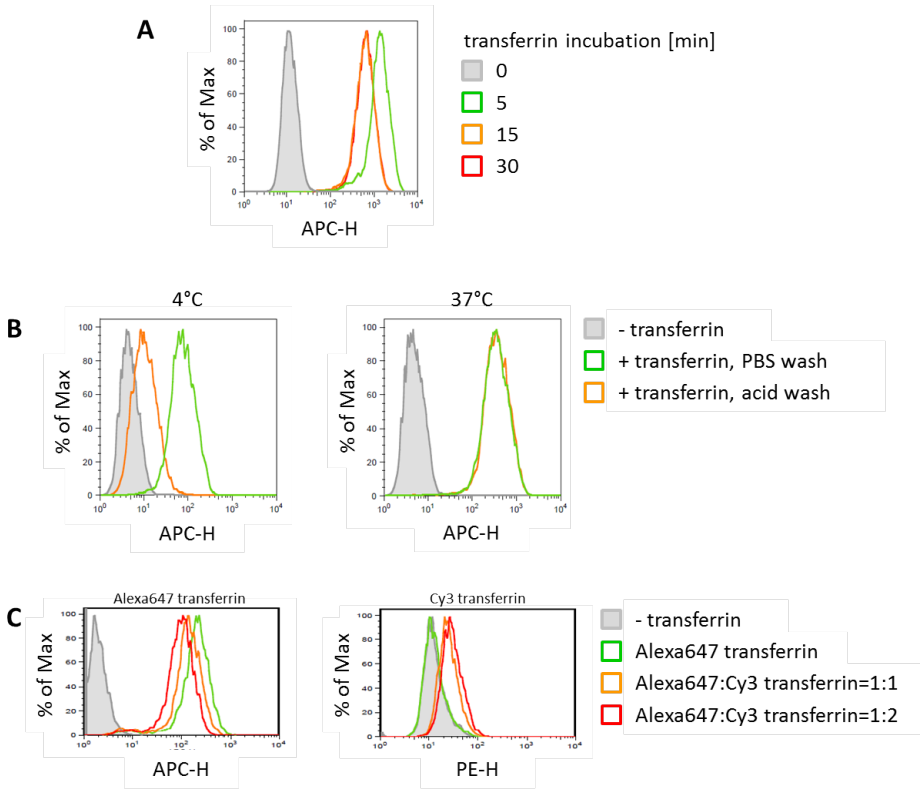

Figure 19 – Analysis of transferrin-uptake in T-REx-293 cells. Alexa647-transferrin was applied at a concentration of 25 µg/ml. **(A)** Time series of transferrin-uptake. T-REx-293 cells were incubated with Alexa647-transferrin at 37°C for the indicated periods of time and transferrin-uptake was assessed by FACS-analysis. **(B)** Dependency of transferrin-uptake in T-REx-293 cells on temperature and prevention of unspecific binding. T-REx-293 cells were incubated for 10 min at 4°C and subsequently incubated with Alexa647-transferrin for 30 min at 4°C. Further on cells were incubated for 15 min at 4°C (left histogram) or 37°C (right histogram) and were subsequently washed with PBS or were subjected to acid wash. Transferrin-uptake was analyzed by FACS. **(C)** Competition of transferrin-uptake in T-REx-293 cells. T-REx-293 cells were incubated for 10 min at 4°C and subsequently incubated with Alexa647-transferrin alone or a mixture of Alexa647-transferrin and Cy3-transferrin at the ratio of 1:1 (25 µg/ml of each) or 1:2 (25 µg/ml Alexa647-transferrin and 50 µg/ml Cy3-transferrin) for 30 min at 4°C. Internalization was carried out at 37°C for 15 min. Uptake of differentially tagged transferrin-conjugates was monitored by FACS-analysis of their fluorescent tag – Alexa647-transferrin-uptake (left histogram), Cy3-transferrin--uptake (right histogram). Cells not incubated with transferrin (filled histograms) serve as a negative control.

After establishing the protocol for analysis of transferrin-uptake in T-REx-293 cells the focus was set on the effect of dominant-negative dynamin on transferrin-uptake in these cells. T-REx-293 cells were transfected with increasing amounts of K44A dynamin/GFP and incubated with Alexa647-transferrin (Figure 20). Figure 20A shows the concomitant increase of the dynamin- and GFP-signal upon transfection of increasing amounts of K44A dynamin/GFP. Transfected cells were analyzed by flow cytometry. As shown in Figure 20B with transfection of increasing amounts of K44A dynamin/GFP more and more counted cells shift to the GFP^+ population and show reduced Alexa647-fluorescence indicating a reduction

in transferrin-uptake. Cells not transfected with dynamin were transfected with a construct encoding IRES-GFP in order to have a GFP^+ population where transferrin-uptake is not perturbed.

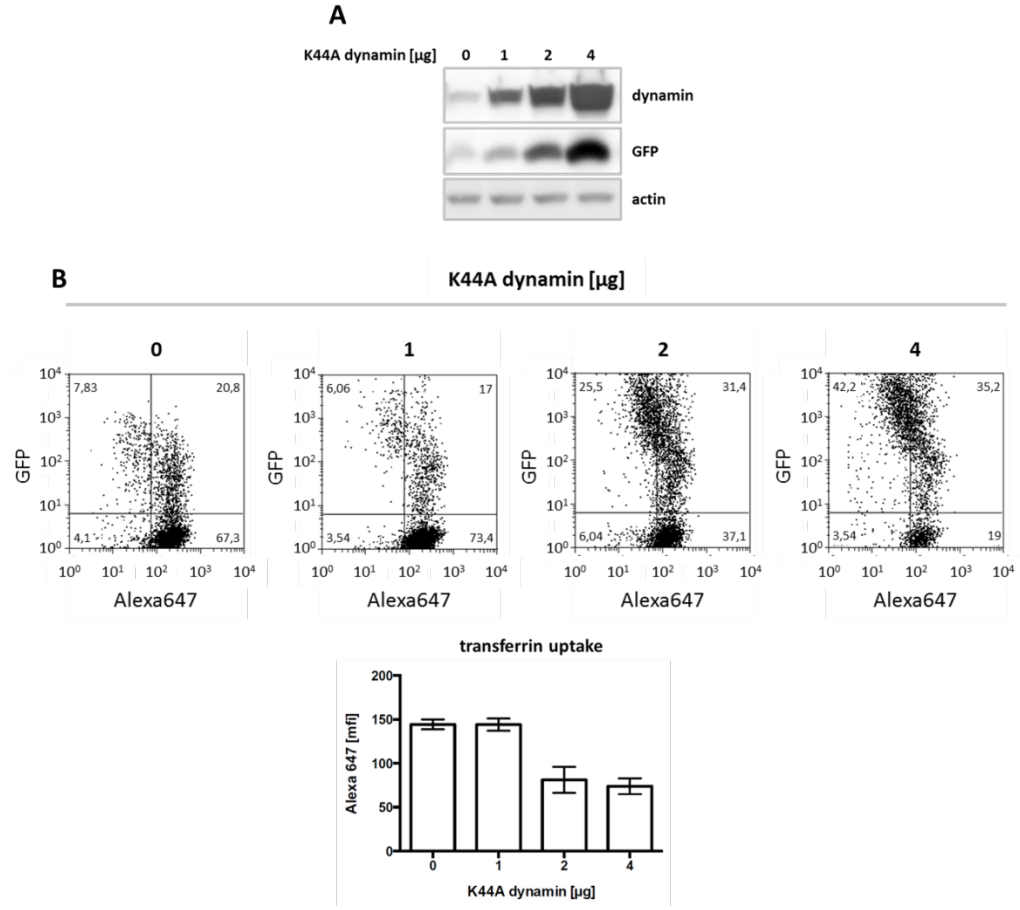

Figure 20 – Effect of dominant-negative dynamin on transferrin-uptake in T-REx-293 cells. (A) and **(B)** T-REx-293 cells were transiently transfected with increasing amounts of an expression vector encoding dominant-negative K44A dynamin and GFP. **(A)** TCLs were analyzed by immunoblotting using Abs against dynamin, GFP and actin as loading control. **(B)** Cells were first incubated for 10 min at 4°C and subsequently incubated with 25 µg/ml Alexa647-transferrin for 30 min at 4°C. Internalization was performed for 15 min at 37°C. K44A dynamin expression and transferrin-uptake were assessed via FACS-analysis (upper panel). Bar charts represent means and standard deviations of the detected Alexa647-signal from three independent experiments (lower panel).

3.2.2.3. Dominant-negative dynamin leads to cell membrane accumulation of WTgp130 and CAgp130 in a dose-dependent manner

In order to analyze the effect of dominant-negative dynamin on ligand-independent endocytosis of WTgp130 and endocytosis of CAgp130, T-REx-293-WTgp130-mCherry and T-REx-293-CAgp130-mCherry were transfected with increasing amounts of K44A dynamin/GFP. Subsequently receptor expression was induced and cells were analyzed by flow cytometry.

GFP$^+$ and therefore dynamin-transfected cells were analyzed with respect to overall and surface receptor expression (Figure 21).

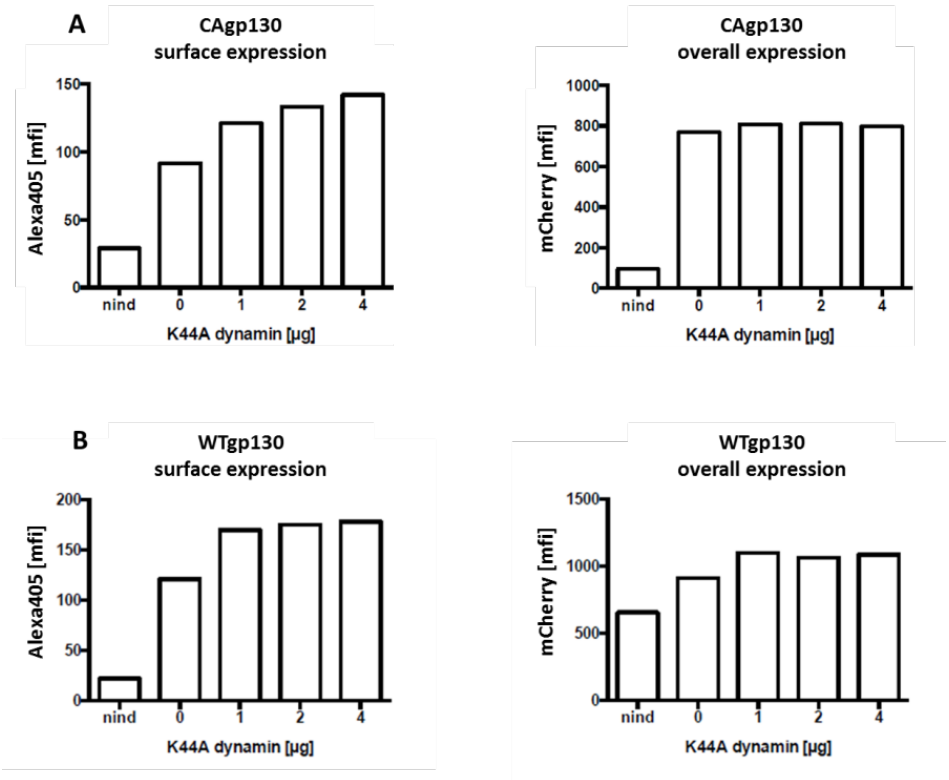

Figure 21 – Effect of dominant-negative dynamin on surface expression of CAgp130 and WTgp130. T-REx-293-CAgp130-mCherry **(A)** and T-REx-293-WTgp130-mCherry **(B)** were transfected with increasing amounts of dominant-negative K44A dynamin. Cells were left untreated (non-induced, nind) or receptor expression was induced with 20 ng/ml dox for 24 h. Overall receptor expression was assessed by FACS-analysis of the fluorescent tag (right panels) and surface receptor expression was verified using the gp130 Ab B-P8 and an Alexa405-labeled secondary Ab (left panels).

Overall receptor expression was verified via the mCherry-tag and surface receptor was monitored using the gp130 Ab B-P8 and an Alexa405-labeled secondary Ab. As shown in Figure 21 overall receptor expression of CAgp130 and WTgp130 is largely unaffected by transfection of dominant-negative dynamin (right diagrams). Non-induced cells serve as a negative control. On the contrary, the amount of cell surface receptor increases with transfection of increasing amounts of K44A dynamin/GFP not only for WTgp130 as expected but also for CAgp130 (left diagrams). This result indicates that CAgp130 gets internalized in a dynamin-dependent way which is blocked by dominant-negative K44A dynamin.

3.2.2.4. Inhibition of endocytosis does not interfere with constitutive signaling

To find out whether inhibition of receptor endocytosis interferes with signaling of CAgp130, TCLs of cells transfected with increasing amounts of K44Adynamin/GFP were subjected to WB-analysis and probed for pSTAT3 (Figure 22). Surprisingly, inhibition of endocytosis does not seem to interfere with constitutive signaling. This result implies that receptor at the cell surface and receptor molecules upon endocytosis do not considerably contribute to signaling of CAgp130 if they contribute at all.

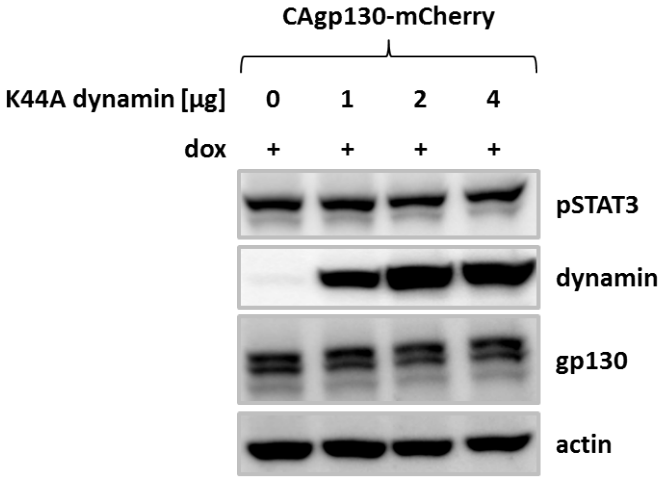

Figure 22 – Effect of dominant-negative dynamin on signaling of CAgp130. T-REx-293-CAgp130-mCherry were transfected with increasing amounts of dominant-negative K44A dynamin. Expression of CAgp130 was induced with 20 ng/ml dox for 24 h. TCLs were analyzed by immunoblotting using Abs against pSTAT3(Y705), dynamin, gp130 and actin as loading control.

3.3. Targeting constitutive signaling emanating from CAgp130

3.3.1. Neutralizing antibodies do not block constitutive signaling

In order to further substantiate the finding that cell surface as well as endocytosed receptor molecules do not essentially contribute to the constitutive activity of CAgp130 we tried to inhibit mutant receptor with antagonistic gp130 Abs. The applied Abs used in this study were developed in previous work by Wijdenes et al. [160] to inhibit the biological activity of distinct IL-6-type cytokines through gp130. Taking into account the recent publication by Sommer et al. [161] where CAgp130 was reported to be inhibited by a gp130 Ab that specifically neutralizes IL-11-signaling, we included the referred Ab B-P4 in our study. In addition we utilized gp130 Abs B-T2 and B-R3. B-T2 was originally shown to downregulate IL-6-induced signaling and proliferation of a human myeloma cell line. B-R3 was shown to downregulate IL-6- as well as IL-11-induced signaling. As mentioned before B-R3 targets domain D2 of gp130 and is not able to bind to CAgp130. Thus it serves in the context of the mutant receptor as a negative control.

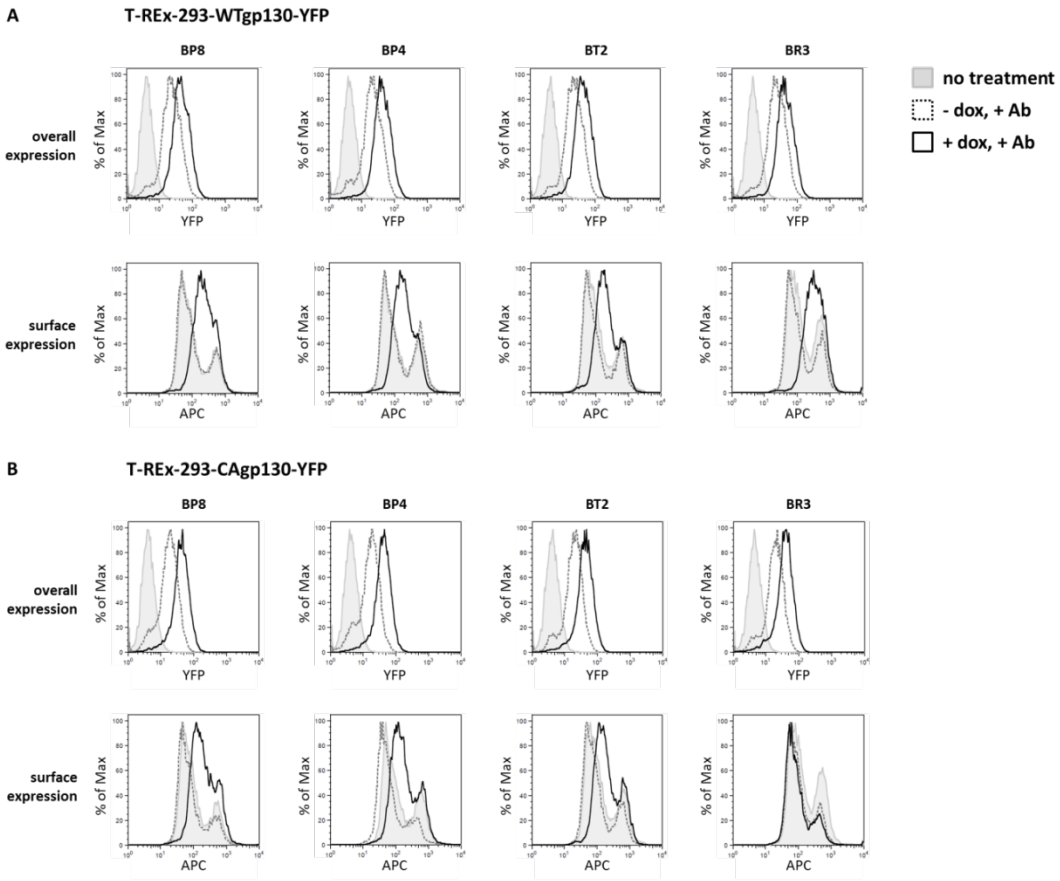

Figure 23 – Binding of neutralizing gp130 Abs to WTgp130 and CAgp130. T-REx-293-WTgp130-YFP (upper panel) and T-REx-293-CAgp130-YFP (lower panel) were left untreated (dotted line) or expression was induced with 20 ng/ml dox for 24 h (solid line). Surface receptor

was stained with gp130 Abs B-P8, B-P4, B-T2 and B-R3 and binding of primary Abs was assessed by an APC-labeled secondary Ab. Non-treated cells (filled histograms) served as negative controls.

T-REx-293-WTgp130-YFP and T-REx-293-CAgp130-YFP were treated with dox to induce receptor expression and were incubated with the given concentrations of Abs B-P4, B-T2 or B-R3. Binding of the Abs was verified by FACS-analysis using an APC-tagged secondary Ab (Figure 23). In order to analyze the inhibitory effect on WTgp130 expressing cells, stimulation was performed with IL-6 and sIL-6Rα. TCLs were subjected to WB-analysis and probed for STAT3-phosphorylation (Figure 24). As shown in Figure 24A IL-6-induced STAT3-phosphorylation can be inhibited by Abs B-T2 and B-R3 and to some extent with Ab B-P4 in a dose-dependent manner. Strikingly there is no effect of any of the neutralizing Abs on STAT3-phosphorylation caused by CAgp130 (Figure 24B).

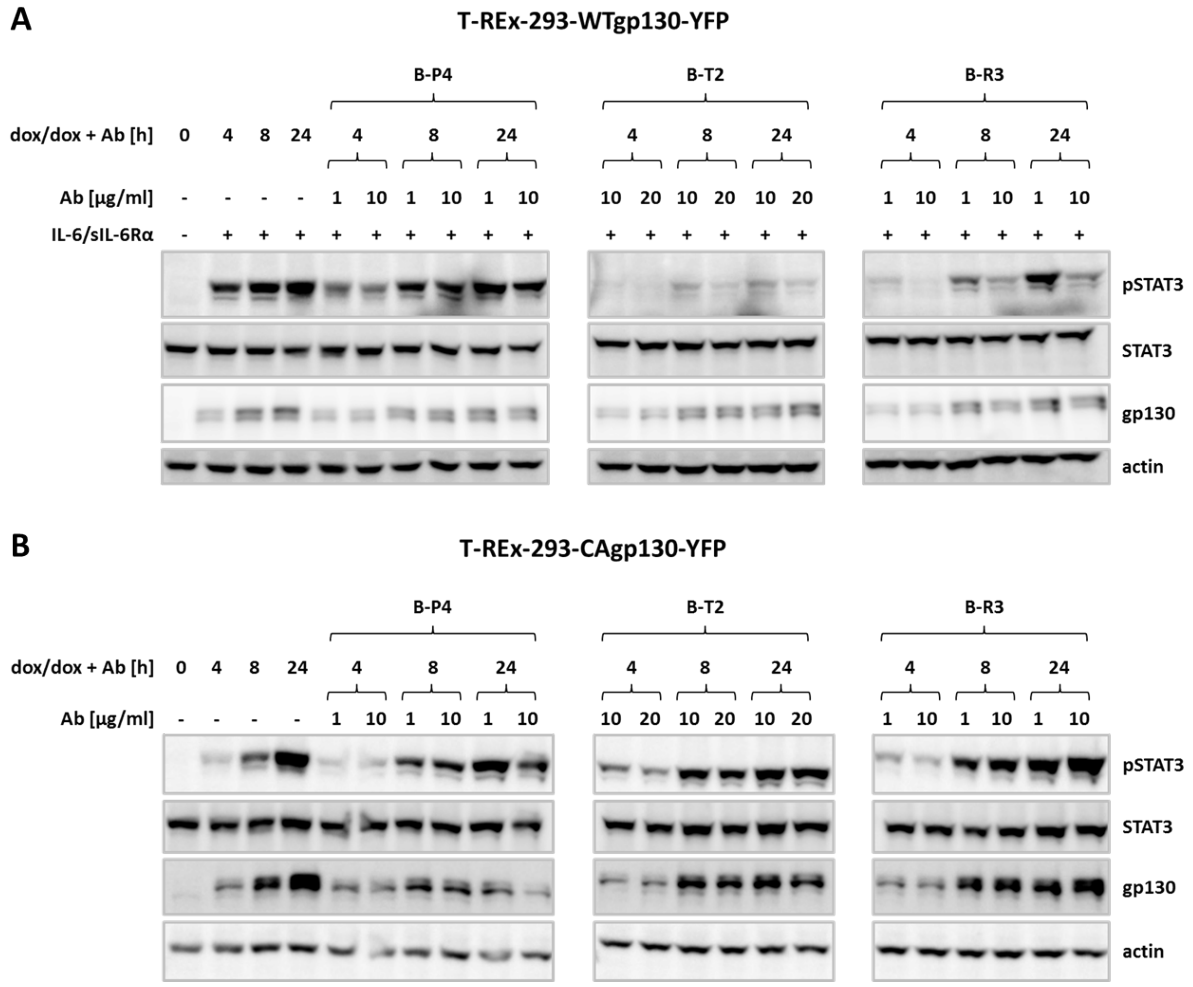

Figure 24 – Effect of neutralizing gp130 Abs on signaling of CAgp130. T-REx-293-WTgp130-YFP **(A)** and T-REx-293-CAgp130-YFP **(B)** were left untreated or expression was induced with 20 ng/ml dox for the indicated periods of time. Cells were simultaneously incubated with indicated amounts of neutralizing gp130 Abs and subsequently stimulated with 200 U/ml IL-6

and 0.5 µg/ml sIL-6Rα for 30 min or left unstimulated. TCLs were analyzed by immunoblotting using Abs against pSTAT3(Y705), STAT3, gp130 and actin as loading control.

3.3.2. Constitutive signaling gets diminished by transfection of a dominant-negative STAT3 mutant

In order to downregulate constitutive STAT3-phosphorylation caused by CAgp130 from within the cell we took advantage of the dominant-negative STAT3-Y705F mutant. STAT3-Y705F impairs WT-STAT3 activity in stimulated cells and was recently reported to act at multiple levels affecting phosphorylation, nuclear translocation and transcriptional activity of WT-STAT3 [162]. Parental T-REx-293 cells and cells inducibly expressing STAT3-Y705F-YFP were transfected with equal amounts of CAgp130-YFP. Upon induction there is an increase in expression of CAgp130 and ligand-independent STAT3-phosphorylation in parental T-REx-293 cells over time (Figure 25). In cells stably transfected with dominant-negative STAT3, expression of transiently transfected CAgp130 as well as STAT3-Y705F-YFP is induced upon dox treatment. STAT3-Y705F-YFP strongly attenuates CAgp130-mediated phosphorylation of endogenous STAT3.

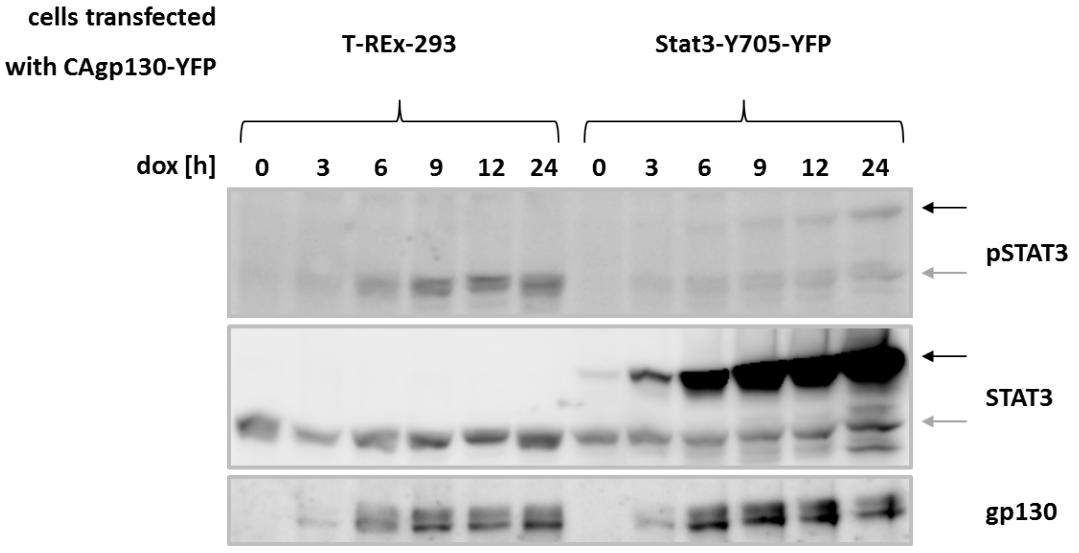

Figure 25 – Effect of dominant-negative STAT3 on signaling of CAgp130. T-REx-293 cells and cells stably transfected with STAT3-Y705F-YFP were transfected with equal amounts of CAgp130-YFP. Expression of CAgp130 or CAgp130 and STAT3-Y705F was induced with 20 ng/ml dox for the indicated periods of time. TCLs were analyzed by immunoblotting using Abs against pSTAT3(Y705), STAT3 and gp130. Black arrows mark induced STAT3-Y705F-YFP and grey arrows mark endogenous STAT3 that serves as loading control.

3.4. The role of SOCS3 in downregulation of ligand-independent signaling originating from CAgp130

As already shown in section 3.1.3.2. CAgp130 leads to a constitutive and ligand-independent activation of STAT3 that translocates into the nucleus and induces expression of several target genes. The most important target gene with immediate consequences for further progression of signaling intensity is the negative feedback inhibitor SOCS3.

In this part of the work the focus was set on the role of SOCS3 that is persistently induced in cells expressing CAgp130. Experiments performed tried to elucidate whether SOCS3 acts through inhibition of kinase activity or if it even functions as an E3-ubiquitin ligase to degrade signaling partners like CAgp130.

3.4.1. SOCS3 mediates its inhibitory effect on CAgp130 via direct kinase inhibition

The primary mechanism of SOCS3 action is via direct inhibition of the catalytic activity of JAKs. In order to reveal whether CAgp130 is sensitive to SOCS3-mediated feedback inhibition two different approaches were taken into consideration. In the first approach we used a mutant of CAgp130 that lacks the SOCS3 recruitment site – CAgp130-Y759F – and therefore should not be inhibited by SOCS3. HEK293 cells were transiently transfected with equal amounts of CAgp130 and its mutant form CAgp130-Y759F.

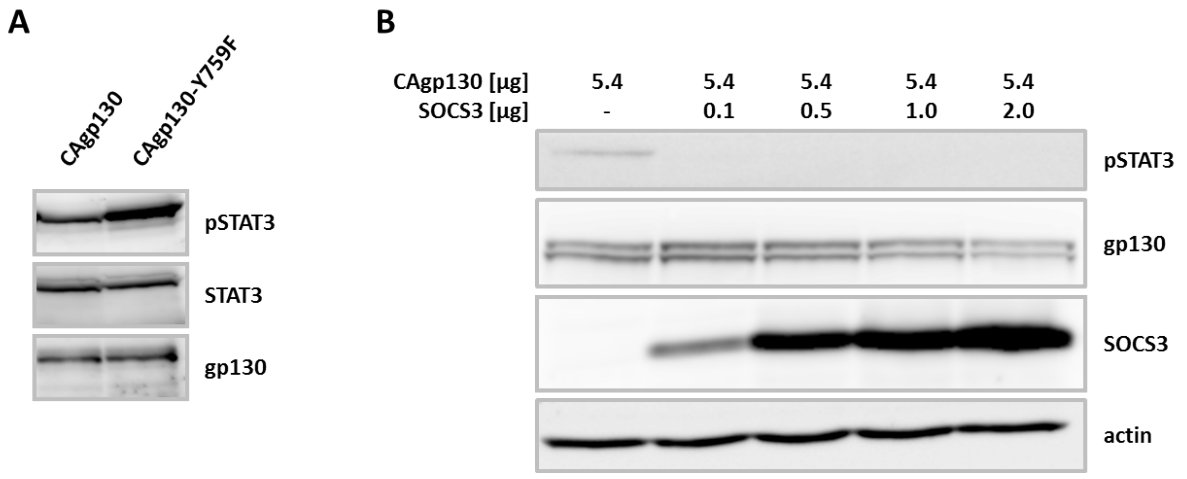

Figure 26 – CAgp130 is sensitive to SOCS3-mediated feedback inhibition. HEK293 cells were transiently transfected with equal amounts of CAgp130-YFP and CAgp130-Y759F-YFP **(A)** or were transiently cotransfected with equal amounts of CAgp130-YFP and increasing amounts of SOCS3 **(B)**. TCLs were analyzed by immunoblotting using Abs against pSTAT3, STAT3 and gp130 **(A)** or pSTAT3, gp130, SOCS3 and actin **(B)**.

As shown in Figure 26A STAT3-phosphorylation caused by CAgp130-Y759F is stronger than the respective signal caused by CAgp130 although cells were transfected with comparable receptor amounts. In the second approach HEK293 cells were cotransfected with equal amounts of receptor and increasing amounts of SOCS3. As evident from Figure 26B already the lowest amount of transfected SOCS3 is much higher than the SOCS3 amount induced by CAgp130 and is able to completely abolish constitutive signaling. Both experiments provide strong evidence that CAgp130 gets feedback inhibited by SOCS3 through direct kinase inhibition. The second approach provides annother interesting finding which is the inverse correlation between SOCS3 and CAgp130. Upon transfection of high amounts of the expression vector encoding SOCS3 the receptor amount decreases. This finding could indicate the negative regulation of the receptor mutant by SOCS3 and brings up its second possible mode of action as an E3-ubiquitin ligase.

3.4.2. SOCS3 mediates lysosomal routing of CAgp130

Besides direct kinase inhibition SOCS3 is believed to act by a second mode of action. This second mode is based on its ability to recruit an E3-ubiquitin ligase complex and thereby induce ubiquitination and degradation of cooperating signaling components.

In order to further verify whether SOCS3 induced by CAgp130 is able to promote downregulation of the receptor the SOCS3 overexpression experiment (Figure 26B) was performed in the context of CAgp130-Y759F that lacks the SOCS3 recruitment site as well as the mutant CAgp130-K648R. The respective Arg-residue within the G-CSF (granulocyte-colony stimulating factor) receptor is the one that gets ubiquitinated by SOCS3 and drives lysosomal routing of the receptor [163]. In analogy to the experimennt in Figure 26B HEK293 cells were cotransfected with equal amounts of receptor and increasing amounts of SOCS3 (Figure 27). In line with previous data overexpression of SOCS3 immediately diminishes constitutive activity of CAgp130 as shown by complete loss of STAT3-phosphorylation. As expected STAT3-phosphorylation caused by CAgp130-Y759F remains largely unperturbed by SOCS3 overexpression. In the case of CAgp130-K648R constitutive activity also gets completely diminished as Y759 recruits SOCS3 that inhibits the associated JAK kinases within its primary mode of action. Verification of the role of SOCS3 as an ubiquitin ligase requires precise analysis of receptor levels. At first sight receptor amounts for CAgp130 and the mutants CAgp130-Y759F and CAgp130-K648R get equally reduced upon coexpression with

SOCS3 (Figure 27A). However, quantification of detected receptor-signal (Figure 27B – upper right panel) reveals that there are clear differences between CAgp130 on the one side and CAgp130-Y759F as well as CAgp130-K648R on the other side regarding changes in receptor levels within the range of 0-1 µg transfected SOCS3-plasmid. The amount of CAgp130 immediately drops upon transfection of 0.1 µg SOCS3. In contrast, the amounts of CAgp130-Y759F and CAgp130-K648R remain stable indicating that both residues – Y759 and K648 – could play a crucial role in SOCS3-mediated receptor degradation.

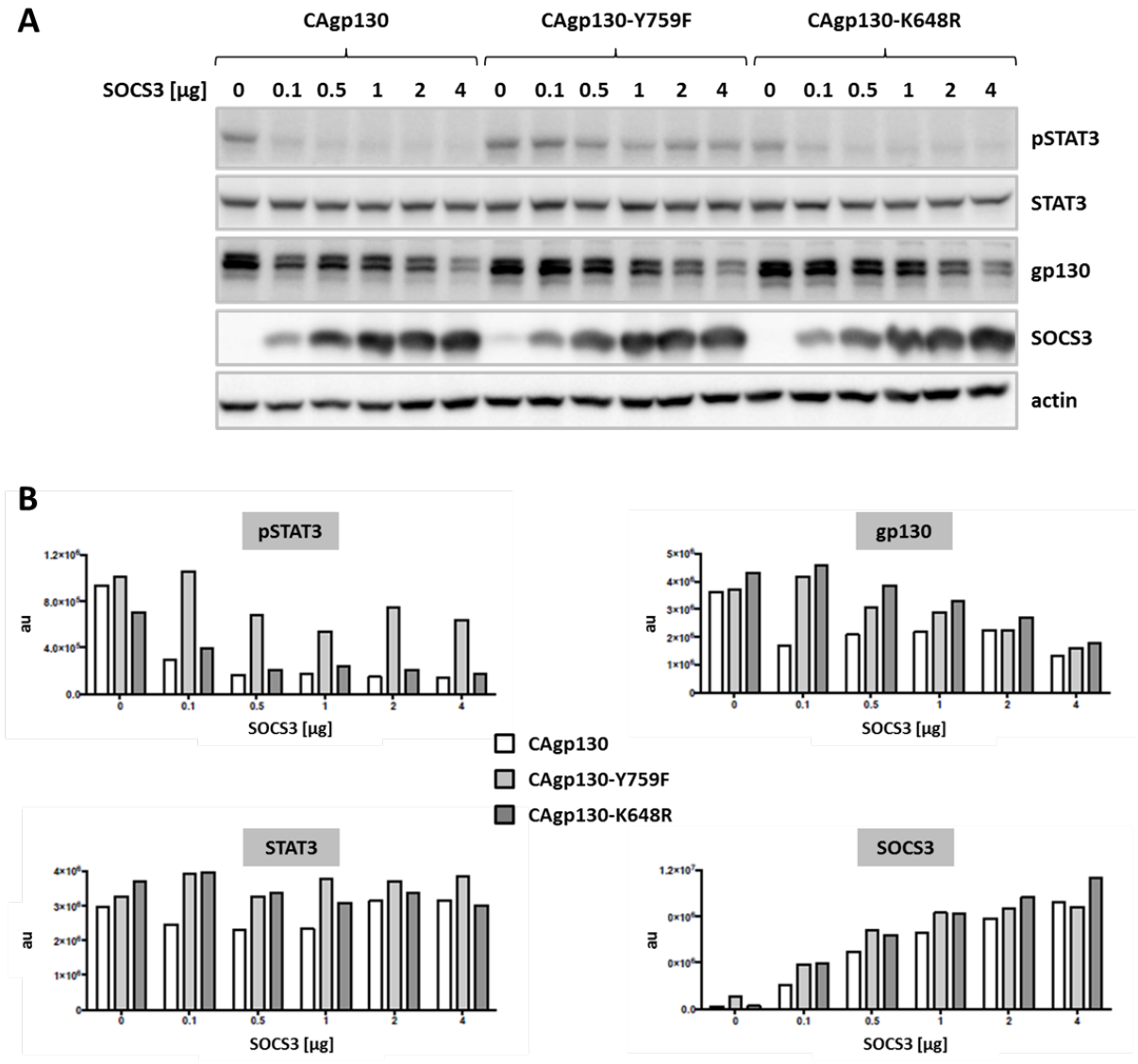

Figure 27 – Residues Y759 and K648 within CAgp130 might play a role in SOCS3-mediated receptor downregulation. (A) HEK293 cells were transiently cotransfected with equal amounts of CAgp130-mCherry, CAgp130-Y759F-mCherry or CAgp130-K648R-mCherry and increasing amounts of SOCS3. TCLs were subjected to immunoblotting using Abs against pSTAT3, STAT3, gp130, SOCS3 and actin as loading control. **(B)** Immunoblotting data from (A) where quantified with MultiGauge and values were normalized to actin. Au – arbitrary unit

To exclude that the drop of receptor levels observed in Figure 27 upon cotransfection of SOCS3 within the range of 2-4 µg was an overexpression artefact, we decided to perform further verification of the degrading properties of SOCS3 with another experimental approach utilizing inhibitors of proteasomal and lysosomal degradation (Figure 28-30).

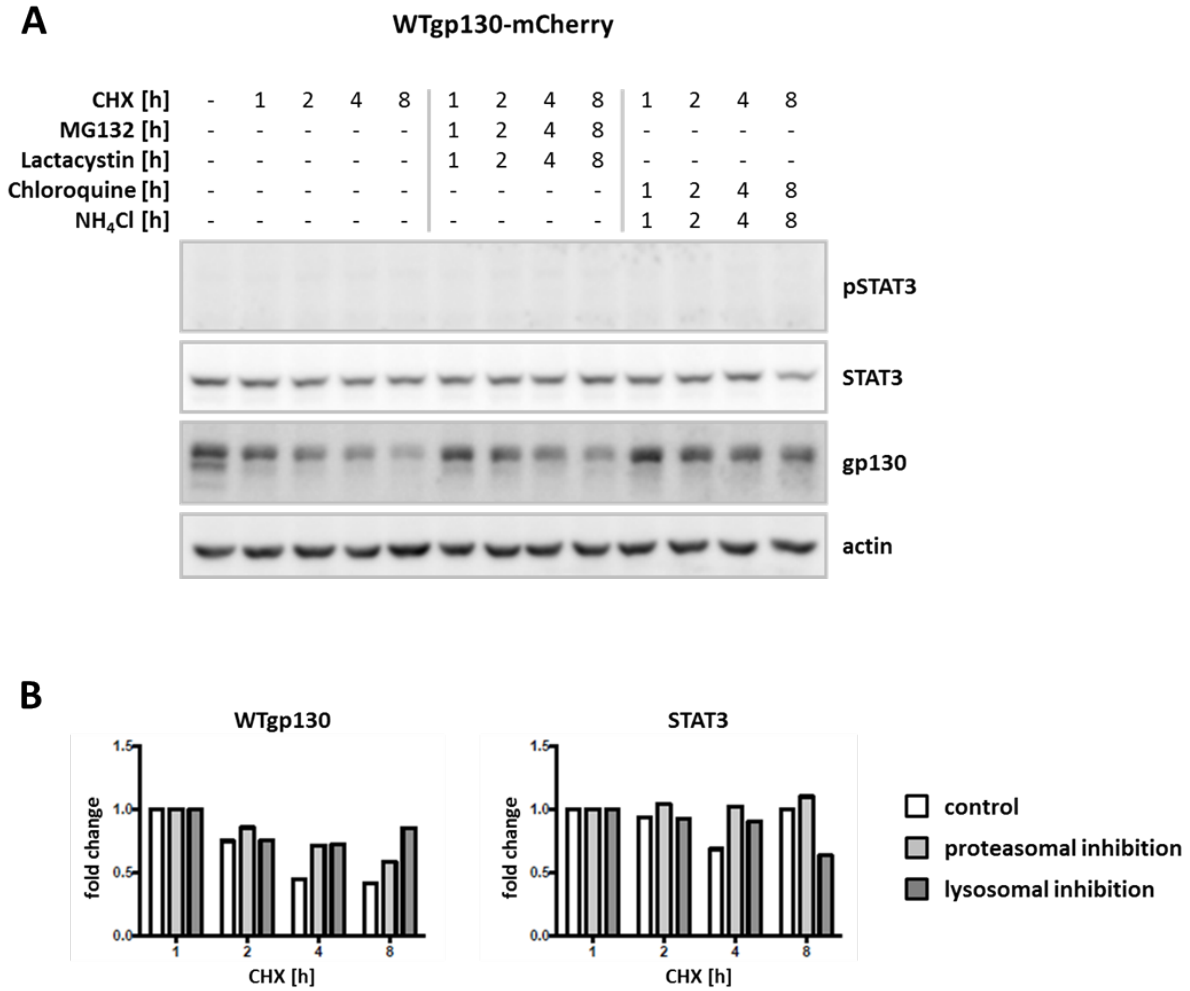

Figure 28 – WTgp130 gets degraded via the proteasomal/lysosomal pathway. (A) T-REx-293-WTgp130-mCherry were treated with 20 ng/ml dox for 24 h. Upon removal of dox cells were either treated with 10 µg/ml CHX alone or coincubated with a combination of CHX and proteasomal or lysosomal inhibitors for the indicated periods of time. MG132 (10 µM) and Lactacystin (5 µM) were used as inhibitors of proteasomal degradation. For inhibition of lysosomal degradation Chloroquin (25 µM) and NH_4Cl (10 mM) were applied. TCLs were analyzed by immunoblotting using Abs against pSTAT3, STAT3, gp130 and actin as loading control. **(B)** Data from (A) were quantified by MultiGauge, normalized to actin and fold changes relative to the 1 h time point were calculated.

The first set of experiments was performed to verify the degradation pathway of unstimulated WTgp130. Receptor expression was induced in T-REx-293-WTgp130-mCherry and upon induction cells were treated with CHX (cycloheximide) to stop protein biosynthesis and inhibitors of proteasomal and lysosomal degradation for up to 8 h. Proteasomal

degradation was inhibited by the use of MG132 and lactacystin. Chloroquine and NH_4Cl were utilized as inhibitors of lysosomal degradation. As shown in Figure 28B (left panel) WTgp130 gets degraded on the proteasomal and lysosomal way without any visible tendency.

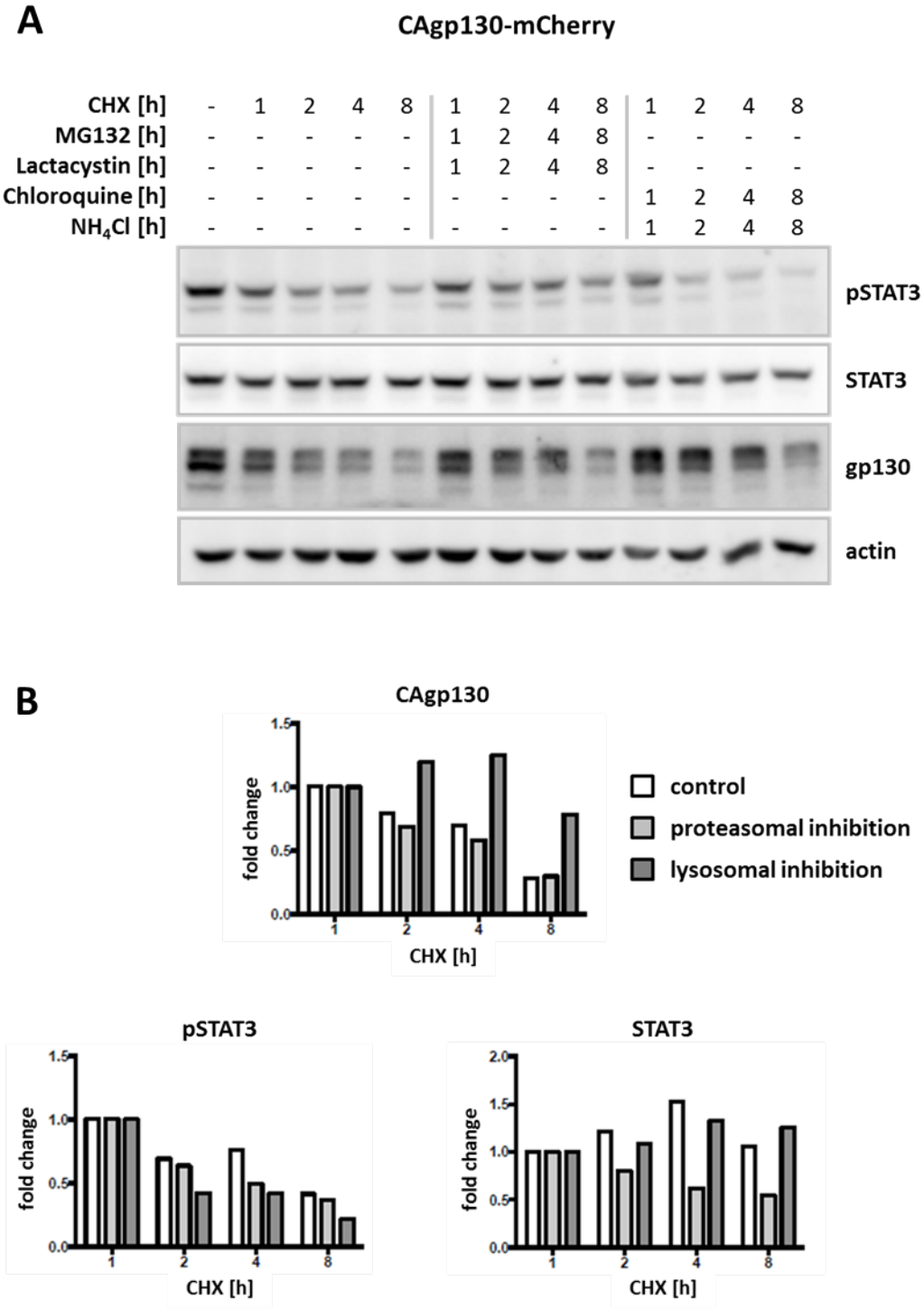

Figure 29 – Degradation of CAgp130 occurs via the lysosomal pathway. (A) T-REx-293-CAgp130-mCherry were treated with 20 ng/ml dox for 24 h. Upon removal of dox cells were either treated with 10 µg/ml CHX alone or coincubated with a combination of CHX and proteasomal or lysosomal inhibitors for the indicated periods of time. MG132 (10 µM) and lactacystin (5 µM) were used as inhibitors of proteasomal degradation. For inhibition of lysosomal degradation chloroquine (25 µM) and NH_4Cl (10 mM) were applied. TCLs were

analyzed by immunoblotting using Abs against pSTAT3, STAT3, gp130 and actin as loading control. **(B)** Data from (A) were quantified by MultiGauge, normalized to actin and fold changes relative to the 1 h time point were calculated.

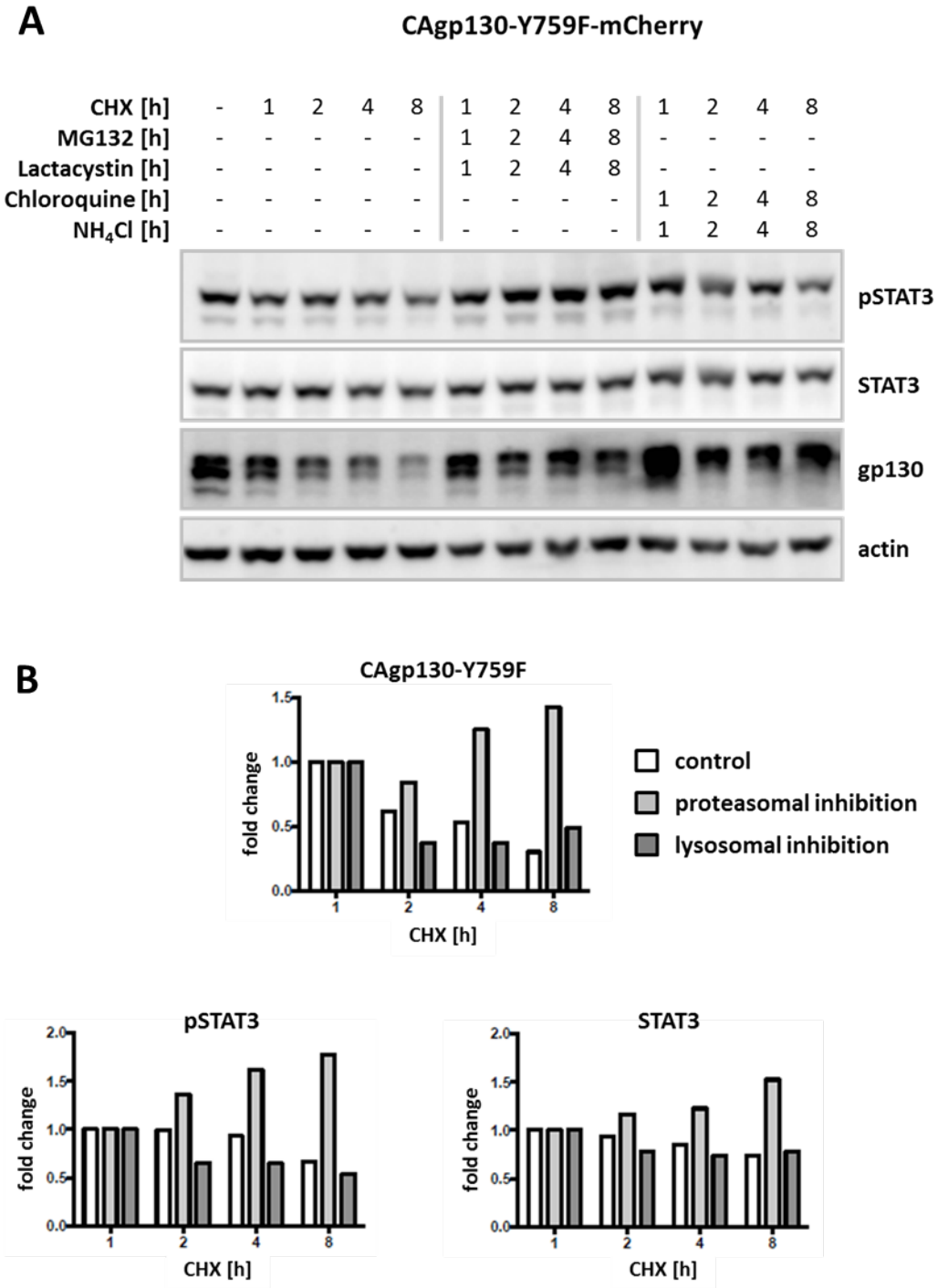

Figure 30 – Degradation of CAgp130-Y759F shifts to the proteasomal pathway. (A) T-REx-293-CAgp130-Y759F-mCherry were treated with 20 ng/ml dox for 24 h. Upon removal of dox cells were either treated with 10 µg/ml CHX alone or coincubated with a combination of CHX and proteasomal or lysosomal inhibitors for the indicated periods of time. MG132 (10 µM) and lactacystin (5 µM) were used as inhibitors of proteasomal degradation. For inhibition of lysosomal degradation chloroquine (25 µM) and NH_4Cl (10 mM) were applied. TCLs were analyzed by immunoblotting using Abs against pSTAT3, STAT3, gp130 and actin as loading control. **(B)** Data from (A) were quantified by MultiGauge, normalized to actin and fold changes relative to the 1 h time point were calculated.

The same experiment performed with cells stably expressing CAgp130 (Figure 29) revealed that levels of the receptor mutant get stabilized by inhibitors of lysosomal degradation meaning that CAgp130 gets preferentially degraded over the lysosomal pathway.
Even more interesting are the results from this experiment in the context of the CAgp130-Y759F mutant (Figure 30). In contrast to CAgp130, degradation of CAgp130-Y759F is sensitive to inhibitors of proteasomal degradation. Both receptors – CAgp130 and CAgp130-Y759F – just differ from each other regarding the SOCS3 recruitment site at Y759 but show deviating degradation fates.
All together these results point to a possible role of SOCS3 in degradation of CAgp130.

3.5. Generating a transgenic mouse model for CAgp130

In order to investigate the tumorigenic potential of CAgp130 *in vivo*, first steps were taken for generation of a transgenic mouse model. Constructs were designed in cooperation with Professor Dr. Christian Trautwein and Dr. Wei Hu of the Department of Internal Medicine III at the University Hospital, RWTH Aachen. In order to facilitate the inducible expression of the receptor mutant the Cre/loxP system was utilized. As apparent in Figure 31A the loxP sites frame the cDNA encoding GFP. Upon retroviral transfection of a Cre recombinase the GFP is being removed and the constitutive CAG promotor drives expression of the mCherry-tagged CAgp130.

In order to verify the Cre/loxP system before starting the transgenic animal approach the expression cassette depicted in Figure 31A was cloned into the pcDNA5 backbone. The resulting plasmid was transiently transfected in HEK293 cells with or without a plasmid encoding the Cre recombinase. TCLs of transfected cells (Figure 31B) as well as the transfected cells themselves (Figure 31C) were analyzed by WB and confocal microscopy respectively. As apparent in Figure 31B cells that are transfected with the CAgp130 encoding plasmid alone do not show any signal neither for the receptor nor its fluorescent tag. A signal for CAgp130 as well as mCherry is first detected upon cotransfection of the Cre recombinase. The GFP-signal does not completely disappear upon cotransfection as the experiment was performed in the mode of transient transfection and not every cell transfected with the CAgp130 encoding plasmid necessarily receives the plasmid encoding

the Cre recombinase. The observations made in the-WB analysis can be partially confirmed by confocal microscopy (Figure 31C). Upon transfection of the Cre recombinase the mCherry-signal representing CAgp130 emerges. Some of the cells depicted show GFP- as well as mCherry-signal and appear yellowish in the merge picture. These cells represent an intermediate state with some of the transfected receptor encoding plasmids having been targeted by the recombinase and others remaining intact.

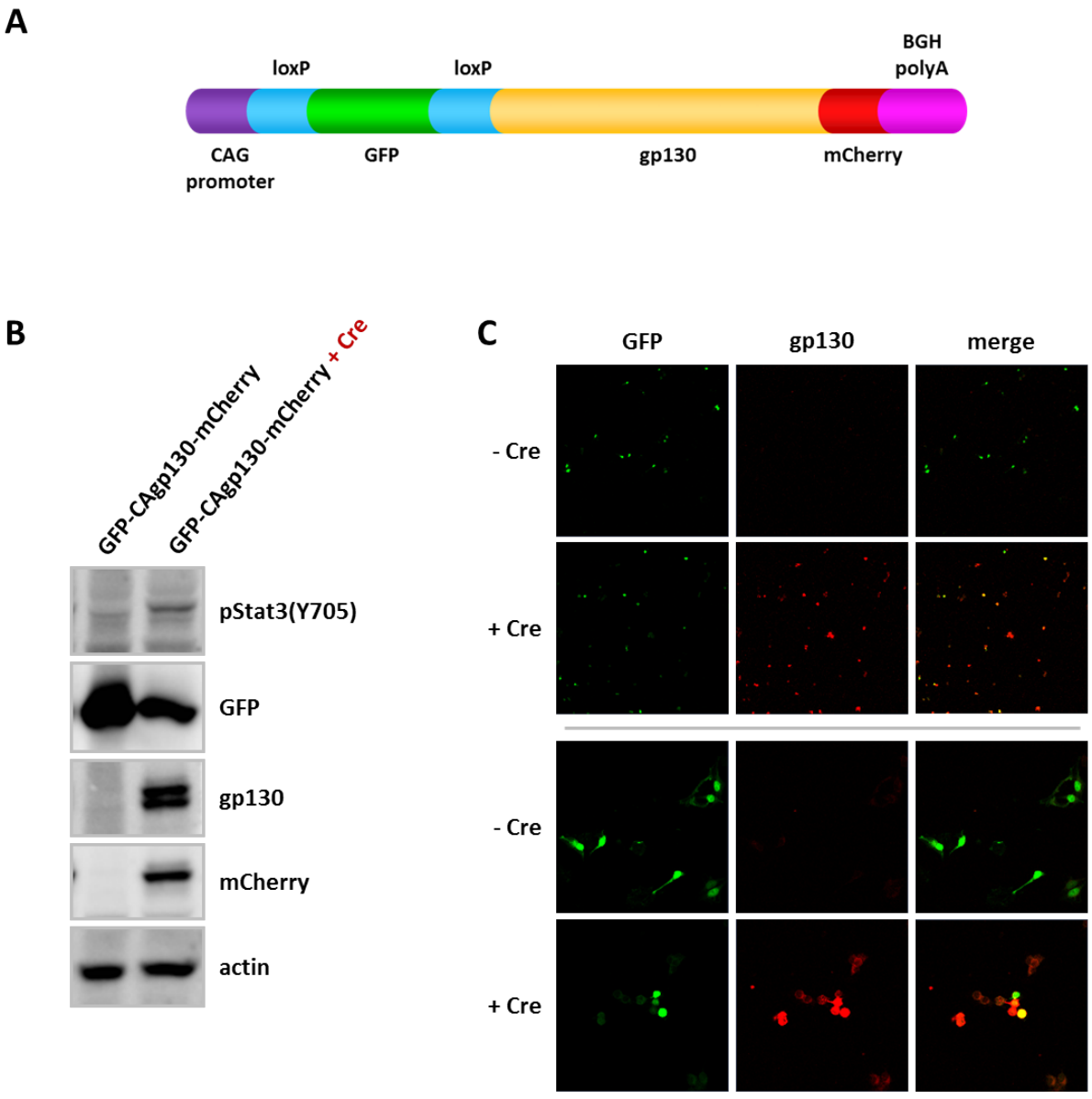

Figure 31 – Verification of the Cre/loxP system for generation of a transgenic mouse model for CAgp130. (A) Schematic representation of the CAgp130 encoding expression cassette used for generation of transgenic mice. **(B)** and **(C)** HEK293 cells were transiently transfected with the receptor encoding plasmid alone or were contransfected with the receptor encoding plasmid and a plasmid encoding the Cre recombinase. TCLs were analyzed by immunoblotting using Abs against pSTAT3(Y705), GFP, gp130, mCherry and actin as loading

control **(B)**. Transfected cells were fixed and GFP- as well as mCherry-fluorescence was analyzed by confocal microscopy **(C)**.

4. Discussion

Short in-frame somatic deletions within the *IL-6ST* gene encoding gp130 are found in 60% of IHCAs. The deletions are localized within domain 2 of the CBM and target the interaction site of gp130 and IL-6. They render gp130 constitutively active and lead further downstream to a constitutive and ligand-independent activation of STAT3 as well as induction of the feedback inhibitor SOCS3 and acute phase genes like CRP and SAA2 [133].

Despite the fact that IHCAs are benign liver tumors, activating gp130 mutations cannot be readily assessed as harmless as there is a serious risk of bleeding and malignant transformation when they coincide with certain mutational hits. According to a recently published time frame of mutations occuring during malignant progression of HCAs, mutations within gp130 appear in the classical HCAs but also play a crucial role in the transformation process when combined with activating mutations within β-catenin [132].

In this work the focus was set on elucidating the trafficking and signaling of constitutively active gp130 and understanding its regulation. For this purpose the most potent and second most frequent of the activating deletion mutants of gp130 was cloned and expressed as a fluorescent fusion protein in a stable and inducible cell system. The results may be of significance for the development of therapeutic approaches.

4.1. Constitutive activation of CAgp130 leads to defects in glycosylation and trafficking

Among the most important cotranslational and post-translational modifications that are performed within the ER is the N-linked glycosylation as it occurs for gp130. The process of N-linked glycosylation begins with the addition of a preformed oligosaccharide precursor comprising three glucose, nine mannose and two N-acetylglucosamine molecules to an Asn-residue on a nascent protein. Substrates for this reaction that is catalyzed by the oligosaccharide-protein transferase are Asn-residues within the tripeptide sequences Asn-X-Ser and Asn-X-Thr. In the case of gp130 there are 11 potential glycosylation sites out of which nine are glycosylated [41]. In a series of reactions catalyzed by three different enzymes all three glucose-residues and one particular mannose-residue are removed within the ER. The remaining high-mannose form of the protein gets transported to the cis Golgi by the use of COP(coat protein complex)II vesicles and is further processed by enzymes

localized sequentially along the cis, medial and trans Golgi compartment to a complex glycosylated form. The high-mannose character of the protein gets definitely lost in the medial Golgi upon removal of five mannose and addition of three N-acetylglucosamine molecules. From this point on the glycoprotein is no longer susceptible to Endo H digestion as the enzyme exclusively removes high-mannose N-linked oligosaccharides.

As a typical glycoprotein gp130 undergoes the glycosylation process along the ER-Golgi axis before reaching the cell membrane and has been described in the past to be detected as a double band [40]. This observation can be reproduced in this work for stably expressed YFP-tagged gp130 (Figure 3A), as well as mCherry-tagged (Figure 28) and non-tagged receptor (Figure 8). The lower band represents the high-mannose receptor form that is shifted upon Endo H digestion (Figure 3B) and mainly resides within the ER and cis Golgi. The higher band is generated by complex glycosylated gp130 that has reached the cell membrane and is not sensitive to Endo H treatment. For WTgp130 the complex glycosylated form is much more prevalent in comparison to the high-mannose form (e.g. Figure 3) meaning that a predominant portion of expressed receptor molecules finds its way to the cell membrane.

Similar to WTgp130 the constitutive mutant CAgp130 is also detected as a double band whether it is expressed as a fluorescent fusion protein (Figures 3A and 29 for the YFP- and mCherry-tagged receptor respectively) or not (Figure 8). However, there is a striking difference concerning the distribution of receptor molecules between the high and low glycosylated form in comparison to WTgp130. The ratio of both forms is virtually reversed for CAgp130 with the receptor mutant being much more prevalent in its high-mannose form (e.g. Figure 3). This observation leads to the conclusion that CAgp130 is probably retained within its processing route and resides to a great extent within the ER and cis Golgi.

The observation that a great portion of CAgp130 is not completely processed and subsequent conclusion concerning its cellular distribution are in line with the data provided by confocal microscopy. Both – WTgp130 and CAgp130 – do not show the membrane-bound distribution that is expected from receptors (Figure 1). This can be assigned to the fact that both receptors are expressed as mCherry-tagged fusion proteins and are therefore detectable before reaching the cell membrane. Probably the signal of membrane-bound receptor gets lost beside the much stronger signal generated by fluorescent receptor molecules that are constantly synthesized and transported to the cell membrane. This strong background signal makes confocal imaging unsuitable to analyze differences in cell

membrane localization of both receptors. The most useful information is provided by the intensity profiles that are depicted next to the confocal images (Figure 1) and demonstrate that WTgp130 is evenly distributed throughout the cell whereas CAgp130 strongly accumulates within intracellular structures. As the predominant part of CAgp130 is detected in its high-mannose form these intracellular structures probably represent to a great extent the first half of the processing route including the ER and cis Golgi. This conclusion is in line with recently published data from Schmidt-Arras et al. who showed that mutant receptor colocalizes strongly with a CFP-tagged ER-marker, colocalization with a CFP-tagged Golgi-marker, however, is much weaker [164]. Furthermore, this study provided convincing data on the colocalization of CAgp130 with Rab5a that is a marker for early endosomes.

In order to draw a more quantitative conclusion on the relative amounts of WTgp130 and CAgp130 present at the cell membrane flow cytometry was performed. Flow cytometry provides the great advantage of monitoring the overall receptor amount (using its fluorescent tag) and the amount of receptor at the plasma membrane (using antibodies against the extracellular part of the receptor) at the same time. As apparent in Figure 2A WTgp130-mCherry and CAgp130-mCherry are induced to a comparable extent with a nearly 3fold induction of the mCherry-signal for both. However, the amount of WTgp130 that reaches the cell membrane is much higher than the amount of CAgp130. The differences in cellular distribution are depicted in the lower ratio of surface to overall receptor expression that is calculated for CAgp130 compared to WTgp130. The lower ratio for the mutant receptor is not an artefact generated by the specific fluorescent tag as the difference to WTgp130 remains and is even more pronounced when the same experiment is performed with the YFP-tagged receptor variants (Figure 2B). YFP is a GFP variant and can be considered as a completely different tag than mCherry.

In order to explain the differences in glycosylation and maturation of WTgp130 and CAgp130 it is important to clarify that both receptors are identical concerning the available glycosylation sites as the deletion of residues 186-190 within the receptor mutant does not lead to loss of any of the existing Asn-residues.

Similar to CAgp130 several constitutively active RTKs (receptor tyrosine kinases) such as FLT3-ITD and constitutively active Kit have been reported to show incomplete glycosylation and impaired cell surface expression. For these RTKs defects in maturation were linked to constitutive kinase activity and receptor-phosphorylation itself [165]. A role of receptor-

phosphorylation can be outruled in the case of CAgp130 as a receptor mutant where all cytoplasmic Tyr-residues are mutated to Phe-residues and therefore cannot be phosphorylated anymore does not show any difference in its overall and particularly in its cell surface expression (Figure 12A).

Most likely the deletion itself causes conformational changes within the newly synthesized receptor that interfere with efficient glycosylation. Indeed, it was recently published that the deletion within CAgp130 destabilizes the EF loop within domain 2 and disrupts hydrophobic interactions within the interface of domains 2 and 3 of the receptor thereby confering constitutive activity within a homodimer [166]. As a result, glycosylation sites that are important for correct folding become unaccessible for the respective glycosylating enzymes.

As a consequence of incomplete glycosylation the receptor mutant is predestined to enter the ER quality control where it is retained and repaired or degraded. In general N-linked glycosylation has been described to be important for the correct folding and stability of several proteins [167]. Here N-glycans act as chaperones that mask hydrophobic residues, increase the solubility and thereby ensure correct folding. Correctly folded proteins are further processed in the Golgi, whereas misfolded ones enter the ER quality control. Within this system proteins are reglucosylated and a further misfolding is prevented by the two related lectins calnexin and calreticulin [168]. An interaction with calnexin could already be confirmed for CAgp130 [164] placing the receptor in the middle of ER quality control. Dissociation of the glycoprotein from the calnexin-calreticulin system is mediated by glucosidase II. As a result of several glucosylation and deglucosylation cycles a glycoprotein is released when having aquired its native conformation or is targeted for degradation through the proteasome. This option is mediated by interaction with the EDEM (ER degradation-enhancing α-mannosidase-like protein) protein that further initiates the ERAD (ER associated degradation) response. In the case of CAgp130 our findings argue against an entry into the ERAD response as the receptor shows a rather lysosomal than proteasomal degradation (Figure 29).

A further control mechanism that is activated upon accumulation of misfolded proteins within the ER is the UPR (unfolded protein response) [169]. The UPR is established amongst others by induction of the chaperone BiP (binding immunoglobulin protein). CAgp130 does not induce BiP and therefore does not activate the UPR (data not shown).

Taken together these data suggest that CAgp130 has an intrinsic glycosylation defect that captures a major part of the receptor within the ER quality control. A smaller portion of synthesized receptor gets repaired and further processed in the Golgi to finally reach the cell membrane. Accumulation of misfolded receptor in the ER does not activate the ERAD response or UPR.

4.2. The reduced cell surface expression of CAgp130 explains the partial activation of the Jak/Erk pathway

Among the initial foci of this work was to investigate the signaling properties of CAgp130 and reveal possible deviations in comparison to signaling emanating from WTgp130.

As already mentioned in sections 1.2.4. and 1.2.5. IL-6-induced signal transduction gets initiated by the formation of the hexameric IL-6/IL-6Rα/gp130 complex. In this complex Jaks that are attached to the cytoplasmic part of the receptor first activate each other and subsequently phosphorylate the receptor.

As apparent in Figure 4 endogenous gp130 as well as stably expressed WTgp130-YFP get phosphorylated upon stimulation with IL-6 and IL-6Rα. In contrast, CAgp130-YFP is phosphorylated without any stimulus applied to the cells. For the induced WTgp130 only the upper band gets phosphorylated. This finding is not very surprising as only mature receptor molecules reach the cell membrane where they can respond to the exogenous stimulus. For CAgp130, however, it seems to be the lower glycosylated form of the receptor that is phosphorylated. This finding is a first hint that incompletely glycosylated and therefore intracellularly retained receptor is activated before reaching its actual destination – the cell membrane. This finding further implies that mutant receptor associates with the Jak kinases and homodimerizes in an early stage of its biosynthesis. Common for both receptors is that their induction leads to a decrease in the phosphorylation of endogenous gp130 upon stimulation. A possible explanation for this reduction might be the amount of Jaks that are available for receptor-phosphorylation. Upon receptor induction endogenous and induced receptor molecules – with the second ones being present to a much higher extent – compete for a limited pool of Jaks. In the context of IL-6-signaling and for constitutive signaling by CAgp130 Jak1 is the main activating kinase [47],[134].

Besides being constitutively phosphorylated itself, CAgp130 is able to cause a stimulus-independent and full-fledged activation of the Jak/STAT pathway. This becomes apparent from the phosphorylation of STAT3 at Y705 as well as its phosphorylation at S727 (Figure 5A) both of which in combination have been reported to be required for maximal transcriptional activation of STAT3 target genes [70]. Whether the Ser-phosphorylation of STAT3 might perform any non-canonical function within mitochondria as reported before [71],[72] has not been assessed in this work. Beyond STAT3, STAT1 is the second STAT factor that gets recruited to WTgp130 upon IL-6 stimulation. STAT1 binds to a more restricted consensus sequence corresponding to the two most membrane-distal Tyr-residues within gp130 [63]2. Nevertheless it shows a clear phosphorylation at Y701 that recurs in the context of CAgp130 upon its induction (Figure 5A). According to the nucleus-cytosol fractionation depicted in Figure 5B, STAT3 activated by CAgp130 translocates into the nucleus with comparable efficacy to STAT3 activated upon stimulation of WTgp130 providing evidence that nuclear import of STAT3 remains unaffected by possible downstream effects of constitutive signaling.

The second most important signaling pathway activated by IL-6 is the Jak/Erk pathway. In contrast, to the Jak/STAT pathway that is activated in its full length by CAgp130 the Jak/Erk pathway just exhibits a partial activation upon induction of the mutant receptor (Figure 7). The first component of this pathway subsequent to the receptor, the phosphatase SHP2, gets strongly phosphorylated upon induction of CAgp130. However, the Erk kinase that proceeds within the pathway later on remains largely unaffected showing just a weak if any activation at all. Fact is that SHP2 that initiates the Jak/Erk pathway and SOCS3 that acts as a feedback inhibitor in the Jak/STAT pathway get recruited to the same Tyr-residue of gp130 at position 759. A possible competitive role of SOCS3 towards SHP2 in the context of CAgp130, however, can be immediately outruled due to detection of the activating SHP2-phosphorylation. A more probable explanation for the partial activation of the Jak/Erk cascade by CAgp130 is based on the limited spatial availability of components of this cascade at intracellular membranes. The adaptor protein Gab1 is necessary for activation of the MAPK cascade upon stimulation with several cytokines such as IL-6 and EGF (epidermal growth factor). Gab1 gets recruited to the plasma membrane via its PH-domain and this recruitment was reported to be mandatory for its activation [170], making activation of the Jak/Erk cascade to a process strictly limited to the plasma membrane. This finding in

combination with the low receptor amount on the cell surface can possibly explain this unexpected result. Similar observations on spatial regulation of receptor activity were made in the case of FLT3-ITD [171]. Targeting of FLT3-ITD to the plasma membrane actually reversed its signaling activity strongly activating MAPK and PI3K pathways and diminishing STAT5-activation. The observation of a partial activation of the MAPK pathway goes in line with the finding that CAgp130 is not able to activate the PI3K/Akt pathway (Figure 10) – a pathway also dependent on the cell membrane localization of its components (see section 1.2.5.3.). However this finding has to be seen in relative terms as activation of the PI3K/Akt pathway has been described to be cell type specific [62] and HEK293 cells belong to the ones that do not activate it upon IL-6 stimulation as apparent in Figure 10.

In order to confirm the unexpected findings on partial activation of the Jak/Erk pathway and even go a step further analyzing the contribution of the single Tyr-residues within the cytoplasmic part of CAgp130 to constitutive signaling, add-back mutants were generated. Within these add-back mutants, single Tyr-residues are available allowing a precise assignment of constitutive signaling activity. As shown in Figure 12A overall and surface expression of CAgp130 remain unperturbed for each of these add-back mutants as well as for the receptor mutant where all Tyr-residues have been mutated. As mentioned in the section before these data confirm that the phosphorylation state of CAgp130 does not influence its predominant intracellular localization. Furthermore, activation of STAT3 can be readily assigned to the four most membrane-distal Tyr-residues (Figure 12B) as has been described for WTgp130 upon stimulation [63]. Interestingly, the STAT3-activation that is partially achieved by the add-back mutants is stronger that the one triggered by CAgp130 itself. A possible reason for this fact could be that add-back mutants that activate STAT3 lack Y759 and hence feedback inhibition through SOCS3. Similar to STAT3, STAT1 seems also to get activated by the four most membrane-distal Tyr-residues of gp130 (Figure 12B). This observation is not completely in line with published data that describe the two most membrane-distal Tyr-residues of gp130 as STAT1 recruitment sites [63]. This finding might be the result of receptor overexpression. As shown in Figure 12C SHP2 activation can be definitely assigned to Y759 as described for WTgp130 [73], whereas activation of Erk is much too weak to be detected. Data on SHP2-activation further imply that there could be some degree of competition between SHP2 and SOCS3 towards binding to Y759. The add-back mutant where Y759 is the only available Tyr-residue causes a stronger SHP2-phosphorylation

compared to CAgp130 itself. According to a possible scenario in cells transfected with this add-back mutant which is not able to activate STAT3 and induce SOCS3 anymore, the respective Tyr-residue can be completely engaged by SHP2 and lead to a stronger SHP2-phosphorylation.

Taken together these data demonstrate that CAgp130 leads to a full activation of the Jak/STAT pathway but just partially activates the Jak/Erk pathway. Changes in receptor-phosphorylation do not have any impact on its cellular distribution and the functional assignment to single Tyr-residues is almost identical between WTgp130 and CAgp130. These findings are once again no artefact generated by the fluorescent tag of the receptor as their main aspects could be reproduced with non-tagged variants of the receptor as apparent in Figure 8. Furthermore, these data outrule the possibility of Erk being the kinase responsible for Ser-phosphorylation of STAT3 [7].

4.3. The ER and Golgi compartments constitute the main signaling platform for CAgp130

The constitutive and ligand-independent activity of CAgp130 probably uncouples the receptor from the necessity to be localized at the cell membrane in order to signal. As a consequence it's signaling might show a completely different spatial distribution in comparison to WTgp130. From a logical point of view the receptor mutant could fire its constitutive signal from three different cellular positions: (1) CAgp130 could be able to signal on its biosynthesic route meaning the ER and Golgi before reaching the cell membrane. First hints for this scenario have been already discussed in section 4.1. with the observation that for CAgp130 only the lower glycosylated and therefore intracellularly retained receptor form gets phosphorylated. (2) Receptor mutant that is present at the cell membrane could furthermore signal upon its endocytosis as has been described for several RTKs like the HGF (hepatocyte growth factor) receptor Met [172] and the epidermal growth factor receptor EGFR [173]. (3) As a third possibility it is conceivable that the smaller portion of CAgp130 that is localized in the cell membrane also shows signaling activity as it is the case for WTgp130 upon stimulation. The results concerning all three possible sources of constitutive signaling are discussed within the following three sections.

4.3.1. CAgp130 activates STAT3 on its way to the cell membrane – the receptor mutant associates with Jaks and homodimerizes long before reaching the cell membrane

In a first attempt to analyze the signaling potential of CAgp130 on its biosynthetic route constructs of WTgp130 and CAgp130 were cloned that were tagged with published ER-retention sequences. Identical to the fluorescent tags the retention sequences were placed at the intracellular C-termini of both receptors in order to avoid any disturbance in formation of the hexameric (in the case of WTgp130) or dimeric (in the case of CAgp130) signaling complexes.

Retention sequences play an important role in intracellular transport processes as they are crucial for maintenance of the protein composition of organelles. Among the best characterized retention signals is the C-terminally localized K(H)DEL sequence that is only suitable for soluble proteins. Of great importance for the retrieval of membrane proteins are Lys- and Arg-based signals [174]. Three out of four signals utilized in this study (Figure 13) are derived from a large combinatorial screening that was performed in mammalian cells [157]. The screening used GFP-tagged CD4 – a type I transmembrane protein like gp130 – as a reporter protein. The fourth retention signal is an Arg-based signal discovered within CD74 [158].

First experiments that were performed with retention mutants of WTgp130 in a transient transfection mode were promising as the amount of surface receptor upon transfection was even lower than the amount of endogenous gp130 (Figure 14). Despite the fact that reduction of surface receptor does not necessarily mean its ER-retention it can provide a first hint in this direction. As already mentioned in section 2.1.1. this observation could be due to formation of preformed dimers between endogenous gp130 and the transfected retention mutants. Such preformed dimers have been described for gp130 in the past, however, they have been reported to be localized at the cell membrane and get stabilized by addition of the ligand [48].

As CAgp130 shows a much lower cell surface expression compared to WTgp130 it was obvious that its ER-retention would be more difficult to detect in a transient transfection experiment. Therefore, the retention mutant of CAgp130 harboring the CD74 retention signal was stably transfected in HEK293 cells. As shown in Figure 15 for three different clones the Arg-based retention signal derived from CD74 is not able to prevent trafficking of

CAgp130 to the cell surface. This is apparent from its surface/overall receptor ratio that does not decrease in comparison to that of CAgp130. Similar results were obtained for the retention mutant of CAgp130 containing the Lys-based signal KKYN although not depicted here. The failure of retention in the case of CAgp130 might be explained by its reduced cell surface expression. In a further scenario conformational differences within the cytoplasmic part of WTgp130 and CAgp130 could be big enough to change the accessibility of one and the same retention signal in these receptors.

In a second approach to analyze the signaling activity of CAgp130 on its way to the cell membrane the pharmacological inhibitor brefeldin A was utilized. Brefeldin A is a potent inhibitor of the secretory pathway and has been reported to inhibit the retrograde transport from the Golgi to the ER [175]. The retrograde transport that is mediated by COPII vesicles is important for the retrieval of ER resident proteins that have escaped to the Golgi during the process of protein secretion [176]. As a consequence of treatment with brefeldin A more and more ER proteins accumulate in the Golgi and an intermediate ER-Golgi compartment is formed. The performed experimental approach was based on the concomitant induction of receptor expression and inhibitor treatment to prevent any receptor molecules from reaching the cell membrane. As shown in Figure 16 brefeldin A is able to prevent cell surface expression of CAgp130 for the first eight hours of induction. Even more important newly synthesized CAgp130 activates STAT3 in these cells (Figure 17) in line with recently published data [164]. This observation is further in line with the finding that only immature receptor gets phosphorylated in the case of CAgp130 (see section 4.1.). The observed decrease in STAT3-phosphorylation correlates with the reduction of overall receptor amount. Another possible explanation would be steric hindrance of receptors accumulating in the brefeldin-induced ER-Golgi compartment. Yet a further interesting scenario would be that receptors at intracellular membranes are less potent in activating signaling pathways than receptors at the plasma membrane, bringing up the spatial regulation of receptor activity. STAT3-activation from within the cell indicates that CAgp130 gets associated with Jaks and exists as an active dimer from its early processing stages within the ER. Jaks have been reported to act as chaperones and enhance cell surface expression for a series of receptors like MPL [177], EPOR [178] or OSMR [179]. Binding of Jaks to these receptors seems to mask a negative regulatory signal, possibly an ER-retention signal. In the case of CAgp130, however, this chaperone activity of Jaks is not sufficient to facilitate cell surface expression.

Interestingly, there is a similar study performed with a constitutive MPL mutant [146]. Mutant MPL was captured in the ER by use of the KDEL retention sequence and was shown to be associated with Jak2. However, it was not able to support factor-independent growth of transfected cells as already reported for CAgp130 [161]. Intracellular signaling was first activated by introduction of a disulfide bond and forced dimerization as it has already been reported for gp130 [180].

4.3.2. CAgp130 does not contribute to constitutive STAT3-phosphorylation upon its endocytosis

In recent years there have been several reports on the intracellular signaling potential of RTKs like the EGFR and GPCRs like the β2AR (β2 adrenergic receptor) upon endocytosis [181]. Elaborate approaches led to the theory of signaling endosomes. Today it is common knowledge that sorting events occurring upon internalization of receptors often regulate the strength and duration of signaling and the theory of signaling endosomes has moved to the next stage and differentiates between signaling emanating from early, late or even recycling endosomes [182].

As already mentioned in section 1.2.3. internalization of gp130 occurs in a constitutive manner independent of the presence of a ligand [56]. Interestingly, the half-life of gp130 at the cell surface as well as its internalization kinetics do not significantly change upon stimulation. From this point of view gp130 behaves less like a signaling receptor whose internalization is triggered by the ligand and more like a nutrient receptor such as the receptor for transferrin or LDL (low density lipoprotein). This comparison fits to the mechanism of endocytosis that was revealed for gp130 and is identical to the one of nutrient receptors. Transferrin for example gets endocytosed via clathrin-coated pits [183] that require the main coat constituent AP-2 for assembly of the clathrin cage [184]. In line with this information gp130 was reported to be constitutively associated with AP-2 leading to the conclusion that its internalization is clathrin-dependent [56].

Of central importance for most endocytic processes is the GTPase dynamin that has been implicated in membrane remodelling [184]. The basic dynamin unit is a dimer that polymerizes around the neck of an endocytic bud. Dependent on GTP hydrolysis dynamin polymers undergo structural reorganization and trigger constriction or stretching and subsequent membrane fission [185]. As GTPase activity is important for the endocytic

process dynamin mutants with impaired GTP binding activity such as dynamin K44A demonstrate dominant-negative effects [186].

Analysis of the signaling activity of CAgp130 upon its endocytosis was performed by transfection of dominant-negative K44A dynamin. If the endocytosed receptor accounts for a part of the constitutive activity as it has been shown for the EGFR [187] this contribution should be omitted upon inhibition of the internalization process. As shown in Figure 20 dominant-negative dynamin is able to inhibit the uptake of transferrin in HEK293 cells. Mutant dynamin furthermore interferes with endocytosis of CAgp130 leading to its accumulation at the cell membrane (Figure 21). However, there is no impairment of constitutive signaling (Figure 22). STAT3-phosphorylation remains unaltered indicating that the endocytosed receptor does not contribute to ligand-independent activity. The data on endosomal signaling of CAgp130 do not coincide with recently published data according to which endosomal signaling represents an essential part of constitutive signaling [164]. These contradictory data might be explained by the differences in the applied experimental approach. The application of the endocytosis-inhibitor dynasore – as it is utilized by Schmidt-Arras et al. – led in our first approaches to detrimental effects on cell viability as revealed by FACS-analysis (Figure 18). Therefore a more elaborate approach was chosen that utilized dominant-negative dynamin. Our results do not rule out the possibility of endosomal signaling in the case of CAgp130. Before giving definite answers to this question the possibility has to be excluded that mutant receptor molecules can somehow circumvent classical receptor trafficking. In a possible scenario a fraction of newly synthesized mutant receptor could be directly transferred from the ER and cis Golgi to endosomal compartments circumventing the plasma membrane. Signal emanating from these molecules would remain unaffected in experimental approaches that interfere with endocytic processes.

4.3.3. Signaling of CAgp130 is unaffected by the use of neutralizing gp130 antibodies

The third and last cellular compartment where constitutive signaling can originate from is the cell membrane. To exclusively target CAgp130 present at the cell membrane we utilized three neutralizing gp130 antibodies [160] as mentioned in section 3.1.. B-P4 was initially described as an Ab leading to neutralization of IL-11-signaling. IL-11 is the other IL-6-type cytokine that signals via a gp130 homodimer [7]. In contrast, B-T2 was reported to neutralize

IL-6-signaling and B-R3 was shown to be a potent inhibitory Ab for both – IL-6 and IL-11 – signaling pathways. As shown in Figure 24A and according to the expectation B-P4 only slightly interferes with IL-6-signaling whereas B-T2 abrogates it almost completely when applied to cells stably expressing WTgp130. B-R3 has an intermediate effect. In the case of CAgp130 B-P4 and B-T2 successfully bind to surface resident receptor (Figure 23B) but are insufficient in blocking its signaling activity (Figure 24B). B-R3 does not bind to the receptor mutant (Figure 23B).

These findings are in contrast to the results of Sommer et al., who reported to block CAgp130 by the Ab B-P4 [161] suggesting that activating mutations of gp130 lead to an IL-11-like signaling. Based on our findings we conclude that the mutant receptor, which localizes to the plasma membrane, does not significantly contribute to constitutive STAT3-activation. In the light of these controversial experimental findings it needs to be taken into account that antibodies were tested on different experimental settings and on different cell lines. Sommer et al. performed proliferation assays with Ba/F3 cells stably transfected with CAgp130. The factor-independent growth of these cells conferred by the constitutive signaling of mutant receptor was abrogated by incubation with the Ab B-P4 over a time period of three days. Although there is no visible neutralizing effect of B-P4 on CAgp130 in our own experiments it is possible that the antagonistic effects is too small to be noticed within the first 24 h, however, adds up as the assay proceeds.

Finally, we were able to inhibit STAT3-activation emanating from CAgp130 by transfection of a dominant-negative STAT3 mutant (Figure 25) [162]. Similarly, signaling of CAgp130 can be blocked through inhibition of Jak1 as has been recently reported [134].

Taken together our data reveal that CAgp130 mainly signals along the biosynthetic route on its way to the cell membrane. The receptor mutant does not contribute to constitutive signaling upon its endocytosis and surprisingly even membrane-bound receptor does not show significant signaling activity. These findings are of importance for therapeutic approaches targeting gp130 mutations in the treatment of HCAs. From the results it is obvious that mutant receptor cannot be targeted with agents that act on the cell surface. As demonstrated by the use of dominant-negative STAT3 downregulation of constitutive activity has to be performed with intracellularly acting agents.

4.4. SOCS3 partially downregulates constitutive activity of CAgp130 and might play a role in lysosomal targeting of the receptor mutant

SOCS3 is the most prominent feedback inhibitor within the IL-6 signaling pathway. As already mentioned in section 1.2.6.3. its inhibitory function consists out of two major parts: the direct kinase inhibition and the recruitment of an E3-ubiquitin ligase complex. Whereas the first mode of action – the direct kinase inhibition – is known for a long time and has been thoroughly characterized in biochemical [89] as well as structural means [90], the second mode of action remains to be fully elucidated. Zhang et al. were the first to report the interaction of the SOCS-box within SOCS3 with elongin B and C [87] suggesting that SOCS proteins might target activated signaling components to degradation. About ten years later Babon et al. showed that a SOCS-box bound to elongin B and C tightly interacts with cullin 5 [91]. In 2014 the same group was able to reconstitute a SOCS3-based E3-ubiquitin ligase complex *in vitro* and showed that this complex efficiently catalyzed ubiquitination of gp130 and Jak2 [93].

The role of SOCS3 in the context of CAgp130 was of particular interest from the beginning of this work. Upon detection of SOCS3 expression in cells stably expressing CAgp130 the focus was set primarily on its kinase inhibitory function. As shown in Figure 6 SOCS3 is induced by CAgp130, however, it is not able to prevent constitutive STAT3-phosphorylation caused by the mutant receptor. In a first approach a receptor mutant was cloned where the SOCS3 recruitment site at Y759 was mutated. As apparent in Figure 26A CAgp130-Y759F is expressed to a comparable extent as CAgp130, however, it causes a stronger STAT3-activation. This finding suggests that CAgp130 gets partially downregulated in its constitutive activity by SOCS3. In a further approach CAgp130 was transiently coexpressed with increasing amounts of SOCS3 (Figure 26B). As it becomes obvious from Figure 26B even the lowest amount of transfected SOCS3 is much higher than the SOCS3 amount induced by the mutant receptor and is able to completely abrogate constitutive activity. The most interesting part of this experiment is the gradual decrease of detected receptor upon transfection of increasing SOCS3 amounts. This observation could provide a hint for the degrading role of SOCS3, however, it should be validated by other means as the experiment

was performed with a high degree of SOCS3 overexpression that increases the possibility of side effects.

A role of SOCS3 in downregulation of gp130 becomes more likely in view of recent publications that assign SOCS3 a decisive role in controlling the lysosomal routing of the G-CSF receptor G-CSFR. G-CSF is the main cytokine in the production of neutrophilic granulocytes [188] and its receptor is closely related to gp130 within the class I cytokine receptor superfamily. For G-CSFR a juxtamembrane Lys-residue at position 632 was reported to play a key role in receptor routing as its mutation caused accumulation of the receptor within early endosomes [163]. According to the prevalent model, SOCS3 that is induced upon G-CSF stimulation binds to Y729 of the G-CSFR that is equivalent to Y759 of gp130 and directly inhibits the associated Jak. Recruited SOCS3, however, additionally leads to recruitment of an E3-ubiquitin ligase complex through its SOCS-box that ubiquitinates a juxtamembrane Lys-residue at position 632. Ubiquitination of K632 is responsible for the transport of G-CSFR from early endosomes to lysosomes where it is degraded. Most importantly K632 lies within the consensus sequence KXXXWXXXPDP (where X is an arbitrary aa) that is conserved within other class I cytokine receptors like LepR and gp130. As a consequence this Lys-residue could play a similar role for the trafficking and downregulation of these receptors as well.

In the light of these reports the mutant CAgp130-K648R was generated (with K648 being equivalent to K632 of G-CSFR) and confronted with increasing amounts of SOCS3 in an experiment of transient coexpression (Figure 27). If K632 was of any importance for lysosomal routing and degradation of gp130 its substitution by an Arg-residue would abrogate or at least interfere with SOCS3-mediated receptor degradation. As shown in the receptor diagram within Figure 27 coexpression of CAgp130 with 0.1 µg SOCS3 reduces the receptor amount to more than 50%. However, cotransfection of the same amount of SOCS3 with identical amounts of CAgp130-Y759F and CAgp130-K648R does not have any effect on the level of these receptors providing a hint for a possible role of SOCS3 and K632 in downregulation of the constitutively active receptor mutant. The amounts of CAgp130-Y759F and CAgp130-K648R first decrease upon transfection of higher SOCS3 amounts that probably cause a series of side effects as speculated before. Interesting as well are the changes in STAT3-phosphorylation detected for all three receptors. As seen before (Figure 26B) constitutive activity of CAgp130 gets completely abrogated by cotransfection of very

low SOCS3 amounts. In contrast, STAT3-phosphorylation generated by CAgp130-Y759F is not influenced (0.1 µg) or at least not influenced as much (0.5-4 µg) as the one emanating from CAgp130. This result is not further surprising as CAgp130-Y759F lacks the SOCS3 binding site and therefore cannot be downregulated in its constitutive activity. It further demonstrates that SOCS3 overexpression is an unreliable tool as there is a reduction in STAT3-phosphorylation from 0.5 µg SOCS3 DNA. For CAgp130-K648R STAT3-phosphorylation is completely abrogated by SOCS3 as the docking site for SOCS3 is intact. Taken together data from the experiment in Figure 27 provide hints that SOCS3 exerts its primary mode of action by kinase inhibition in the case of CAgp130 and CAgp130-K648R. However, it might also play a role in downregulating the receptor itself as detected in the case of CAgp130 and CAgp130-Y759F.

Trying to avoid the overexpression of SOCS3 an experimental approach was designed that was based on inhibition of protein degradation. As there are two main pathways of protein degradation – the proteasomal and lysosomal degradation pathway – we utilized inhibitors of both pathways separately to dissect the contribution of each in downregulating CAgp130 and CAgp130-Y759F. The first experiment was performed with cells stably expressing WTgp130. As shown in Figure 28 the amount of receptor that is set to 1 at the initial time point decreases to about 50% 8 h after withdrawal of dox and inhibition of further protein synthesis by CHX. Excluding the 8 h time point where inhibitors may not work any longer both proteasomal and lysosomal inhibitors interfere with receptor degradation to a comparable extent. This result is just partially consistent with observations made by Tanaka et al. who reported that gp130 is degraded over the proteasome in the absence of IL-6 stimulation [189]. The same experiment performed with CAgp130 (Figure 29) revealed that degradation of the mutant receptor can be abrogated by the use of inhibitors of lysosomal degradation. In contrast, proteasomal inhibitors do not interfere with receptor degradation at all. In the case of CAgp130-Y759F the degradation profile is reversed with inhibitors of the proteasome leading to complete abrogation of receptor degradation [Figure 30]. These data are in line with a possible role of SOCS3 for lysosomal degradation of CAgp130 considering that SOCS3 susceptibility is the only apparent difference between CAgp130 and CAgp130-Y759F. As soon as the receptor mutant loses its SOCS3 binding site its degradation switches from the lysosomal to the proteasomal pathway. These data are preliminary and require further verification.

Abbreviations

Ab	antibody
aa	amino acid
Amp[R]	ampicillin [resistance]
AP-2	adaptor protein-2
APC	allophycocyanin
APP	acute phase protein
APR	acute phase response
APS	ammonium persulfate
BiP	binding immunoglobulin protein
BSA	bovine serum albumin
CA	constitutively active
CBM	cytokine binding module
cDNA	complementary DNA
CFP	cyan fluorescent protein
CHX	cycloheximide
CLC	cardiotrophin-like cytokine
CNTF	ciliary neurotrophic factor
COP	coat protein complex
CRP	C-reactive protein
CT-1	cardiotrophin-1
ddH2O	double-distilled water
DMSO	dimethyl sulfoxide
dox	doxycycline
ds	double stranded
E. coli	Escherichia coli
EDTA	ethylenediaminetetraacetic acid
EGF	epidermal growth factor
Endo H	endoglycosidase H
EPOR	erythropoietin receptor
Erk	extracellular signal regulated kinase
FACS	fluorescence-activated cell sorting
FCS	fetal calf serum
FLT3	Fms-like tyrosine kinase 3
FNIII	fibronectin type III
FRT	Flp recombinase target
FSC	forward scatter
Gab1	Grb2 associated binding protein 1
GAPDH	glyceraldehyde-3-phosphate dehydrogenase
G-CSF	granulocyte-colony stimulating factor
GFP	green fluorescent protein
GOI	gene of interest
Gp130	glycoprotein 130

GPCR	G protein-coupled receptors
HCA[C]	hepatocellular adenoma [carcinoma]
HIF1α	hypoxia-inducible factor 1α
HRP	horseradish peroxidase
hu	human
HygR	hygromycin B resistance
Ig	immunoglobulin
IHCA	inflammatory HCA
IL	interleukin
IRES	internal ribosome entry site
ITD	in-frame tandem duplication
Jak	Janus kinase
JNK	c-jun N-terminal kinase
KanR	kanamycin resistance
KIR	kinase inhibitory region
LB	lysogeny broth
LepR	leptin receptor
LIF	leukaemia inhibitory factor
MAPK	mitogen activated protein kinase
MBS	multiple beam splitter
MCS	multiple cloning site
MeOH	methanol
MPL	thrombopoietin receptor
o/n	over night
OSM	oncostatin M
PAA	polyacrylamide
PBS	phosphate buffered saline
PCR	polymerase chain reaction
PFA	paraformaldehyde
PtdIns	phosphoinositide
PVDF	polyvinylidene fluoride
ROS	reactive oxygen species
rpm	revolutions per minute
rt	room temperature
RTK	receptor tyrosine kinase
SAA	serum amyloid A
SAPK	stress activated protein kinase
sc	single chain
SDS	sodium dodecyl sulfate
SH2	src homology domain 2
SHP2	SH2 containing protein tyrosine phosphatase 2
sIL-6Rα	soluble IL-6Rα
SOCS	suppressor of cytokine signaling
SSC	side scatter
STAT	signal transducer and activator of transcription

TCL	total cell lysate
TEMED	tetramethylethylenediamine
UPR	unfolded protein response
VEGF	vascular endothelial growth factor
WB	western blot
WT	wild type
YFP	yellow fluorescent protein

References

1. **Heinrich PC**, **Behrmann I**, **Müller-Newen G**, **Schaper F**, **Graeve L**. Interleukin-6-type cytokine signalling through the gp130/Jak/STAT pathway. *Biochem J*. 1998; **334 (Pt 2)**:297–314.

2. **Garbers C**, **Hermanns HM**, **Schaper F**, **Müller-Newen G**, **Grötzinger J**, **Rose-John S**, **Scheller J**. Plasticity and cross-talk of Interleukin 6-type cytokines. *Cytokine Growth Factor Rev*. 2012; **23**:85–97.DOI: 10.1016/j.cytogfr.2012.04.001.

3. **Ozaki K**, **Leonard WJ**. Cytokine and Cytokine Receptor Pleiotropy and Redundancy. *Journal of Biological Chemistry*. 2002; **277**:29355–29358.DOI: 10.1074/jbc.R200003200.

4. **Banchereau J**, **Pascual V**, **O'Garra A**. From IL-2 to IL-37: the expanding spectrum of anti-inflammatory cytokines. *Nat Immunol*. 2012; **13**:925–931.DOI: 10.1038/ni.2406.

5. **Rose-John S**. IL-6 trans-signaling via the soluble IL-6 receptor: importance for the pro-inflammatory activities of IL-6. *International Journal of Biological Sciences*. 2012; **8**:1237–1247.DOI: 10.7150/ijbs.4989.

6. **Bazan JF**. Structural design and molecular evolution of a cytokine receptor superfamily. *Proceedings of the National Academy of Sciences*. 1990; **87**:6934–6938.DOI: 10.1073/pnas.87.18.6934.

7. **Heinrich PC**, **Behrmann I**, **Haan S**, **Hermanns HM**, **Müller-Newen G**, **Schaper F**. Principles of interleukin (IL)-6-type cytokine signalling and its regulation. *Biochem J*. 2003; **374**:1–20.DOI: 10.1042/BJ20030407.

8. **Heinrich PC**, **Castell JV**, **Andus T**. Interleukin-6 and the acute phase response. *Biochem J*. 1990; **265**:621–636.

9. **Cantor SB**, **Elting LS**, **Hudson DV**, **Rubenstein EB**. Pharmacoeconomic analysis of oprelvekin (recombinant human interleukin-11) for secondary prophylaxis of thrombocytopenia in solid tumor patients receiving chemotherapy. *Cancer*. 2003; **97**:3099–3106.DOI: 10.1002/cncr.11447.

10. **Kawashima I**, **Ohsumi J**, **Mita-Honjo K**, **Shimoda-Takano K**, **Ishikawa H**, **Sakakibara S**, **Miyadai K**, *et al.* Molecular cloning of cDNA encoding adipogenesis inhibitory factor and identity with interleukin-11. *FEBS Lett*. 1991; **283**:199–202.DOI: 10.1016/0014-5793(91)80587-S.

11. **Larousserie F**, **Charlot P**, **Bardel E**, **Froger J**, **Kastelein RA**, **Devergne O**. Differential Effects of IL-27 on Human B Cell Subsets. *J Immunol*. 2006; **176**:5890–5897.DOI: 10.4049/jimmunol.176.10.5890.

12. **Cheung PFY**, **Wong CK**, **Ho AWY**, **Hu S**, **Chen DP**, **Lam CWK**. Activation of human eosinophils and epidermal keratinocytes by Th2 cytokine IL-31: implication for the immunopathogenesis of atopic dermatitis. *International Immunology*. 2010; **22**:453–467.DOI: 10.1093/intimm/dxq027.

13. **Dillon SR**, **Sprecher C**, **Hammond A**, **Bilsborough J**, **Rosenfeld-Franklin M**, **Presnell SR**, **Haugen HS**, *et al.* Interleukin 31, a cytokine produced by activated T cells, induces dermatitis in mice. *Nat Immunol*. 2004; **5**:752–760.DOI: 10.1038/ni1084.

14. **Stewart CL**, **Kaspar P**, **Brunet LJ**, **Bhatt H**, **Gadi I**, **Köntgen F**, **Abbondanzo SJ**. Blastocyst implantation depends on maternal expression of leukaemia inhibitory factor. *Nature*. 1992; **359**:76–79.DOI: 10.1038/359076a0.

15. **Rowe DD**, **Collier LA**, **Seifert HA**, **Chapman CB**, **Leonardo CC**, **Willing AE**, **Pennypacker KR**. Leukemia inhibitor factor promotes functional recovery and oligodendrocyte survival in rat models of focal ischemia. *Eur J Neurosci*. 2014:n/a–n/a.DOI: 10.1111/ejn.12675.

16. **Zarling JM**, **Shoyab M**, **Marquardt H**, **Hanson MB**, **Lioubin MN**, **Todaro GJ**. Oncostatin M: a growth regulator produced by differentiated histiocytic lymphoma cells. *Proceedings of the National Academy of Sciences*. 1986; **83**:9739–9743.DOI: 10.1073/pnas.83.24.9739.

17. **Walker EC**, **McGregor NE**, **Poulton IJ**, **Solano M**, **Pompolo S**, **Fernandes TJ**, **Constable MJ**, *et al.* Oncostatin M promotes bone formation independently of resorption when signaling through leukemia inhibitory factor receptor in mice. *J Clin Invest*. 2010; **120**:582–592.DOI: 10.1172/JCI40568.

18. **Emsley JG**, **Hagg T**. Endogenous and exogenous ciliary neurotrophic factor enhances forebrain neurogenesis in adult mice. *Exp Neurol*. 2002; **183**:298–310.DOI: 10.1016/S0014-4886(03)00129-8.

19. **Lu C**, **Meng D**, **Cao J**, **Xiao Z**, **Cui Y**, **Fan J**, **Cui X**, *et al.* Collagen scaffolds combined with collagen-binding ciliary neurotrophic factor facilitate facial nerve repair in mini-pigs. *J. Biomed. Mater. Res.* 2014:n/a–n/a.DOI: 10.1002/jbm.a.35305.

20. **Pennica D**, **King KL**, **Shaw KJ**, **Luis E**, **Rullamas J**, **Luoh SM**, **Darbonne WC**, *et al.* Expression cloning of cardiotrophin 1, a cytokine that induces cardiac myocyte hypertrophy. *Proceedings of the National Academy of Sciences*. 1995; **92**:1142–1146.DOI: 10.1073/pnas.92.4.1142.

21. **Oppenheim RW**, **Wiese S**, **Prevette D**, **Armanini M**, **Wang S**, **Houenou LJ**, **Holtmann B**, *et al.* Cardiotrophin-1, a muscle-derived cytokine, is required for the survival of subpopulations of developing motoneurons. *J. Neurosci.* 2001; **21**:1283–1291.

22. **Senaldi G**, **Varnum BC**, **Sarmiento U**, **Starnes C**, **Lile J**, **Scully S**, **Guo J**, *et al.* Novel neurotrophin-1/B cell-stimulating factor-3: A cytokine of the IL-6 family. *Proceedings of the National Academy of Sciences*. 1999; **96**:11458–11463.DOI: 10.1073/pnas.96.20.11458.

23. **Elson GC**, **Lelièvre E**, **Guillet C**, **Chevalier S**, **Plun-Favreau H**, **Froger J**, **Suard I**, *et al.* CLF associates with CLC to form a functional heteromeric ligand for the CNTF receptor complex. *Nat. Neurosci.* 2000; **3**:867–872.DOI: 10.1038/78765.

24. **Pflanz S**, **Timans JC**, **Cheung J**, **Rosales R**, **Kanzler H**, **Gilbert J**, **Hibbert L**, *et al.* IL-27, a Heterodimeric Cytokine Composed of EBI3 and p28 Protein, Induces Proliferation of Naive CD4+ T Cells. *Immunity*. 2002; **16**:779–790.DOI: 10.1016/S1074-7613(02)00324-2.

25. **Devergne O**, **Birkenbach M**, **Kieff E**. Epstein-Barr virus-induced gene 3 and the p35 subunit of interleukin 12 form a novel heterodimeric hematopoietin. *Proceedings of the National Academy of Sciences*. 1997; **94**:12041–12046.DOI: 10.1073/pnas.94.22.12041.

26. **Collison LW**, **Workman CJ**, **Kuo TT**, **Boyd K**, **Wang Y**, **Vignali KM**, **Cross R**, *et al.* The inhibitory cytokine IL-35 contributes to regulatory T-cell function. *Nature*. 2007; **450**:566–569.DOI: 10.1038/nature06306.

27. **Robledo O**, **Fourcin M**, **Chevalier S**, **Guillet C**, **Auguste P**, **Pouplard-Barthelaix A**, **Pennica D**, *et al.* Signaling of the Cardiotrophin-1 Receptor: Evidence for a third receptor component. *Journal of Biological Chemistry*. 1997; **272**:4855–4863.DOI: 10.1074/jbc.272.8.4855.

28. **Zhang Q**, **Putheti P**, **Zhou Q**, **Liu Q**, **Gao W**. Structures and biological functions of IL-31 and IL-31 receptors. *Cytokine Growth Factor Rev*. 2008; **19**:347–356.DOI: 10.1016/j.cytogfr.2008.08.003.

29. **Ritchie DG**, **Fuller GM**. Hepatocyte-stimulating factor: a monocyte-derived acute-phase regulatory protein. *Ann N Y Acad Sci*. 1983; **408**:490–502.DOI: 10.1111/j.1749-6632.1983.tb23268.x.

30. **Somers W**, **Stahl M**, **Seehra JS**. 1.9 A crystal structure of interleukin 6: implications for a novel mode of receptor dimerization and signaling. *EMBO J.* 1997; **16**:989–997.DOI: 10.1093/emboj/16.5.989.

31. **Paonessa G**, **Graziani R**, **De Serio A**, **Savino R**, **Ciapponi L**, **Lahm A**, **Salvati AL**, *et al.* Two distinct and independent sites on IL-6 trigger gp 130 dimer formation and signalling. *EMBO J.* 1995; **14**:1942–1951.

32. **Kimura A**, **Kishimoto T**. IL-6: regulator of Treg/Th17 balance. *Eur J Immunol*. 2010; **40**:1830–1835.DOI: 10.1002/eji.201040391.

33. **Tanaka T**, **Kishimoto T**. Targeting interleukin-6: all the way to treat autoimmune and inflammatory diseases. *International Journal of Biological Sciences*. 2012; **8**:1227–1236.DOI: 10.7150/ijbs.4666.

34. **Yawata H**, **Yasukawa K**, **Natsuka S**, **Murakami M**, **Yamasaki K**, **Hibi M**, **Taga T**, *et al.* Structure-function analysis of human IL-6 receptor: dissociation of amino acid residues required for IL-6-binding and for IL-6 signal transduction through gp130. *EMBO J.* 1993; **12**:1705–1712.

35. **Fischer M**, **Goldschmitt J**, **Peschel C**, **Brakenhoff JPG**, **Kallen K-J**, **Wollmer A**, **Grötzinger J**, *et al.* A bioactive designer cytokine for human hematopoietic progenitor cell expansion. *Nat Biotechnol*. 1997; **15**:142–145.DOI: 10.1038/nbt0297-142.

36. **Scheller J**, **Chalaris A**, **Garbers C**, **Rose-John S**. ADAM17: a molecular switch to control inflammation and tissue regeneration. *Trends Immunol*. 2011; **32**:380–387.DOI: 10.1016/j.it.2011.05.005.

37. **Müllberg J**, **Schooltink H**, **Stoyan T**, **Günther M**, **Graeve L**, **Buse G**, **Mackiewicz A**, *et al.* The soluble interleukin-6 receptor is generated by shedding. *Eur J Immunol*. 1993; **23**:473–480.DOI: 10.1002/eji.1830230226.

38. **Dittrich A**, **Quaiser T**, **Khouri C**, **Görtz D**, **Mönnigmann M**, **Schaper F**. Model-driven experimental analysis of the function of SHP-2 in IL-6-induced Jak/STAT signaling. *Molecular BioSystems*. 2012; **8**:2119–2134.DOI: 10.1039/c2mb05488d.

39. **Yoshida K**, **Taga T**, **Saito M**, **Suematsu S**, **Kumanogoh A**, **Tanaka T**, **Fujiwara H**, *et al.* Targeted disruption of gp130, a common signal transducer for the interleukin 6 family of cytokines, leads to myocardial and hematological disorders. *Proceedings of the National Academy of Sciences*. 1996; **93**:407–411.DOI: 10.1073/pnas.93.1.407.

40. **Gerhartz C**, **Dittrich E**, **Stoyan T**, **Rose-John S**, **Yasukawa K**, **Heinrich PC**, **Graeve L**. Biosynthesis and half-life of the interleukin-6 receptor and its signal transducer gp130. *Eur J Biochem*. 1994; **223**:265–274.

41. **Moritz RL**, **Hall NE**, **Connolly LM**, **Simpson RJ**. Determination of the Disulfide Structure andN-Glycosylation Sites of the Extracellular Domain of the Human Signal Transducer gp130. *Journal of Biological Chemistry*. 2001; **276**:8244–8253.DOI: 10.1074/jbc.M009979200.

42. **Yanagisawa M**, **Yu RK**. N-glycans modulate the activation of gp130 in mouse embryonic neural precursor cells. *Biochem Biophys Res Commun*. 2009; **386**:101–104.DOI: 10.1016/j.bbrc.2009.05.132.

43. **Waetzig GH**, **Chalaris A**, **Rosenstiel P**, **Suthaus J**, **Holland C**, **Karl N**, **Valles Uriarte L**, *et al.* N-Linked Glycosylation Is Essential for the Stability but Not the Signaling Function of the Interleukin-6 Signal Transducer Glycoprotein 130. *Journal of Biological Chemistry*. 2010; **285**:1781–1789.DOI: 10.1074/jbc.M109.075952.

44. **Horsten U**, **Schmitz-Van de Leur H**, **MÜLLBERG J**, **Heinrich PC**, **Rose-John S**. The membrane distal half of gp130 is responsible for the formation of a ternary complex with IL-6 and the IL-6 receptor. *FEBS Lett*. 1995; **360**:43–46.DOI: 10.1016/0014-5793(95)00053-C.

45. **Kurth I**, **Horsten U**, **Pflanz S**, **Timmermann A**, **Küster A**, **Dahmen H**, **Tacken I**, *et al.* Importance of the Membrane-Proximal Extracellular Domains for Activation of the Signal Transducer Glycoprotein 130. *J Immunol*. 2000; **164**:273–282.DOI: 10.4049/jimmunol.164.1.273.

46. **Lütticken C**, **Wegenka UM**, **Yuan J**, **Buschmann J**, **Schindler C**, **Ziemiecki A**, **Harpur AG**, *et al.* Association of transcription factor APRF and protein kinase Jak1 with the interleukin-6 signal transducer gp130. *Science*. 1994; **263**:89–92.DOI: 10.1126/science.8272872.

47. **Guschin D**, **Rogers N**, **Briscoe J**, **Witthuhn B**, **Watling D**, **Horn F**, **Pellegrini S**, *et al.* A major role for the protein tyrosine kinase JAK1 in the JAK/STAT signal transduction pathway in response to interleukin-6. *EMBO J.* 1995; **14**:1421–1429.

48. **Giese B**, **Roderburg C**, **Sommerauer M**, **Wortmann SB**, **Metz S**, **Heinrich PC**, **Müller-Newen G**. Dimerization of the cytokine receptors gp130 and LIFR analysed in single cells. *J Cell Sci*. 2005; **118**:5129–5140.DOI: 10.1242/jcs.02628.

49. **Murakami M**, **Narazaki M**, **Hibi M**, **Yawata H**, **Yasukawa K**, **Hamaguchi M**, **Taga T**, *et al.* Critical cytoplasmic region of the interleukin 6 signal transducer gp130 is conserved in the cytokine receptor family. *Proceedings of the National Academy of Sciences*. 1991; **88**:11349–11353.DOI: 10.1073/pnas.88.24.11349.

50. **Haan C**, **Heinrich PC**, **Behrmann I**. Structural requirements of the interleukin-6 signal transducer gp130 for its interaction with Janus kinase 1: the receptor is crucial for kinase activation. *Biochem J*. 2002; **361**:105.DOI: 10.1042/0264-6021:3610105.

51. **Haan C**, **Hermanns HM**, **Heinrich PC**, **Behrmann I**. A single amino acid substitution (Trp666→Ala) in the interbox1/2 region of the interleukin-6 signal transducer gp130 abrogates binding of JAK1, and dominantly impairs signal transduction. *Biochem J*. 2000; **349**:261.DOI: 10.1042/0264-6021:3490261.

52. **Nesbitt JE**, **Fuller GM**. Differential regulation of interleukin-6 receptor and gp130 gene expression in rat hepatocytes. *Mol Biol Cell*. 1992; **3**:103–112.DOI: 10.1091/mbc.3.1.103.

53. **Zohlnhöfer D**, **Graeve L**, **Rose-John S**, **Schooltink H**, **DITTRICH E**, **Heinrich PC**. The hepatic interleukin-6 receptor Down-regulation of the interleukin-6 binding subunit (gp80) by its ligand. *FEBS Lett*. 1992; **306**:219–222.DOI: 10.1016/0014-5793(92)81004-6.

54. **Dittrich E**, **Rose-John S**, **Gerhartz C**, **Müllberg J**, **Stoyan T**, **Yasukawa K**, **Heinrich PC**, *et al.* Identification of a region within the cytoplasmic domain of the interleukin-6 (IL-6) signal transducer gp130 important for ligand-induced endocytosis of the IL-6 receptor. *Journal of Biological Chemistry*. 1994; **269**:19014–19020.

55. **Dittrich E**, **Haft CR**, **Muys L**, **Heinrich PC**, **Graeve L**. A di-leucine motif and an upstream serine in the interleukin-6 (IL-6) signal transducer gp130 mediate ligand-induced endocytosis and down-regulation of the IL-6 receptor. *J Biol Chem*. 1996; **271**:5487–5494.

56. **Thiel S**, **Dahmen H**, **Martens A**, **Müller-Newen G**, **Schaper F**, **Heinrich PC**, **Graeve L**. Constitutive internalization and association with adaptor protein-2 of the interleukin-6 signal transducer gp130. *FEBS Lett*. 1997; **441**:231–234.DOI: 10.1016/S0014-5793(98)01559-2.

57. **Schmitz J**, **Weissenbach M**, **Haan S**, **Heinrich PC**, **Schaper F**. SOCS3 exerts its inhibitory function on interleukin-6 signal transduction through the SHP2 recruitment site of gp130. *Journal of Biological Chemistry*. 2000; **275**:12848–12856.DOI: 10.1074/jbc.275.17.12848.

58. **Boulanger MJ**, **Chow D-C**, **Brevnova EE**, **Garcia KC**. Hexameric structure and assembly of the interleukin-6/IL-6 alpha-receptor/gp130 complex. *Science*. 2003; **300**:2101–2104.DOI: 10.1126/science.1083901.

59. **Müller-Newen G**. The cytokine receptor gp130: faithfully promiscuous. *Sci Signal*. 2003.DOI: 10.1126/stke.2003.201.pe40].

60. **Pellegrini S**, **Dusanter-Fourt I**. The structure, regulation and function of the Janus kinases (JAKs) and the signal transducers and activators of transcription (STATs). *Eur J Biochem*. 1997; **248**:615–633.DOI: 10.1111/j.1432-1033.1997.00615.x.

61. **Rane SG**, **Reddy EP**. Janus kinases: components of multiple signaling pathways. *Oncogene*. 2000; **19**:5662–5679.DOI: 10.1038/sj.onc.1203925.

62. **Kortylewski M**, **Feld F**, **Krüger K-D**, **Bahrenberg G**, **Roth RA**, **Joost H-G**, **Heinrich PC**, *et al.* Akt modulates STAT3-mediated gene expression through a FKHR (FOXO1a)-dependent mechanism. *Journal of Biological Chemistry*. 2003; **278**:5242–5249.DOI: 10.1074/jbc.M205403200.

63. **Gerhartz C**, **Heesel B**, **Sasse J**, **Hemmann U**, **Landgraf C**, **SchneiderMergener J**, **Horn F**, *et al.* Differential activation of acute phase response factor/STAT3 and STAT1 via the cytoplasmic domain of the interleukin 6 signal transducer gp130 .1. Definition of a novel phosphotyrosine motif mediating STAT1 activation. *Journal of Biological Chemistry*. 1996; **271**:12991–12998.DOI: 10.1074/jbc.271.22.12991.

64. **Schmitz J**, **Dahmen H**, **Grimm C**, **Gendo C**, **Müller-Newen G**, **Heinrich PC**, **Schaper F**. The Cytoplasmic Tyrosine Motifs in Full-Length Glycoprotein 130 Have Different Roles in IL-6 Signal Transduction. *J Immunol*. 2000; **164**:848–854.DOI: 10.4049/jimmunol.164.2.848.

65. **Kaptein A**, **Paillard V**, **Saunders M**. Dominant Negative Stat3 Mutant Inhibits Interleukin-6-induced Jak-STAT Signal Transduction. *Journal of Biological Chemistry*. 1996; **271**:5961–5964.DOI: 10.1074/jbc.271.11.5961.

66. **Shuai K**, **Stark G**, **Kerr I**, **Darnell J**. A single phosphotyrosine residue of Stat91 required for gene activation by interferon-gamma. *Science*. 1993; **261**:1744–1746.DOI: 10.1126/science.7690989.

67. **Starr R**, **Willson TA**, **Viney EM**, **Murray LJ**, **Rayner JR**. A family of cytokine-inducible inhibitors of signalling. *Nature*. 1997; **387**:917–921.DOI: 10.1038/43206.

68. **Eilers A**, **Georgellis D**, **Klose B**, **Schindler C**, **Ziemiecki A**, **Harpur AG**, **Wilks AF**, *et al.* Differentiation-regulated serine phosphorylation of STAT1 promotes GAF activation in macrophages. *Mol Cell Biol*. 1995; **15**:3579–3586.

69. **Zhang X**, **Blenis J**, **Li H**, **Schindler C**, **Chen-Kiang S**. Requirement of serine phosphorylation for formation of STAT-promoter complexes. *Science*. 1995; **267**:1990–1994.DOI: 10.1126/science.7701321.

70. **Wen Z**, **Zhong Z**, **Darnell JE Jr.** Maximal activation of transcription by statl and stat3 requires both tyrosine and serine phosphorylation. *Cell*. 1995; **82**:241–250.DOI: 10.1016/0092-8674(95)90311-9.

71. **Wegrzyn J**, **Potla R**, **Chwae Y-J**, **Sepuri NBV**, **Zhang Q**, **Koeck T**, **Derecka M**, *et al.* Function of mitochondrial Stat3 in cellular respiration. *Science*. 2009; **323**:793–797.DOI: 10.1126/science.1164551.

72. **Gough DJ**, **Corlett A**, **Schlessinger K**, **Wegrzyn J**, **Larner AC**, **Levy DE**. Mitochondrial STAT3 Supports Ras-Dependent Oncogenic Transformation. *Science*. 2009; **324**:1713–1716.DOI: 10.1126/science.1171721.

73. **Stahl N**, **Farruggella T**, **Boulton T**, **Zhong Z**, **Darnell J**, **Yancopoulos G**. Choice of STATs and other substrates specified by modular tyrosine-based motifs in cytokine receptors. *Science*. 1995; **267**:1349–1353.DOI: 10.1126/science.7871433.

74. **Lock LS**, **Royal I**, **Naujokas MA**, **Park M**. Identification of an Atypical Grb2 Carboxyl-terminal SH3 Domain Binding Site in Gab Docking Proteins Reveals Grb2-dependent and -independent Recruitment of Gab1 to Receptor Tyrosine Kinases. *Journal of Biological Chemistry*. 2000; **275**:31536–31545.DOI: 10.1074/jbc.M003597200.

75. **Schaeper U**, **Gehring NH**, **Fuchs KP**, **Sachs M**, **Kempkes B**, **Birchmeier W**. Coupling of Gab1 to c-Met, Grb2, and Shp2 mediates biological responses. *The Journal of Cell Biology*. 2000; **149**:1419–1432.DOI: 10.1083/jcb.149.7.1419.

76. **Isakoff SJ**, **Cardozo T**, **Andreev J**, **Li Z**, **Ferguson KM**, **Abagyan R**, **Lemmon MA**, *et al.* Identification and analysis of PH domain-containing targets of phosphatidylinositol 3-kinase using a novel in vivo assay in yeast. *EMBO J.* 1998; **17**:5374–5387.DOI: 10.1093/emboj/17.18.5374.

77. **Maroun CR**, **Moscatello DK**, **Naujokas MA**, **Holgado-Madruga M**, **Wong AJ**, **Park M**. A Conserved Inositol Phospholipid Binding Site within the Pleckstrin Homology Domain of the Gab1 Docking Protein Is Required for Epithelial Morphogenesis. *Journal of Biological Chemistry*. 1999; **274**:31719–31726.DOI: 10.1074/jbc.274.44.31719.

78. **Stephens LR**, **Jackson TR**, **Hawkins PT**. Agonist-stimulated synthesis of phosphatidylinositol(3,4,5)-trisphosphate. *Biochimica et Biophysica Acta (BBA) - Molecular Cell Research*. 1993; **1179**:27–75.DOI: 10.1016/0167-4889(93)90072-W.

79. **Vara JÁF**, **Casado E**, **de Castro J**, **Cejas P**, **Belda-Iniesta C**, **González-Barón M**. PI3K/Akt signalling pathway and cancer. *Cancer Treatment Reviews*. 2004; **30**:193–204.DOI: 10.1016/j.ctrv.2003.07.007.

80. **Pluskey S**, **Wandless TJ**, **Walsh CT**, **Shoelson SE**. Potent stimulation of SH-PTP2 phosphatase activity by simultaneous occupancy of both SH2 domains. *Journal of Biological Chemistry*. 1995; **270**:2897–2900.

81. **Lehmann U**, **Schmitz J**, **Weissenbach M**, **Sobota RM**, **Hortner M**, **Friederichs K**, **Behrmann I**, *et al.* SHP2 and SOCS3 contribute to Tyr-759-dependent attenuation of interleukin-6 signaling through gp130. *Journal of Biological Chemistry*. 2003; **278**:661–671.DOI: 10.1074/jbc.M210552200.

82. **Liu B**, **Liao J**, **Rao X**, **Kushner SA**, **Chung CD**, **Chang DD**, **Shuai K**. Inhibition of Stat1-mediated gene activation by PIAS1. *Proceedings of the National Academy of Sciences*. 1998; **95**:10626–10631.DOI: 10.1073/pnas.95.18.10626.

83. **Chung CD**, **Liao J**, **Liu B**, **Rao X**, **Jay P**, **Berta P**, **Shuai K**. Specific inhibition of Stat3 signal transduction by PIAS3. *Science*. 1997; **278**:1803–1805.DOI: 10.1126/science.278.5344.1803.

84. **Yoshimura A**, **Ohkubo T**, **Kiguchi T**, **Jenkins NA**, **Gilbert DJ**, **Copeland NG**, **Hara T**, *et al.* A novel cytokine-inducible gene CIS encodes an SH2-containing protein that binds to tyrosine-phosphorylated interleukin 3 and erythropoietin receptors. *EMBO J.* 1995; **14**:2816–2826.

85. **Hilton DJ**, **Richardson RT**, **Alexander WS**, **Viney EM**, **Willson TA**, **Sprigg NS**, **Starr R**, *et al.* Twenty proteins containing a C-terminal SOCS box form five structural classes. *Proceedings of the National Academy of Sciences*. 1998; **95**:114–119.DOI: 10.1073/pnas.95.1.114.

86. **Krebs DL**, **Hilton DJ**. SOCS proteins: negative regulators of cytokine signaling. *Stem Cells*. 2001; **19**:378–387.DOI: 10.1634/stemcells.19-5-378.

87. **Zhang JG**, **Farley A**, **Nicholson SE**, **Willson TA**, **Zugaro LM**, **Simpson RJ**, **Moritz RL**, *et al.* The conserved SOCS box motif in suppressors of cytokine signaling binds to elongins B and C and may couple bound proteins to proteasomal degradation. *Proceedings of the National Academy of Sciences*. 1999; **96**:2071–2076.DOI: 10.1073/pnas.96.5.2071.

88. **Croker BA**, **Kiu H**, **Pellegrini M**, **Toe J**, **Preston S**, **Metcalf D**, **O'Donnell JA**, *et al.* IL-6 promotes acute and chronic inflammatory disease in the absence of SOCS3. *Immunol Cell Biol*. 2011; **90**:124–129.DOI: 10.1038/icb.2011.29.

89. **Sasaki A**, **Yasukawa H**, **Suzuki A**, **Kamizono S**, **Syoda T**, **Kinjyo I**, **Sasaki M**, *et al.* Cytokine-inducible SH2 protein-3 (CIS3/SOCS3) inhibits Janus tyrosine kinase by binding through the N-terminal kinase inhibitory region as well as SH2 domain. *Genes Cells*. 1999; **4**:339–351.DOI: 10.1046/j.1365-2443.1999.00263.x.

90. **Kershaw NJ**, **Murphy JM**, **Liau NPD**, **Varghese LN**, **Laktyushin A**, **Whitlock EL**, **Lucet IS**, *et al.* SOCS3 binds specific receptor–JAK complexes to control cytokine signaling by direct kinase inhibition. *Nat Struct Mol Biol*. 2013; **20**:469–476.DOI: 10.1038/nsmb.2519.

91. **Babon JJ**, **Sabo JK**, **Soetopo A**, **Yao S**, **Bailey MF**, **Zhang J-G**, **Nicola NA**, *et al.* The SOCS Box Domain of SOCS3: Structure and Interaction with the ElonginBC-Cullin5 Ubiquitin Ligase. *Journal of Molecular Biology*. 2008; **381**:928–940.DOI: 10.1016/j.jmb.2008.06.038.

92. **Petroski MD**, **Deshaies RJ**. Function and regulation of cullin-RING ubiquitin ligases. *Nat. Rev. Mol. Cell Biol.* 2005; **6**:9–20.DOI: 10.1038/nrm1547.

93. **Kershaw NJ**, **Laktyushin A**, **Nicola NA**, **Babon JJ**. Reconstruction of an active SOCS3-based E3 ubiquitin ligase complex in vitro: identification of the active components and JAK2 and gp130 as substrates. *Growth Factors*. 2014; **32**:1–10.DOI: 10.3109/08977194.2013.877005.

94. **Hanahan D**, **Weinberg RA**. Hallmarks of cancer: the next generation. *Cell*. 2011; **144**:646–674.DOI: 10.1016/j.cell.2011.02.013.

95. **Grivennikov SI**, **Karin M**. Inflammation and oncogenesis: a vicious connection. *Curr. Opin. Genet. Dev.* 2010; **20**:65–71.DOI: 10.1016/j.gde.2009.11.004.

96. **Coussens LM**, **Werb Z**. Inflammation and cancer. *Nature*. 2002; **420**:860–867.DOI: 10.1038/nature01322.

97. **Mantovani A**, **Allavena P**, **Sica A**, **Balkwill F**. Cancer-related inflammation. *Nature*. 2008; **454**:436–444.DOI: 10.1038/nature07205.

98. **Punturieri A**, **Szabo E**, **Croxton TL**, **Shapiro SD**, **Dubinett SM**. Lung Cancer and Chronic Obstructive Pulmonary Disease: Needs and Opportunities for Integrated Research. *JNCI Journal of the*

National Cancer Institute. 2009; **101**:554–559.DOI: 10.1093/jnci/djp023.

99. **Roder DM**. The epidemiology of gastric cancer. *Gastric Cancer*. 2002; **5 Suppl 1**:5–11.DOI: 10.1007/s10120-002-0203-6.

100. **Karin M**. Nuclear factor-kappaB in cancer development and progression. *Nature*. 2006; **441**:431–436.DOI: 10.1038/nature04870.

101. **Waldner MJ**, **Neurath MF**. Colitis-associated cancer: the role of T cells in tumor development. *Seminars in Immunopathology*. 2009; **31**:249–256.DOI: 10.1007/s00281-009-0161-8.

102. **Nickoloff BJ**, **Ben-Neriah Y**, **Pikarsky E**. Inflammation and Cancer: Is the Link as Simple as We Think? *J Investig Dermatol*. 2005; **124**:x–xiv.DOI: 10.1111/j.0022-202X.2005.23724.x.

103. **Sparmann A**, **Bar-Sagi D**. Ras-induced interleukin-8 expression plays a critical role in tumor growth and angiogenesis. *Cancer cell*. 2004; **6**:447–458.DOI: 10.1016/j.ccr.2004.09.028.

104. **Sumimoto H**, **Imabayashi F**, **Iwata T**, **Kawakami Y**. The BRAF-MAPK signaling pathway is essential for cancer-immune evasion in human melanoma cells. *J Exp Med*. 2006; **203**:1651–1656.DOI: 10.1084/jem.20051848.

105. **Shchors K**, **Shchors E**, **Rostker F**, **Lawlor ER**, **Brown-Swigart L**, **Evan GI**. The Myc-dependent angiogenic switch in tumors is mediated by interleukin 1beta. *Genes Dev*. 2006; **20**:2527–2538.DOI: 10.1101/gad.1455706.

106. **Hussain SP**, **Hofseth LJ**, **Harris CC**. Radical causes of cancer. *Nat Rev Cancer*. 2003; **3**:276–285.DOI: 10.1038/nrc1046.

107. **Colotta F**, **Allavena P**, **Sica A**, **Garlanda C**, **Mantovani A**. Cancer-related inflammation, the seventh hallmark of cancer: links to genetic instability. *Carcinogenesis*. 2009; **30**:1073–1081.DOI: 10.1093/carcin/bgp127.

108. **Okazaki I-M**, **Kotani A**, **Honjo T**. Role of AID in Tumorigenesis. In: *AID for Immunoglobulin Diversity*.Vol 94. Advances in Immunology. Elsevier; 2007:245–273.DOI: 10.1016/S0065-2776(06)94008-5.

109. **Chen X**, **Xu H**, **Yuan P**, **Fang F**, **Huss M**, **Vega VB**, **Wong E**, *et al.* Integration of External Signaling Pathways with the Core Transcriptional Network in Embryonic Stem Cells. *Cell*. 2008; **133**:1106–1117.DOI: 10.1016/j.cell.2008.04.043.

110. **Lewis CE**, **Pollard JW**. Distinct role of macrophages in different tumor microenvironments. *Cancer research*. 2006; **66**:605–612.DOI: 10.1158/0008-5472.CAN-05-4005.

111. **de Visser KE**, **Eichten A**, **Coussens LM**. Paradoxical roles of the immune system during cancer development. *Nat Rev Cancer*. 2006; **6**:24–37.DOI: 10.1038/nrc1782.

112. **Bollrath J**, **Phesse TJ**, **Burstin von VA**, **Putoczki T**, **Bennecke M**, **Bateman T**, **Nebelsiek T**, *et al.* gp130-Mediated Stat3 Activation in Enterocytes Regulates Cell Survival and Cell-Cycle Progression during Colitis-Associated Tumorigenesis. *Cancer cell*. 2009; **15**:91–102.DOI: 10.1016/j.ccr.2009.01.002.

113. **Bromberg JF**, **Wrzeszczynska MH**, **Devgan G**, **Zhao Y**, **Pestell RG**, **Albanese C**, **Darnell JE**. Stat3 as an oncogene. *Cell*. 1999; **98**:295–303.DOI: 10.1016/S0092-8674(00)81959-5.

114. **Real PJ**, **Sierra A**, **De Juan A**, **Segovia JC**, **Lopez-Vega JM**, **Fernandez-Luna JL**. Resistance to chemotherapy via Stat3-dependent overexpression of Bcl-2 in metastatic breast cancer cells. *Oncogene*. 2002; **21**:7611–7618.DOI: 10.1038/sj.onc.1206004.

115. **Rahaman SO**, **Harbor PC**, **Chernova O**, **Barnett GH**, **Vogelbaum MA**, **Haque SJ**. Inhibition of constitutively active Stat3 suppresses proliferation and induces apoptosis in glioblastoma multiforme cells. *Oncogene*. 2002; **21**:8404–8413.DOI: 10.1038/sj.onc.1206047.

116. **Kanda N**, **Seno H**, **Konda Y**, **Marusawa H**, **Kanai M**, **Nakajima T**, **Kawashima T**, *et al.* STAT3 is constitutively activated and supports cell survival in association with survivin expression in gastric cancer cells. *Oncogene*. 2004; **23**:4921–4929.DOI: 10.1038/sj.onc.1207606.

117. **Ivanov VN**, **Bhoumik A**, **Krasilnikov M**, **Raz R**, **Owen-Schaub LB**, **Levy D**, **Horvath CM**, *et al.* Cooperation between STAT3 and c-jun suppresses Fas transcription. *Mol Cell*. 2001; **7**:517–528.DOI: 10.1016/S1097-2765(01)00199-X.

118. **Wei D**, **Le X**, **Zheng L**, **Wang L**, **Frey JA**, **Gao AC**, **Peng Z**, *et al.* Stat3 activation regulates the expression of vascular endothelial growth factor and human pancreatic cancer angiogenesis and metastasis. *Oncogene*. 2003; **22**:319–329.DOI: 10.1038/sj.onc.1206122.

119. **Niu G**, **Wright KL**, **Huang M**, **Song L**, **Haura E**, **Turkson J**, **Zhang S**, *et al.* Constitutive Stat3 activity up-regulates VEGF expression and tumor angiogenesis. *Oncogene*. 2002; **21**:2000–2008.DOI: 10.1038/sj.onc.1205260.

120. **Dang EV**, **Barbi J**, **Yang H-Y**, **Jinasena D**, **Yu H**, **Zheng Y**, **Bordman Z**, *et al.* Control of TH17/Treg Balance by Hypoxia-Inducible Factor 1. *Cell*. 2011; **146**:772–784.DOI: 10.1016/j.cell.2011.07.033.

121. **Ahluwalia A**, **Tarnawski AS**. Critical role of hypoxia sensor-HIF-1α in VEGF gene activation. Implications for angiogenesis and tissue injury healing. *Current medicinal chemistry*. 2012.DOI: 10.2174/092986712803413944.

122. **Xie T-X**, **Huang F-J**, **Aldape KD**, **Kang S-H**, **Liu M**, **Gershenwald JE**, **Xie K**, *et al.* Activation of stat3 in human melanoma promotes brain metastasis. *Cancer research*. 2006; **66**:3188–3196.DOI: 10.1158/0008-5472.CAN-05-2674.

123. **Sullivan NJ**, **Sasser AK**, **Axel AE**, **Vesuna F**, **Raman V**, **Ramirez N**, **Oberyszyn TM**, *et al.* Interleukin-6 induces an epithelial–mesenchymal transition phenotype in human breast cancer cells. *Oncogene*. 2009; **28**:2940–2947.DOI: 10.1038/onc.2009.180.

124. **Demaria M**, **Giorgi C**, **Lebiedzinska M**, **Esposito G**, **D'Angeli L**, **Bartoli A**, **Gough DJ**, *et al.* A STAT3-mediated metabolic switch is involved in tumour transformation and STAT3 addiction. *Aging*. 2010; **2**:823–842.

125. **Darnell JE**. STAT3, HIF-1, glucose addiction and Warburg effect. *Aging*. 2010; **2**:890–891.

126. **Bourgeais J**, **Gouilleux-Gruart V**, **Gouilleux F**. Oxidative metabolism in cancer: A STAT affair? *jak-stat*. 2013; **2**:e25764.DOI: 10.4161/jkst.25764.

127. **Hutchins AP**, **Diez D**, **Miranda-Saavedra D**. The IL-10/STAT3-mediated anti-inflammatory response: recent developments and future challenges. *Brief Funct Genomics*. 2013; **12**:489–498.DOI: 10.1093/bfgp/elt028.

128. **Bettelli E**, **Carrier Y**, **Gao W**, **Korn T**, **Strom TB**, **Oukka M**, **Weiner HL**, *et al.* Reciprocal developmental pathways for the generation of pathogenic effector TH17 and regulatory T cells.

Nature. 2006; **441**:235–238.DOI: 10.1038/nature04753.

129. **Kolls JK**, **Lindén A**. Interleukin-17 family members and inflammation. *Immunity*. 2004; **21**:467–476.DOI: 10.1016/j.immuni.2004.08.018.

130. **Nault JC**, **Bioulac-Sage P**, **Zucman-Rossi J**. Hepatocellular Benign Tumors—From Molecular Classification to Personalized Clinical Care. *Gastroenterology*. 2013; **144**:888–902.DOI: 10.1053/j.gastro.2013.02.032.

131. **Rooks JB**, **Ory HW**, **Ishak KG**, **Strauss LT**, **Greenspan JR**, **Hill AP**, **Tyler CW**. Epidemiology of hepatocellular adenoma. The role of oral contraceptive use. *JAMA*. 1979; **242**:644–648.

132. **Pilati C**, **Letouzé E**, **Nault JC**, **Imbeaud S**, **Boulai A**, **Calderaro J**, **Poussin K**, *et al.* Genomic Profiling of Hepatocellular Adenomas Reveals Recurrent FRK-Activating Mutations and the Mechanisms of Malignant Transformation. *Cancer cell*. 2014; **25**:428–441.DOI: 10.1016/j.ccr.2014.03.005.

133. **Rebouissou S**, **Amessou M**, **Couchy G**, **Poussin K**, **Imbeaud S**, **Pilati C**, **Izard T**, *et al.* Frequent in-frame somatic deletions activate gp130 in inflammatory hepatocellular tumours. *Nature*. 2009; **457**:200–204.DOI: 10.1038/nature07475.

134. **Poussin K**, **Pilati C**, **Couchy G**, **Calderaro J**, **Bioulac-Sage P**, **Bacq Y**, **Paradis V**, *et al.* Biochemical and functional analyses of gp130 mutants unveil JAK1 as a novel therapeutic target in human inflammatory hepatocellular adenoma. *oncoimmunology*. 2013; **2**:e27090.DOI: 10.4161/onci.27090.

135. **Pilati C**, **Amessou M**, **Bihl MP**, **Balabaud C**, **Van Nhieu JT**, **Paradis V**, **Nault JC**, *et al.* Somatic mutations activating STAT3 in human inflammatory hepatocellular adenomas. *J Exp Med*. 2011; **208**:1359–1366.DOI: 10.1084/jem.20110283.

136. **Seifert R**, **Wenzel-Seifert K**. Constitutive activity of G-protein-coupled receptors: cause of disease and common property of wild-type receptors. *Naunyn Schmiedebergs Arch Pharmacol*. 2002; **366**:381–416.DOI: 10.1007/s00210-002-0588-0.

137. **Leff P**. The two-state model of receptor activation. *Trends Pharmacol Sci*. 1995; **16**:89–97.DOI: 10.1016/S0165-6147(00)88989-0.

138. **Tonacchera M**, **Van Sande J**, **Cetani F**, **Swillens S**, **Schvartz C**, **Winiszewski P**, **Portmann L**, *et al.* Functional characteristics of three new germline mutations of the thyrotropin receptor gene causing autosomal dominant toxic thyroid hyperplasia. *The Journal of Clinical Endocrinology & Metabolism*. 1996; **81**:547–554.DOI: 10.1210/jcem.81.2.8636266.

139. **Kosugi S**, **Shenker A**, **Mori T**. Constitutive activation of cyclic AMP but not phosphatidylinositol signaling caused by four mutations in the 6th transmembrane helix of the human thyrotropin receptor. *FEBS Lett*. 1994; **356**:291–294.DOI: 10.1016/0014-5793(94)01286-5.

140. **Duprez L**, **Parma J**, **Costagliola S**, **Hermans J**, **Van Sande J**, **Dumont JE**, **Vassart G**. Constitutive activation of the TSH receptor by spontaneous mutations affecting the N-terminal extracellular domain. *FEBS Lett*. 1997; **409**:469–474.DOI: 10.1016/S0014-5793(97)00532-2.

141. **Schaffer K**, **McBride EW**, **Beinborn M**, **Kopin AS**. Interspecies Polymorphisms Confer Constitutive Activity to theMastomys Cholecystokinin-B/Gastrin Receptor. *Journal of Biological Chemistry*. 1998; **273**:28779–28784.DOI: 10.1074/jbc.273.44.28779.

142. **Latronico AC**, **Anasti J**, **Arnhold IJ**, **Mendonça BB**, **Domenice S**, **Albano MC**, **Zachman K**, *et al.* A

novel mutation of the luteinizing hormone receptor gene causing male gonadotropin-independent precocious puberty. *The Journal of Clinical Endocrinology & Metabolism*. 1995; **80**:2490–2494.DOI: 10.1210/jcem.80.8.7629248.

143. **Yoshimura A**, **Longmore G**, **Lodish HF**. Point mutation in the exoplasmic domain of the erythropoietin receptor resulting in hormone-independent activation and tumorigenicity. *Nature*. 1990; **348**:647–649.DOI: 10.1038/348647a0.

144. **Watowich SS**, **Yoshimura A**, **Longmore GD**, **Hilton DJ**, **Yoshimura Y**, **Lodish HF**. Homodimerization and constitutive activation of the erythropoietin receptor. *Proceedings of the National Academy of Sciences*. 1992; **89**:2140–2144.

145. **White DW**, **Wang DW**, **Chua SC**, **Morgenstern JP**, **Leibel RL**, **Baumann H**, **Tartaglia LA**. Constitutive and impaired signaling of leptin receptors containing the Gln --> Pro extracellular domain fatty mutation. *Proceedings of the National Academy of Sciences*. 1997; **94**:10657–10662.DOI: 10.1073/pnas.94.20.10657.

146. **Marty C**, **Chaligné R**, **Lacout C**, **Constantinescu SN**, **Vainchenker W**, **Villeval J-L**. Ligand-independent thrombopoietin mutant receptor requires cell surface localization for endogenous activity. *Journal of Biological Chemistry*. 2009; **284**:11781–11791.DOI: 10.1074/jbc.M808703200.

147. **Matsumura I**, **Mizuki M**, **Kanakura Y**. Roles for deregulated receptor tyrosine kinases and their downstream signaling molecules in hematologic malignancies. *Cancer Sci*. 2008; **99**:479–485.DOI: 10.1111/j.1349-7006.2007.00717.x.

148. **Furitsu T**, **Tsujimura T**, **Tono T**, **Ikeda H**, **Kitayama H**, **Koshimizu U**, **Sugahara H**, *et al.* Identification of mutations in the coding sequence of the proto-oncogene c-kit in a human mast cell leukemia cell line causing ligand-independent activation of c-kit product. *Journal of Clinical Investigation*. 1993; **92**:1736–1744.DOI: 10.1172/JCI116761.

149. **Tsujimura T**, **Morimoto M**, **Hashimoto K**, **Moriyama Y**, **Kitayama H**, **Matsuzawa Y**, **Kitamura Y**, *et al.* Constitutive activation of c-kit in FMA3 murine mastocytoma cells caused by deletion of seven amino acids at the juxtamembrane domain. *Blood*. 1996; **87**:273–283.

150. **London CA**, **Galli SJ**, **Yuuki T**, **Hu ZQ**, **Helfand SC**, **Geissler EN**. Spontaneous canine mast cell tumors express tandem duplications in the proto-oncogene c-kit. *Exp Hematol*. 1999; **27**:689–697.

151. **Hirota S**, **Isozaki K**, **Moriyama Y**, **Hashimoto K**, **Nishida T**, **Ishiguro S**, **Kawano K**, *et al.* Gain-of-function mutations of c-kit in human gastrointestinal stromal tumors. *Science*. 1998; **279**:577–580.

152. **Nakao M**, **Yokota S**, **Iwai T**, **Kaneko H**, **Horiike S**, **Kashima K**, **Sonoda Y**, *et al.* Internal tandem duplication of the flt3 gene found in acute myeloid leukemia. *Leukemia*. 1996; **10**:1911–1918.

153. **Arcone R**, **Pucci P**, **Zappacosta F**, **Fontaine V**, **Malorni A**, **Marino G**, **Ciliberto G**. Single-step purification and structural characterization of human interleukin-6 produced in Escherichia coli from a T7 RNA polymerase expression vector. *Eur J Biochem*. 1991; **198**:541–547.DOI: 10.1111/j.1432-1033.1991.tb16048.x.

154. **Weiergraber O**, **Hemmann U**, **Küster A**, **Müller-Newen G**, **Schneider J**, **Rose-John S**, **Kurschat P**, *et al.* Soluble Human Interleukin-6 Receptor. Expression in Insect Cells, Purification and Characterization. *Eur J Biochem*. 1995; **234**:661–669.DOI: 10.1111/j.1432-1033.1995.661_b.x.

155. **Morrison DK**, **Davis RJ**. Regulation of MAP kinase signaling modules by scaffold proteins in mammals. *Annu. Rev. Cell Dev. Biol.* 2003; **19**:91–118.DOI:

10.1146/annurev.cellbio.19.111401.091942.

156. **Böing I**, **Stross C**, **Radtke S**, **Lippok BE**, **Heinrich PC**, **Hermanns HM**. Oncostatin M-induced activation of stress-activated MAP kinases depends on tyrosine 861 in the OSM receptor and requires Jak1 but not Src kinases. *Cellular Signalling*. 2006; **18**:50–61.DOI: 10.1016/j.cellsig.2005.03.015.

157. **Zerangue N**, **Malan MJ**, **Fried SR**, **Dazin PF**, **Jan YN**, **Jan LY**, **Schwappach B**. Analysis of endoplasmic reticulum trafficking signals by combinatorial screening in mammalian cells. *Proceedings of the National Academy of Sciences*. 2001; **98**:2431–2436.DOI: 10.1073/pnas.051630198.

158. **Schwartz V**, **Lue H**, **Kraemer S**, **Korbiel J**, **Krohn R**, **Ohl K**, **Bucala R**, *et al.* A functional heteromeric MIF receptor formed by CD74 and CXCR4. *FEBS Lett*. 2009; **583**:2749–2757.DOI: 10.1016/j.febslet.2009.07.058.

159. **Tenhumberg S**, **Schuster B**, **Zhu L**, **Kovaleva M**, **Scheller J**, **Kallen K-J**, **Rose-John S**. gp130 dimerization in the absence of ligand: Preformed cytokine receptor complexes. *Biochem Biophys Res Commun*. 2006; **346**:649–657.DOI: 10.1016/j.bbrc.2006.05.173.

160. **Wijdenes J**, **Heinrich PC**, **Müller-Newen G**, **Roche C**, **Gu Z-J**, **Clément C**, **Klein B**. Interleukin-6 signal transducer gp130 has specific binding sites for different cytokines as determined by antagonistic and agonistic anti-gp130 monoclonal antibodies. *Eur J Immunol*. 1995; **25**:3474–3481.DOI: 10.1002/eji.1830251240.

161. **Sommer J**, **Effenberger T**, **Volpi E**, **Waetzig GH**, **Bernhardt M**, **Suthaus J**, **Garbers C**, *et al.* Constitutively Active Mutant gp130 Receptor Protein from Inflammatory Hepatocellular Adenoma Is Inhibited by an Anti-gp130 Antibody That Specifically Neutralizes Interleukin 11 Signaling. *Journal of Biological Chemistry*. 2012; **287**:13743–13751.DOI: 10.1074/jbc.M111.349167.

162. **Mohr A**, **Fahrenkamp D**, **Rinis N**, **Müller-Newen G**. Dominant-negative activity of the STAT3-Y705F mutant depends on the N-terminal domain. *Cell Commun. Signal*. 2013; **11**:83.DOI: 10.1186/1478-811X-11-83.

163. **Irandoust MI**, **Aarts LHJ**, **Roovers O**, **Gits J**, **Erkeland SJ**, **Touw IP**. Suppressor of cytokine signaling 3 controls lysosomal routing of G-CSF receptor. *EMBO J.* 2007; **26**:1782–1793.DOI: 10.1038/sj.emboj.7601640.

164. **Schmidt-Arras D**, **Muller M**, **Stevanovic M**, **Horn S**, **Schutt A**, **Bergmann J**, **Wilkens R**, *et al.* Oncogenic deletion mutants of gp130 signal from intracellular compartments. *J Cell Sci*. 2014; **127**:341–353.DOI: 10.1242/jcs.130294.

165. **Schmidt-Arras D-E**, **Böhmer A**, **Markova B**, **Choudhary C**, **Serve H**, **Böhmer F-D**. Tyrosine phosphorylation regulates maturation of receptor tyrosine kinases. *Mol Cell Biol*. 2005; **25**:3690–3703.DOI: 10.1128/MCB.25.9.3690-3703.2005.

166. **Schütt A**, **Zacharias M**, **Schneider N**, **Horn S**, **Grötzinger J**, **Rose-John S**, **Schmidt-Arras D**. gp130 activation is regulated by D2–D3 interdomain connectivity. *Biochem J*. 2013; **450**:487–496.DOI: 10.1042/BJ20121660.

167. **Mitra N**, **Sinha S**, **Ramya TNC**, **Surolia A**. N-linked oligosaccharides as outfitters for glycoprotein folding, form and function. *Trends Biochem. Sci.* 2006; **31**:156–163.DOI: 10.1016/j.tibs.2006.01.003.

168. **Ellgaard L**, **Helenius A**. Quality control in the endoplasmic reticulum. *Nat. Rev. Mol. Cell Biol.* 2003; **4**:181–191.DOI: 10.1038/nrm1052.

169. **Hetz C**. The unfolded protein response: controlling cell fate decisions under ER stress and beyond. *Nat. Rev. Mol. Cell Biol.* 2012; **13**:89–102.DOI: 10.1038/nrm3270.

170. **Eulenfeld R**, **Schaper F**. A new mechanism for the regulation of Gab1 recruitment to the plasma membrane. *J Cell Sci*. 2009; **122**:574–574.DOI: 10.1242/jcs.049551.

171. **Schmidt-Arras D**, **Bohmer SA**, **Koch S**, **Muller JP**, **Blei L**, **Cornils H**, **Bauer R**, *et al.* Anchoring of FLT3 in the endoplasmic reticulum alters signaling quality. *Blood*. 2009; **113**:3568–3576.DOI: 10.1182/blood-2007-10-121426.

172. **Joffre C**, **Barrow R**, **Ménard L**, **Calleja V**, **Hart IR**, **Kermorgant S**. A direct role for Met endocytosis in tumorigenesis. *Nat Cell Biol*. 2011; **13**:827–837.DOI: 10.1038/ncb2257.

173. **Brankatschk B**, **Wichert SP**, **Johnson SD**, **Schaad O**, **Rossner MJ**, **Gruenberg J**. Regulation of the EGF Transcriptional Response by Endocytic Sorting. *Sci Signal*. 2012; **5**:ra21–ra21.DOI: 10.1126/scisignal.2002351.

174. **Teasdale RD**, **Jackson MR**. Signal-mediated sorting of membrane proteins between the endoplasmic reticulum and the golgi apparatus. *Annu. Rev. Cell Dev. Biol.* 1996; **12**:27–54.DOI: 10.1146/annurev.cellbio.12.1.27.

175. **Jackson CL**, **Casanova JE**. Turning on ARF: the Sec7 family of guanine-nucleotide-exchange factors. *Trends Cell Biol*. 2000; **10**:60–67.DOI: 10.1016/S0962-8924(99)01699-2.

176. **Springer S**, **Spang A**, **Schekman R**. A primer on vesicle budding. *Cell*. 1999; **97**:145–148.

177. **Royer Y**, **Staerk J**, **Costuleanu M**, **Courtoy PJ**, **Constantinescu SN**. Janus Kinases Affect Thrombopoietin Receptor Cell Surface Localization and Stability. *Journal of Biological Chemistry*. 2005; **280**:27251–27261.DOI: 10.1074/jbc.M501376200.

178. **Huang LJ**, **Constantinescu SN**, **Lodish HF**. The N-terminal domain of Janus kinase 2 is required for Golgi processing and cell surface expression of erythropoietin receptor. *Mol Cell*. 2001; **8**:1327–1338.DOI: 10.1016/S1097-2765(01)00401-4.

179. **Radtke S**, **Hermanns HM**, **Haan C**, **Schmitz-Van de Leur H**, **Gascan H**, **Heinrich PC**, **Behrmann I**. Novel Role of Janus Kinase 1 in the Regulation of Oncostatin M Receptor Surface Expression. *Journal of Biological Chemistry*. 2002; **277**:11297–11305.DOI: 10.1074/jbc.M100822200.

180. **Stuhlmann-Laeisz C**. Forced Dimerization of gp130 Leads to Constitutive STAT3 Activation, Cytokine-independent Growth, and Blockade of Differentiation of Embryonic Stem Cells. *Mol Biol Cell*. 2006; **17**:2986–2995.DOI: 10.1091/mbc.E05-12-1129.

181. **Sorkin A**, **Zastrow von M**. Endocytosis and signalling: intertwining molecular networks. *Nat. Rev. Mol. Cell Biol.* 2009; **10**:609–622.DOI: 10.1038/nrm2748.

182. **Sadowski L**, **Pilecka I**, **Miaczynska M**. Signaling from endosomes: Location makes a difference. *Experimental Cell Research*. 2009; **315**:1601–1609.DOI: 10.1016/j.yexcr.2008.09.021.

183. **Wang J**, **Pantopoulos K**. Regulation of cellular iron metabolism. *Biochem J*. 2011; **434**:365–381.DOI: 10.1042/BJ20101825.

184. **Conner SD**, **Schmid SL**. Regulated portals of entry into the cell. *Nature*. 2003; **422**:37–44.DOI: 10.1038/nature01451.

185. **Ferguson SM**, **De Camilli P**. Dynamin, a membrane-remodelling GTPase. *Nat. Rev. Mol. Cell Biol.* 2012.DOI: 10.1038/nrm3266.

186. **van der Bliek AM**, **Redelmeier TE**, **Damke H**, **Tisdale EJ**, **Meyerowitz EM**, **Schmid SL**. Mutations in human dynamin block an intermediate stage in coated vesicle formation. *The Journal of Cell Biology*. 1993; **122**:553–563.DOI: 10.1083/jcb.122.3.553.

187. **Tomas A**, **Futter CE**, **Eden ER**. EGF receptor trafficking: consequences for signaling and cancer. *Trends Cell Biol*. 2014; **24**:26–34.DOI: 10.1016/j.tcb.2013.11.002.

188. **Avalos BR**, **Gasson JC**, **Hedvat C**, **Quan SG**, **Baldwin GC**, **Weisbart RH**, **Williams RE**, *et al.* Human granulocyte colony-stimulating factor: biologic activities and receptor characterization on hematopoietic cells and small cell lung cancer cell lines. *Blood*. 1990; **75**:851–857.

189. **Tanaka Y**, **Tanaka N**, **Saeki Y**, **Tanaka K**, **Murakami M**, **Hirano T**, **Ishii N**, *et al.* c-Cbl-dependent monoubiquitination and lysosomal degradation of gp130. *Mol Cell Biol*. 2008; **28**:4805–4818.DOI: 10.1128/MCB.01784-07.

Acknowledgements

First of all, I would like to express my gratitude to my doctoral adviser Gerhard Müller-Newen not only for his guidance over the past few years but also for his invigorating enthusiasm that fortunately infected me and for his apparently sheer endless patience.

To Björn Usadel I am indepted for his willingness to be my second supervisor.

Mein herzlicher Dank gilt unserer technischen Assistenz, Andrea und Hildegard, die sich in jegliches Klonierungsunterfangen gestürzt haben um mir einen schnellen und reibungslosen Arbeitsablauf zu ermöglichen. Wenn es im Labor so etwas wie eine Hierarchie gibt dann sitzt ihr beide meiner Auffassung nach ganz weit oben.

An dieser Stelle möchte ich des Weiteren meine Kollegen aus Labor 10 Alison, Caro und Marlies und aus Labor 11 Thomas und Oindi erwähnen, auch wenn sie teilweise schon lange das Labor verlassen haben und in der Weltgeschichte mitmischen. Einen besonderen Dank möchte ich Christiane Becker aussprechen, die mich mit ihrem Wesen und ihrer Lebenseinstellung durch einige schwierige Momente getragen hat. Euch allen verdanke ich, dass ich diesen Schritt zu Ende gehen kann.

Mein wichtigster Dank und größter Respekt gilt Marcel Kuhny für seinen Wissenschaftlergeist und seine menschliche Integrität. Danke für deinen Glauben an mich, für deine Zuversicht, für deine Härte und Güte zugleich.